

AMRL-TR-67-62

AD 663762



## CONFIGURATION INVESTIGATION FOR LITHIUM OXIDE CARBON DIOXIDE CONTROL SYSTEMS

DANIEL A. BORYTA  
EUGENE W. DEZMELYK

FOOTE MINERAL COMPANY  
RESEARCH AND ENGINEERING CENTER

OCTOBER 1967

D D C  
REFINED  
JAN 12 1968  
RUBBER  
C

Distribution of this document is unlimited. It  
may be released to the Clearinghouse, Depart-  
ment of Commerce, for sale to the general public.

AEROSPACE MEDICAL RESEARCH LABORATORIES  
AEROSPACE MEDICAL DIVISION  
AIR FORCE SYSTEMS COMMAND  
WRIGHT-PATTERSON AIR FORCE BASE, OHIO

159

## NOTICES

When US Government drawings, specifications, or other data are used for any purpose other than a definitely related Government procurement operation, the Government thereby incurs no responsibility nor any obligation whatsoever, and the fact that the Government may have formulated, furnished, or in any way supplied the said drawings, specifications, or other data, is not to be regarded by implication or otherwise, as in any manner licensing the holder or any other person or corporation, or conveying any rights or permission to manufacture, use, or sell any patented invention that may in any way be related thereto.

Federal Government agencies and their contractors registered with Defense Documentation Center (DDC) should direct requests for copies of this report to:

DDC  
Cameron Station  
Alexandria, Virginia 22314

Non-DDC users may purchase copies of this report from:

Chief, Storage and Dissemination Section  
Clearinghouse for Federal Scientific & Technical Information (CFSTI)  
Sills Building  
5285 Port Royal Road  
Springfield, Virginia 22151

Organizations and individuals receiving reports via the Aerospace Medical Research Laboratories' automatic mailing lists should submit the addressograph plate stamp on the report envelope or refer to the code number when corresponding about change of address or cancellation.

Do not return this copy. Retain or destroy.

700 - January 1967 - CO455 - 18-362

ACCESSION NO.	
CFSTI	WHITE SECTION <input checked="" type="checkbox"/>
DDC	BUFF SECTION <input type="checkbox"/>
UNANNOUNCED	<input type="checkbox"/>
JUSTIFICATION	
.....	
BY	
DISTRIBUTION/AVAILABILITY CODE	
DIST.	AVAIL and/or SPECIAL
/	

## FOREWORD

This study was initiated by the Biomedical Laboratory of the Aerospace Medical Research Laboratories, Aerospace Medical Division, Wright-Patterson Air Force Base, Ohio. The research was conducted by the Foote Mineral Company, Research and Engineering Center, Exton, Pennsylvania, under Contract No. AF33(615)-3382. Mr. Eugene W. Dezmelyk was the principal investigator for Foote Mineral Company and Mr. Daniel A. Boryta was the project supervisor. Mr. Clemens M. Meyer of the Biotechnology Branch, Life Support Division, was the contract monitor for the Aerospace Medical Research Laboratories. The work was performed in support of project 6373, "Equipment for Life Support in Aerospace," and task 637302, "Respiratory Support Equipment." The research sponsored by this contract was conducted between December 1965 and December 1966.

This technical report has been reviewed and is approved.

WAYNE H. McCANDLESS  
Technical Director  
Biomedical Laboratory  
Aerospace Medical Research Laboratories

AMRL-TR-67-62

## **CONFIGURATION INVESTIGATION FOR LITHIUM OXIDE CARBON DIOXIDE CONTROL SYSTEMS**

**DANIEL A. BORYTA  
EUGENE W. DEZMEYER**

Distribution of this document is unlimited. It  
may be released to the Clearinghouse, Depart-  
ment of Commerce, for sale to the general public.

## ABSTRACT

The bulk density of lithium oxide shapes and granules has been increased substantially while retaining good reactivity. Absorbent forms of the oxide can be prepared in the bulk density range of 0.18 to 0.28 g/cc. For granular oxide, results indicate a reasonable compromise between reactivity and absorbent volume efficiency is about 0.20 g/cc in passive systems and 0.26 to 0.28 g/cc in semipassive or dynamic systems. The improvement results from use of high (about  $18 \text{ m}^2/\text{g}$ ) surface area lithium peroxide raw material and techniques in processing the peroxide to oxide. Tests indicate the oxide forms developed can equal (passive exposure) or exceed (semipassive or dynamic exposure) the 0.8 g  $\text{CO}_2/\text{g LiOH}$  capacity of granular lithium hydroxide before 2% breakthrough. Dusting of the granular oxide form was reduced by controlled abrasion and fabric encasement techniques. Tests at one-third and normal atmospheres indicated higher carbon dioxide absorption rates at the lower pressure. A marked improvement was found in oxygen-helium as compared to oxygen and oxygen-nitrogen atmospheres. Atmospheric moisture conditions required for efficient absorption were defined. Exploratory work indicates partial hydration of the oxide is one method for initiating absorption under low humidity conditions. Gravimetric analysis work, which confirmed that density limitations are presently imposed by reaction product-substrate molar volume relations, should provide useful guidelines for absorbent design and further experimentation.

## TABLE OF CONTENTS

<u>Section</u>	<u>Page</u>
<b>I. Introduction</b>	1
1. General Considerations	1
2. Lithium Oxide Preparation	4
a. Lithium Peroxide	5
b. Lithium Peroxide Decomposition	5
3. Processes For Lithium Oxide Configurations	7
4. Li <sub>2</sub> O and Reaction Product Analysis	10
a. Lithium Oxide	10
b. Reaction Products	10
c. Lithium Peroxide	10
<b>II. Preliminary Screening Tests</b>	13
1. Experimental Approach	13
2. Passive Tests - Gravimetric Analysis	13
a. Supported Bed Forms	17
(1) Granules from Li <sub>2</sub> O <sub>2</sub> Powder	17
(2) Granules from Packed Li <sub>2</sub> O Tablets	19
(3) Tablets from Li <sub>2</sub> O <sub>2</sub> Tablets	23
(4) Granules from Pelletized Li <sub>2</sub> O Powder	23
(5) Granules from Li <sub>2</sub> O <sub>2</sub> Pellets	26
(6) Granules from Granular LiOH	26
(7) Comparative LiOH Granules	29
b. Self-supported Shapes	29
(1) From Pressed Li <sub>2</sub> O Powder	29
(2) Sintered Shapes from Li <sub>2</sub> O <sub>2</sub> Powder	32
(3) Sintered Shapes from Granular Li <sub>2</sub> O <sub>2</sub>	32
c. Gas Velocity Effect	32
d. Reaction Product Composition	35
e. Analysis of Results	35
3. Dynamic Tests	38
a. Apparatus and Procedure	38
b. Test Data	40
c. Analysis of Results	40

<u>Section</u>	<u>Page</u>
III. Configuration Tests with Low Moisture Availability	52
1. Apparatus and Procedures	52
2. Exploratory Runs	54
3. Passive Tests	54
4. Dynamic Tests	70
a. Dynamic Test Unit	70
b. Tests	70
c. Analysis of Results	74
IV. Absorber Development and Testing at 1-Atmosphere	77
1. Apparatus	77
2. Granular Li <sub>2</sub> O Development	80
a. Granule Coating	80
b. Dedusting	81
c. Fabric Encasement	83
3. Solid Li <sub>2</sub> O Configuration Development	87
4. Configuration Testing	90
5. Analysis of Results	110
V. Tests at One-Third Atmosphere	120
1. General Considerations	120
2. Apparatus	120
3. Configuration Tests	122
a. Dynamic Exposure, Packed Granular Bed	122
b. Passive Exposure, Granular Belt	123
c. Semipassive Exposure, Pierced Cylinder	126
4. Analysis of Results	129
VI. Effect of Atmosphere Composition	130
1. General Considerations	130
2. Apparatus	130
3. Experimental Data	131
4. Analysis of Results	131

<u>Section</u>	<u>Page</u>
VII. Conclusions	137
1. Lithium Oxide Preparation and Performance	137
2. Effect of Atmosphere Variations	138
3. Configuration Design	139
References	143

LIST OF ILLUSTRATIONS

<u>Figure</u>	<u>Page</u>
1. Lithium Peroxide Decomposer	6
2. Gravimetric Analysis Absorption Chamber	14
3. Gravimetric Curves; Samples 349-9-5, 349-11-2, 349-13-2	16
4. Gravimetric Curves; Samples 349-16-2, 349-18-2, 349-21-2	16
5. Gravimetric Curve, Sample 349-23-2	20
6. Gravimetric Curves; Samples 358-7-1, 349-35-3, 349-42-1C	20
7. Gravimetric Curves; Samples 349-42-4, 358-2-3, 358-7-3	22
8. Li <sub>2</sub> O <sub>2</sub> Tablets After Decomposition	24
9. Gravimetric Curves; Samples 349-42-1B, 349-42-3, 358-2-1	22
10. Gravimetric Curves; Samples 358-11-1, 358-10-1, 358-21-1	28
11. Gravimetric Curves; Samples 358-24-1, 358-21-1, 358-31-1	28
12. Gravimetric Curves; Granular LiOH	30
13. Porous Solid Li <sub>2</sub> O Shapes	30
14. Gravimetric Curves; Samples 349-11-1, 359-13-1, 349-18-1	33
15. Bulk Density of Li <sub>2</sub> O versus Time for Complete Carbonation	37
16. Dynamic Screening Test Apparatus	39
17. Bulk Density of Granular Li <sub>2</sub> O versus CO <sub>2</sub> Absorption in a Single Pass	43
18. Log 4- by 10-mesh Bulk Density versus % CO <sub>2</sub> Input Absorbed in a Single Pass	45
19. Dynamic Test, Effluent Gas Temperature and Relative Humidity, 1% CO <sub>2</sub> and 50% R.H. Input	46

<u>Figure</u>	<u>Page</u>
20. Dynamic Test, Effluent Gas Temperature and Relative Humidity, 50% and 88% R.H. Input	51
21. Apparatus For 1-Atmosphere Tests	53
22. Passive Test Profiles, Granule Rectangular Bed (Run 368-39)	56
23. Passive Cylindrical Bed Configuration	60
24. Passive Test Profiles, Granule Cylindrical Bed (Run 368-45)	62
25. Passive Test Profiles, Granule Cylindrical Bed (Run 376-11)	63
26. Passive Test Profiles, Granule Cylindrical Bed (Run 376-13)	65
27. Passive Test Profiles, Granule Cylindrical Bed (Run 376-15)	66
28. Granule Belt Configuration	67
29. Granule Belt Configuration in Test Apparatus	68
30. Passive Test Profiles, Granule Belt (Run 376-16-1)	68
31. Passive Test Profiles, Granule Belt (Run 376-17-1)	69
32. Dynamic Absorption Unit	71
33. Dynamic Absorber in Test Apparatus	72
34. Dynamic Test Profiles (Run 376-19)	73
35. Dynamic Test Profiles (Run 376-38-1)	75
36. Apparatus For 1-Atmosphere Tests	79
37. Dedusting Apparatus	82
38. Microphotograph, Li <sub>2</sub> O Granule Before Dedusting	84
39. Microphotograph, Li <sub>2</sub> O Granule After Dedusting	85
40. Pierced Cylinder Configuration, Decomposed Li <sub>2</sub> O Powder	88
41. Pierced Cylinder Configuration, Decomposed Li <sub>2</sub> O <sub>2</sub> Granules	89

<u>Figure</u>	<u>Page</u>
42. Test Profiles (Runs 361-26 and 361-30)	92
43. Apparatus Arrangement, Pierced Cylinder Configuration	93
44. Test Profiles (Run 361-21)	95
45. Apparatus Arrangement, Passive Belt Configuration	97
46. Test Profiles (Run 361-29 and 361-34)	98
47. Test Profiles (Run 361-43)	101
48. Test Profiles (Run 361-46)	102
49. Test Profiles, Passive 8-Hour Mission (Run 397-1)	105
50. Apparatus Arrangement, Dynamic Granular Bed	106
51. Test Profiles (Runs 361-48 and 390-6)	108
52. Semipassive Configuration	111
53. Granular Li <sub>2</sub> O Bed For Semipassive Configuration	112
54. Apparatus Arrangement, Semipassive Test	114
55. Test Profiles, Semipassive 8-Hour Mission (Run 397-3)	116
56. Apparatus Arrangement, One-third Atmosphere Tests	121
57. Test Profiles, Passive 8-Hour Mission at One-Third Atmosphere (Run 390-46)	125
58. Cross-section of Pierced Cylinder Configuration	127
59. Test Profiles, Semipassive 8-Hour Mission at One-Third Atmosphere (Run 397-19)	128
60. Gravimetric Curves For O <sub>2</sub> , O <sub>2</sub> -N <sub>2</sub> , and O <sub>2</sub> -He Atmospheres at 50% Relative Humidity	133
61. Gravimetric Curves For O <sub>2</sub> and O <sub>2</sub> -N <sub>2</sub> Atmospheres at 25, 50, and 75% Relative Humidity	134
62. Gravimetric Curves for Partially Hydrated Li <sub>2</sub> O	135

LIST OF TABLES

<u>Table</u>	<u>Page</u>
I Maximum Reactant Densities	4
II Process For Supported Bed Li <sub>2</sub> O Forms	8
III Processes For Self-supported Li <sub>2</sub> O Forms	9
IV Gravimetric Test Data, Process 2a-(2)	18
V Gravimetric Test Data, Process 2a-(1)	21
VI Gravimetric Test Data, Process 2a-(3)	25
VII Gravimetric Test Data, Process 2a-(4) and 2a-(5)	27
VIII Gravimetric Test Data, Porous Solid Li <sub>2</sub> O	31
IX Gravimetric Tests, Gas Velocity Effect	34
X Gravimetric Tests, Reaction Product Analyses	36
XI Dynamic Test Data at 50% R.H. Input	41
XII Reaction Product Molar Ratios	48
XIII Dynamic Test Results	49
XIV Passive Test Data, Granule Rectangular Bed	55
XV Test Data At 1 Atmosphere	57
XVI Chamber Gas Velocities With Fan Operating	78
XVII Chamber CO <sub>2</sub> Concentration With Zero Absorption	80
XVIII Dedusting of 4- by 10-Mesh, Granular Li <sub>2</sub> O	83
XIX Dusting Tests With Fabric Encasement	86
XX Test Data, Runs 361-26 and 361-30	91
XXI Test Data, Run 361-21	96
XXII Test Data, Runs 361-29 and 361-24	99
XXIII Test Data, Runs 361-43 and 361-46	103
XXIV Test Data, Passive 8-Hour Mission, Run 397-1	104
XXV Test Data, Runs 361-48 and 390-6	109

<u>Table</u>	<u>Page</u>
XXVI Configuration Dimensions and Gas Velocities, Run 397-3	113
XXVII Test Data, Semipassive 8-Hour Mission, Run 397-3	115
XXVIII Comparison of Passive Belt and Dynamic Bed	118
XXIX Test Data, Runs 390-46 and 397-19	124
XXX Absorption Tests in Various Atmospheres	132

## SECTION I

### INTRODUCTION

#### 1. GENERAL CONSIDERATIONS

Previous comparisons of the carbon dioxide absorption capacity of nonregenerable chemical absorbents have indicated that lithium oxide is theoretically unsurpassed (references 1, 2,12). CO<sub>2</sub> absorption with high (0.32 g/cc) and low (0.10 g/cc) bulk density forms of Li<sub>2</sub>O has been demonstrated with nearly complete utilization of the oxide's capacity. One obstacle in the practical application of Li<sub>2</sub>O has been the low CO<sub>2</sub> absorption rate of high density forms of the oxide. A principal aim of this investigation was to establish the optimum bulk density and configuration for absorbing 45 g CO<sub>2</sub>/hr while maintaining CO<sub>2</sub> concentration below 7.6 mm Hg partial pressure in an atmosphere at 50% relative humidity and 18 to 29°C temperature.

From a weight and volume efficiency standpoint (weight of CO<sub>2</sub> removed per unit weight and volume of Li<sub>2</sub>O), the ideal form of Li<sub>2</sub>O would be a single solid shape at its true density. However, there are two requirements for reasonable absorption rate and utilization which preclude use of this form. The gas must: (1) contact large absorbent surface areas for reasonable rate, and (2) have access to fresh absorbent for continued reaction. To meet these requirements, three types of void spaces can be visualized:

- a. Channel voids or passages of regular geometric form.

Typical examples are free space between slabs or holes through blocks of absorbent.

b. Bulk voids or passages of irregular geometric form.

The voids occurring in powdered or granular beds of absorbent illustrate this type.

c. Pore voids or passages of irregular form in the discrete particles of absorbent.

Providing gas-solid contact by any of the above techniques necessarily increases the gross volume occupied by the absorbent, with a corresponding decrease in volume efficiency. Thus, an important step in developing Li<sub>2</sub>O absorbent configurations is evaluating void types, or combinations of them, which maximize volume efficiency. The selection of the macroscopic void types, bulk and channel voids, also involves consideration of gas pressure loss in flow-through systems. The characteristics of channel voids (such as gas-flow area, exposed absorbent area, and total void volume) can be readily controlled by fabricating to suitable dimensions, but channel voids have the inherent limitation of low exposed absorbent surface area. The characteristics of bulk voids can be controlled by altering particle size and packing, and larger surface areas can be provided than with channel voids. Pore voids are the only means for providing truly large absorbent surface areas. Their production and control is more difficult than providing macroscopic void types, since pore voids are governed by Li<sub>2</sub>O preparation techniques.

The theoretical maximum bulk density of the absorbent, consistent with CO<sub>2</sub> absorption, can be approximately predicted from

molar volume relations (reference 4). If the molar volume of the reaction product is greater than the equivalent molar volume of the reactive substrate, the reaction product can completely coat the substrate. If this coating is not disrupted during density changes, it is nonporous and shields the substrate from further reaction. Therefore, the reaction product to substrate molar volume ratio is a measure of the coating effect on the reaction, with ratios exceeding unity indicating the presence of potentially protective coatings. Molar volume ratios related to lithium oxide and intermediates in the  $\text{CO}_2$  absorption process are given below. These indicate  $\text{Li}_2\text{CO}_3$  is marginally protective on a  $\text{LiOH}$  substrate and nonprotective on  $\text{LiOH}\cdot\text{H}_2\text{O}$ . Also significant is the indication that  $\text{LiOH}$  and  $\text{LiOH}\cdot\text{H}_2\text{O}$  can be quite protective on a  $\text{Li}_2\text{O}$  substrate. Since both forms of the hydroxide are necessary intermediates in the carbonation of  $\text{Li}_2\text{O}$ , it is essential to minimize their protective effect by void and density adjustment techniques.

Substrate Compound	True Density g/cc	Molar Volume cc/g Mol	Molar Volume Ratio		
			$\text{Li}_2\text{CO}_3$ Coat.	$\text{LiOH}$ Coat.	$\text{LiOH}\cdot\text{H}_2\text{O}$ Coat.
$\text{Li}_2\text{O}$	2.01	14.87	2.355	2.253	3.737
$\text{LiOH}$	1.43	16.75	1.045	---	1.659
$\text{LiOH H}_2\text{O}$	1.51	27.79	0.635	---	---

NOTE:  $\text{Li}_2\text{CO}_3$  specific gravity 2.11; molar volume 35.02

The volume ratio concept can be extended to predicting density limitations and is therefore useful in guiding experimental work. For example, the molar volume ratio of a granule of  $\text{Li}_2\text{O}$ , at its true density of 2.01 g/cc, reacting with water to yield

$\text{LiOH}\cdot\text{H}_2\text{O}$  is 3.74. The ratio, and protective effect of the  $\text{LiOH}\cdot\text{H}_2\text{O}$ , can be reduced by decreasing the  $\text{Li}_2\text{O}$  density. Thus, a porous granule of  $\text{Li}_2\text{O}$  at 0.53 g/cc apparent density yields a calculated ratio of unity. Since this ratio is borderline between a protective and nonprotective  $\text{LiOH}\cdot\text{H}_2\text{O}$  coating, an upper limit has been defined for the apparent density of a  $\text{Li}_2\text{O}$  granule under the stated conditions. Table I gives apparent density limits for porous reactants yielding various nonporous products at a molar volume ratio of unity. For given granule sizes, the apparent density of the single granules can be translated to the bulk densities of beds of such granules. Thus, table I predicts for the stated reactions the maximum density attainable for configurations containing only pore voids and configurations based on 4- by 10-mesh granules containing both pore and bulk voids.

TABLE I  
MAXIMUM REACTANT DENSITIES

<u>Porous Reactant</u>	<u>Nonporous Product</u>	Reactant Density- g/cc	
		<u>Single Granule</u>	<u>4- by 10-Mesh Bulk Bed</u>
$\text{Li}_2\text{O}$	$\text{LiOH}\cdot\text{H}_2\text{O}$	0.537	0.32
$\text{Li}_2\text{O}$	$\text{LiOH}$	0.912	0.54
$\text{Li}_2\text{O}$	$\text{Li}_2\text{CO}_3$	0.853	0.51
$\text{LiOH}$	$\text{LiOH}\cdot\text{H}_2\text{O}$	0.861	0.51

## 2. LITHIUM OXIDE PREPARATION

Lithium oxide can be prepared via two procedures, the dehydration of  $\text{LiOH}$  and the decomposition of  $\text{Li}_2\text{O}_2$ . In the former

process, granular LiOH is dehydrated at high temperature and under vacuum. For  $\text{CO}_2$  absorption applications, slow dehydration and careful temperature control are required to obtain the oxide in a porous and reactive form. The product is typically hard, white, 4- by 14-mesh granules with a bulk density of 0.35 g/cc and surface area of 0.94  $\text{m}^2/\text{g}$ . The low surface area is a prime disadvantage of this process. For comparison purposes in the reported work a few experimental runs were made using LiOH based oxide. The major effort was concentrated on  $\text{Li}_2\text{O}_2$  based oxide with preparation as outlined below.

a. Lithium Peroxide

The  $\text{Li}_2\text{O}_2$  used for experimental work was obtained from Foote Mineral Company production facility. The  $\text{Li}_2\text{O}_2$  was obtained in the form of a white powder with 0.28 g/cc bulk density. Typical analysis was 97.9%  $\text{Li}_2\text{O}_2$  with 0.7% LiOH and 1.1%  $\text{Li}_2\text{CO}_3$ . Surface area ranged from 16.2 to 19.7  $\text{m}^2/\text{g}$ .

b. Lithium Peroxide Decomposition

The atmospheric pressure decomposition apparatus (see figure 1) consisted of a glass beaker housed within an aluminum vessel, the assembly being set in a muffle furnace. Since the  $\text{Li}_2\text{O}$  product density is critical and varies with decomposition temperature, several precautions were taken to insure uniform and reproducible temperatures within the decomposer. The beaker containing the  $\text{Li}_2\text{O}_2$  was supported to avoid glass to metal contact and resulting hot spots, and temperatures on the aluminum vessel and within the beaker were correlated. The aluminum vessel was continuously flushed with dry heated nitrogen

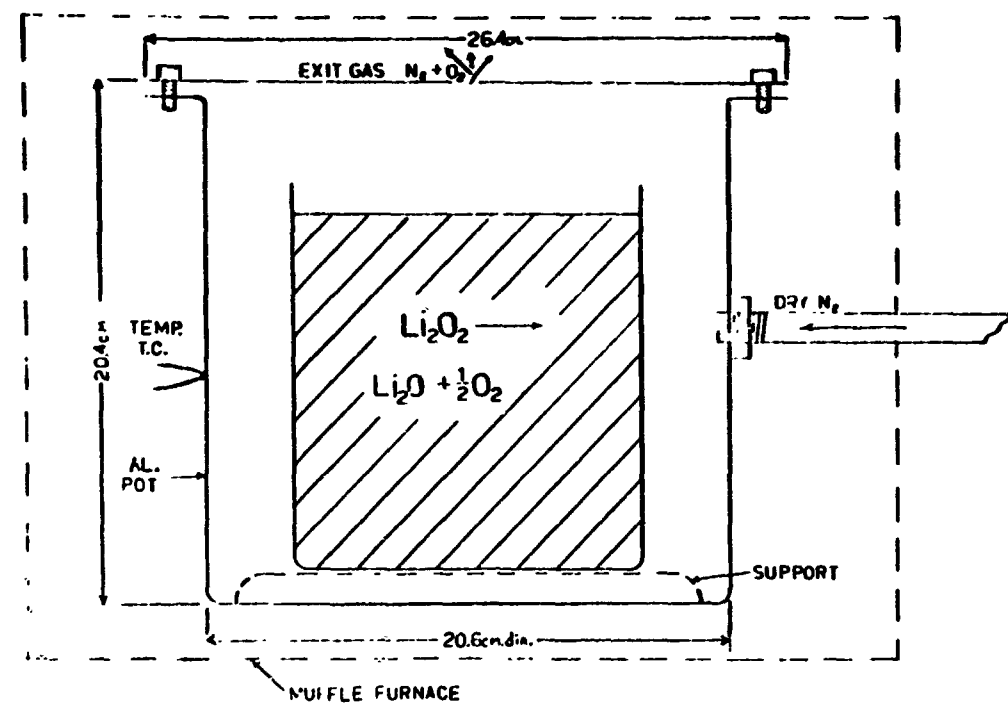


Fig. 1. Lithium Peroxide Decomposer

during operation. Peroxide decompositions under vacuum were conducted in a metal autoclave, and temperature uniformity did not equal that of the atmospheric pressure decomposer.  $\text{Li}_2\text{O}$  that was prepared by this method did not indicate any advantage in vacuum decomposition, therefore, no effort was spent in refining this apparatus.

### 3. PROCESSES FOR LITHIUM OXIDE CONFIGURATIONS

Two general methods can be used for presenting  $\text{Li}_2\text{O}$  surfaces to a carbon dioxide-containing atmosphere. In the first method, the oxide is displayed in the form of supported beds composed of relatively loosely packed particles or granules. The advantages of this technique are the possibility of fabricating configurations of virtually any shape, and the ability to alter oxide density (bulk and particulate) over a wide range. Potential penalties of the supported bed approach are weight of the support media and relatively high overall volume. The second method involves fabricating the oxide into self-supporting shapes, with required mechanical strength developed through interlocking or sintering of the oxide particles or granules. The potential advantages are weight and volume reduction. A major drawback is reduced ability to alter oxide density, since density and mechanical strength become interrelated in self-supported shapes. In the reported work, supported and self-supported configurations were prepared by a number of processes. Steps in the various processes are summarized in tables II and III. More detailed descriptions, process observations, and

TABLE II  
PROCESSES FOR SUPPORTED BED  $\text{Li}_2\text{O}$  FORMS

Process No.	Raw Mat <sub>1</sub>	Treatment	Decomposition		Post-Decomposition Processing		Final Product
			$\text{Li}_2\text{O}_2$ Feed	$\text{Li}_2\text{O}$ Product Form	Sintered Cake	Crushed	
2a-(1)	$\text{Li}_2\text{O}_2$ Powder	None	Powder	---	---	Crushed	$\text{Li}_2\text{O}$ Granules
2a-(2)	$\text{Li}_2\text{O}_2$	Tabletted	Packed Tablets	Sintered Cake	---	Crushed	$\text{Li}_2\text{O}$ Granules
2a-(3)	$\text{Li}_2\text{O}_2$	Tabletted	Loose Tablets	Loose Tablets	---	---	$\text{Li}_2\text{O}$ Tablets
2a-(4)	$\text{Li}_2\text{O}_2$ Powder	None	Powder	Sintered Cake	Pulverized	Crushed	$\text{Li}_2\text{O}$ Granules
2a-(5)	$\text{Li}_2\text{O}_2$ Powder	Pelletized	Pellets	Sintered Pellets	Pelletized	Crushed	$\text{Li}_2\text{O}$ Granules
2a-(6)	$\text{LiOH}$ Granules	None	$\text{LiOH}$ Granules	$\text{Li}_2\text{O}$ Granules	---	---	$\text{Li}_2\text{O}$ Granules
2a-(7)	$\text{LiOH}$ Granules	None	---	---	---	---	$\text{LiOH}$ Granules

Note: Process details and test results are given in section II, under paragraphs corresponding to process numbers.

TABLE III  
PROCESSES FOR SELF-SUPPORTED Li<sub>2</sub>O FORMS

Process No.	Raw Matl	Treatment	Li <sub>2</sub> O Feed Form			Post-Decomposition Processing			Final Product
			Powder	Sintered Cake	Pulverized	Pelletized			
2b-(1)	Li <sub>2</sub> O <sub>2</sub> Powder	None	Powder	Sintered Cake					Li <sub>2</sub> O Cylinders
2b-(2)	Li <sub>2</sub> O <sub>2</sub> Powder	None	Powder	Sintered Cake	---	---	---	Carved to Shape	Li <sub>2</sub> O Cylinders
2b-(3)	Li <sub>2</sub> O <sub>2</sub> Powder	Pelletized & Crushed	Granules	Sintered Cake					Li <sub>2</sub> O Cylinders

Note: Process details and test results are given in section II, under paragraphs corresponding to process numbers.

the corresponding results in  $\text{CO}_2$  absorption screening tests are reported in section II.

#### 4. $\text{Li}_2\text{O}$ AND REACTION PRODUCT ANALYSIS

All chemical analyses were conducted at the Foote Mineral Company, under the following procedures:

##### a. Lithium Oxide

Samples were prepared in a dry box and titrated with 1 normal  $\text{HCl}$  to the modified methyl orange endpoint for total alkalinity. This includes  $\text{Li}_2\text{O}$ ,  $\text{LiOH}$ ,  $\text{Li}_2\text{CO}_3$  and  $\text{Li}_2\text{O}_2$ . Another portion of the sample was then titrated with 1 normal  $\text{HCl}$  after addition of neutral 15-percent  $\text{BaCl}_2$  to the cresol red endpoint for total hydroxide which included  $\text{Li}_2\text{O}$ ,  $\text{LiOH}$  and  $\text{Li}_2\text{O}_2$  but excluded  $\text{Li}_2\text{CO}_3$ . For  $\text{Li}_2\text{O}_2$  content,  $\text{Li}_2\text{O}_2$  samples were acidified with 1:1  $\text{H}_2\text{SO}_4$  and titrated immediately with 0.1 normal  $\text{KMnO}_4$  to a pink endpoint. The final results are obtained with appropriate calculations and corrections programmed for a computer.

##### b. Reaction Products

Samples were prepared with minimum atmospheric exposure. A Knorr Alkalimeter (reference 13) was used to selectively analyze for  $\text{Li}_2\text{CO}_3$ . Another portion was then titrated for total alkalinity with 1 normal  $\text{HCl}$  to the modified methyl orange endpoint which includes  $\text{Li}_2\text{CO}_3$ ,  $\text{Li}_2\text{O}$ ,  $\text{LiOH}$  and  $\text{LiOH}\cdot\text{H}_2\text{O}$ . Water was determined by difference.

##### c. Lithium Peroxide

Lithium peroxide samples were dissolved in 1:1  $\text{H}_2\text{SO}_4$

solution and titrated immediately with 0.1 normal  $\text{KMnO}_4$  to a permanent pink endpoint.

## SECTION II

### PRELIMINARY SCREENING TESTS

#### 1. EXPERIMENTAL APPROACH

Two preliminary  $\text{CO}_2$  absorption screening tests were used to expedite selection of the most promising forms of  $\text{Li}_2\text{O}$  for further evaluation. The first was basically a passive test, with small  $\text{Li}_2\text{O}$  samples being continuously weighed while exposed to a controlled atmosphere. The second was a dynamic test with gas flowing through sample beds. The tests yielded data on the effect of  $\text{Li}_2\text{O}$  surface area, bulk density, and shape as related to reactivity and absorption rate.

#### 2. PASSIVE TESTS - GRAVIMETRIC ANALYSIS

Passive tests were made using the recording balance of a thermogravimetric analysis apparatus (reference 6) to continuously weigh a sample of  $\text{Li}_2\text{O}$  suspended in a gas-filled tube. The absorption section of the apparatus is shown in figure 2. Oxygen containing 1% (vol)  $\text{CO}_2$ , before humidifying to 50% relative humidity at 22 C, was passed through the tube. Gas velocity, based on the cross-sectional area of the tube, was 81 cm/min at 500 cc/min gas flow rate. Under these conditions (0.54 g  $\text{CO}_2$  feed/hr) the minimum time required to completely carbonate 1 g of pure  $\text{Li}_2\text{O}$  would be 2.7 hours, assuming 100%  $\text{CO}_2$  removal from the feed stream.

Reaction mechanisms can be ascribed to various sections of the gravimetric analysis curves (cumulative weight gain versus time) derived in these tests. Initial  $\text{CO}_2$  absorption, reaction

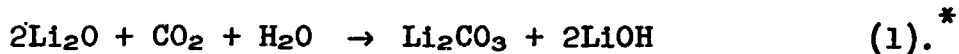


Fig. 2. Gravimetric Analysis Absorption Chamber

Tube: 2.8 cm inside diameter

Sample suspension basket: 400-mesh, stainless steel, screen cloth; 43.5% open area; 1.9 cm diameter by 4.2 cm deep.

(1) below, results from reactions (2), (3), and (4):

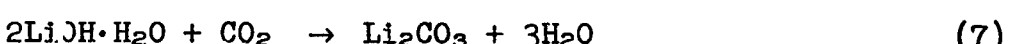
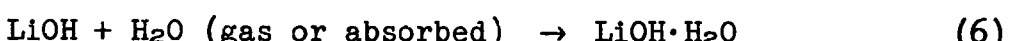


The rate of reaction (2) governs reaction (3). Therefore, a molar ratio of  $\text{H}_2\text{O}/\text{CO}_2$  exceeding unity should be provided to maximize the rate of reaction (3). The theoretical weight gain resulting from reaction (1) is 1.038 g/g  $\text{Li}_2\text{O}$  and the heat of reaction and free energy change per mole  $\text{Li}_2\text{O}$  are:

$$\Delta H^{25} \quad -43.39 \text{ kcal}$$

$$\Delta F^{25} \quad -29.28 \text{ kcal}$$

Subsequent reactions in the  $\text{CO}_2$  absorption process are given below. A weight loss occurs in reaction (7) because the weight of water evolved exceeds the weight of  $\text{CO}_2$  absorbed.



The foregoing reaction mechanisms are illustrated by gravimetric curves developed for samples 349-11-2 and 349-13-2 (figure 3) and sample 349-16-2 (figure 4). In each case, constant rate weight gain occurs up to about 1.1 g gain/g  $\text{Li}_2\text{O}$  followed by a decreasing rate and then a weight loss as the secondary reactions proceed.

---

\*Such numbers refer to reactions throughout this report.

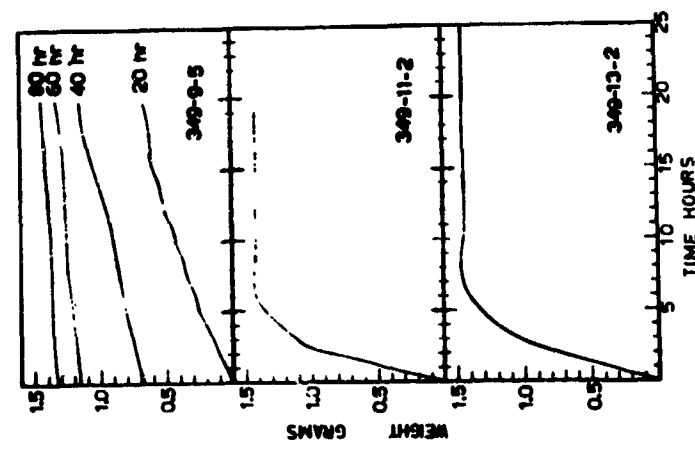


Fig. 3. Gravimetric Curves  
Samples 349-9-5, 349-11-2, 349-13-2

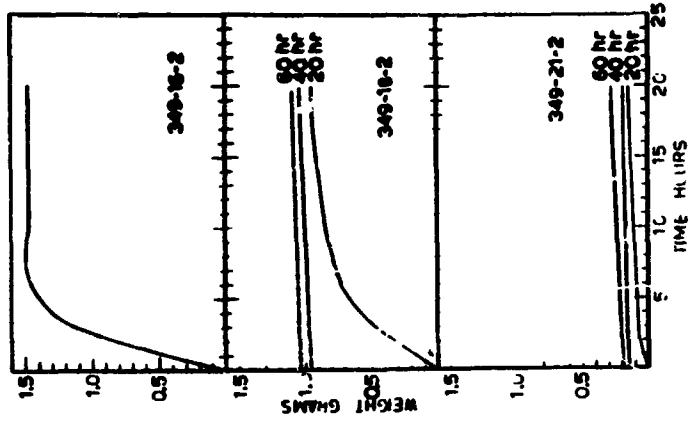


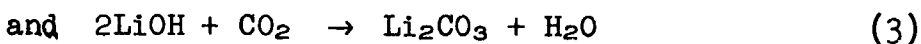
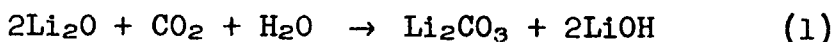
Fig. 4. Gravimetric Curves  
Samples 349-16-2, 349-18-2, 349-21-2

$\text{Li}_2\text{O}$  was prepared by a variety of processes in forms applicable to supported beds and self-supported shapes. Gravimetric  $\text{CO}_2$  absorption tests were then run on the various forms. The processes and observations on them, and information developed in absorption screening tests are outlined as follows:

a. Supported Bed Forms

(1) Granules From  $\text{Li}_2\text{O}_2$  Powder

High surface area (16.2 to 19.7  $\text{m}^2/\text{g}$ )  $\text{Li}_2\text{O}_2$  powder was thermally decomposed at atmospheric pressure and various temperatures. The material sintered during decomposition, and the resulting cake was crushed and sieved to 4- by 10-mesh  $\text{Li}_2\text{O}$  granules. Generally, increasing decomposition temperature raised bulk density and hardness but reduced surface area (see table IV). Samples which were decomposed below 325  $^{\circ}\text{C}$  swelled and compressed against the vessel walls before sintering (suggesting a possible technique for preparing self-supporting shapes as subsequently reported). Decreasing conversion to  $\text{Li}_2\text{CO}_3$  with increasing bulk density is evident in the results in table IV. The approximate times for reactions



are indicated by inflection points in the gravimetric curves of figure 3 (samples 349-11-2 and 349-13-2) and figure 4 (sample 349-16-2). The curves also illustrate the rate reduction occurring at bulk densities of about 0.34  $\text{g}/\text{cc}$  as typified by samples 349-9-5 and 349-18-2. These samples contained  $\text{Li}_2\text{O}$ ,  $\text{LiOH}$ , and  $\text{LiOH}\cdot\text{H}_2\text{O}$  in their reaction products as indicated by x-ray

TABLE IV  
GRAVIMETRIC TEST DATA, PROCESS 2a-(1)

1 Gram 4- by 10-Mesh Granular  $\text{Li}_2\text{O}$  exposed to Oxygen Gas, 1% (Vol)  $\text{CO}_2$ , 50% R.H.  
Preparation:  $\text{Li}_2\text{O}_2$  Powder decomposed, Sintered Cake crushed and sieved

Sample No. 349-	Decomp. Temp. C	Bulk Density g/cc	Surf. Area $\text{m}^2/\text{g}$	Hardness No.	Reaction Time (b) hr	Reaction Time (c) hr	Constant Wt. hr	Exposure Time hr	Product $\text{Li}_2\text{CO}_3$ %	
18	11-2	285	0.100	14.70	66.3	2.5	5.5	8	20	99.9
	13-2	325	0.124	13.35	59.3	3.0	7.0	10	25	97.7
	16-2	325	0.123	13.80	54.6	2.8	6.3	10	20	97.6
	18-2	350	0.341	3.85	93.1	---	---	(d)	190	85.1
	21-2	385	0.573	0.28	98.2	---	---	(d)	64	22.9
	23-2	430	0.630	---	92.6	---	---	(d)	95	26.6
	9-5(a)	644	0.341	0.94	89.2	---	---	(d)	80	90.0

Notes: (a) Sample 349-9-5 prepared from  $\text{LiOH}$  at variable decomposition temperature, 644 C being maximum

(b) For reaction  $2\text{Li}_2\text{O} + \text{CO}_2 + \text{H}_2\text{O} \rightarrow \text{Li}_2\text{CO}_3 + 2\text{LiOH}$

(c) For reaction  $2\text{LiOH} + \text{CO}_2 \rightarrow \text{Li}_2\text{CO}_3 + \text{H}_2\text{O}$

(d) Constant weight not attained during total exposure

diffraction analysis. This thermodynamically unstable condition (references 7,8) can only be explained by kinetic factors such as the formation of a nonporous coating of  $\text{LiOH}\cdot\text{H}_2\text{O}$  on the  $\text{LiOH}$  and  $\text{Li}_2\text{O}$ . The remaining samples with even higher bulk density were virtually unreactive as illustrated by the gravimetric curve of figure 5 (sample 349-23-2).

#### (2) Granules From Packed $\text{Li}_2\text{O}_2$ Tablets

$\text{Li}_2\text{O}_2$  powder was pressed into small tablets, each 6.35 mm diameter by 3.3 mm thick, weighing 0.08 g, and compressed to 31% of true  $\text{Li}_2\text{O}_2$  density. Loosely packed tablets, in 100 g quantities, were decomposed at various temperatures to explore the preparation of  $\text{Li}_2\text{O}$  tablets and void-containing shapes. The decompositions were run in the low temperature range as suggested by earlier results with the  $\text{Li}_2\text{O}_2$  powder. In all cases, the entire mass swelled, compressed itself into a cake containing few bulk voids, and then became sintered. The mass shrunk away from the vessel walls during sintering, the amount of shrinkage varying with decomposition temperature. The cakes were crushed and sieved to 4- by 10-mesh  $\text{Li}_2\text{O}$  granules. Granule characteristics and absorption test results are given in table V. Bulk density increased with decomposition temperature while surface area remained relatively constant over the temperature range studied. All samples exhibited relatively high conversion is evident as bulk density increases. The gravimetric curves of figures 7 and 9 illustrate the declining trend in reaction rate with density increase. This particular preparation technique was a more complex route to granular  $\text{Li}_2\text{O}$  than decomposing

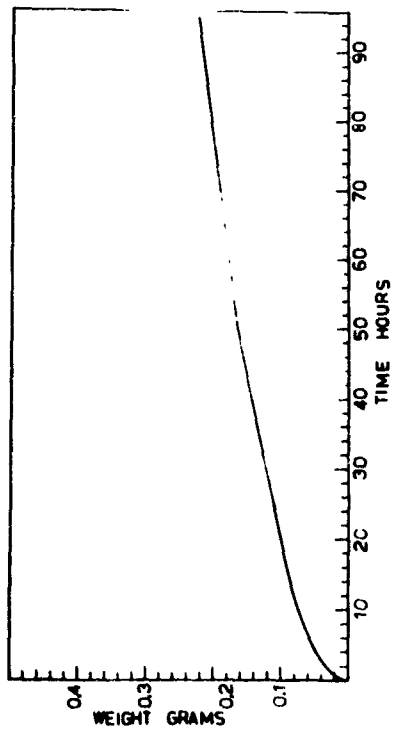


Fig. 5. Gravimetric Curve  
Sample 349-23-2

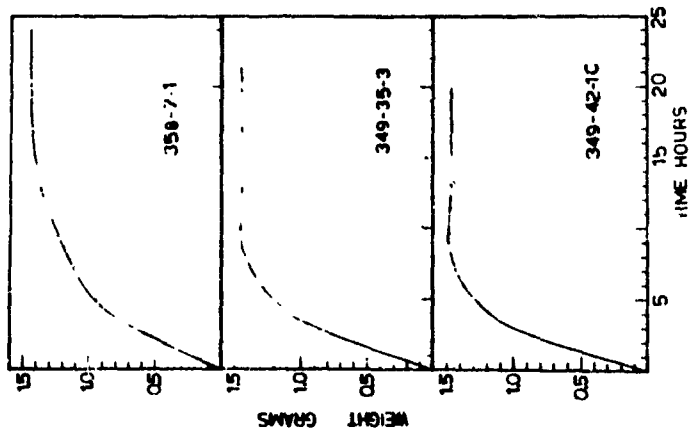


Fig. 6. Gravimetric Curves  
Samples 358-7-1, 349-35-3, 349-42-1C

TABLE V  
GRAVIMETRIC TEST DATA, PROCESS 2a-(2)

1 Gram 4- by 10-Mesh Granular  $\text{Li}_2\text{O}$  exposed to Oxygen Gas, 1% (Vol)  $\text{CO}_2$ , 50% R.H.

Preparation: Loosely packed  $\text{Li}_2\text{O}_2$  Tablets decomposed, sintered, crushed, and sieved

Sample No.	Decomp. Temp. C	Bulk Density g/cc(a)	Surf. Area $\text{m}^2/\text{g}$	Reaction Times		Constant Wt. hr.	Exposure Time hr.	Product $\text{Li}_2\text{CO}_3$ %
				(b) hr.	(c) hr.			
349-35-3	250	0.139	12.6	3.8	8.2	12	22	96.5
349-42-1C	275	0.134	12.8	3.2	10.8	14	20	97.9
349-42-4	300	0.145	13.8	3.6	14.4	18	22	97.2
358-2-3	318	0.186	13.3	5.0	17.0	22	22	96.6
358-7-3	325	0.231	12.7	5.0	15.0	20	22	95.0

Notes: (a) Bulk densities are approximate, being based on 1 g samples.

(b) For reaction  $2\text{Li}_2\text{O} + \text{CO}_2 + \text{H}_2\text{O} \rightarrow \text{Li}_2\text{CO}_3 + 2\text{LiOH}$

(c) For reaction  $2\text{LiOH} + \text{CO}_2 \rightarrow \text{Li}_2\text{CO}_3 + \text{H}_2\text{O}$

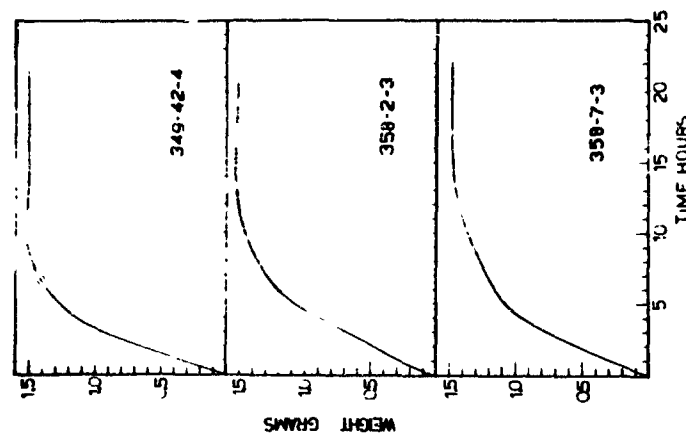


Fig. 7. Gravimetric Curves  
Samples 349-42-4, 358-2-3, 358-7-3

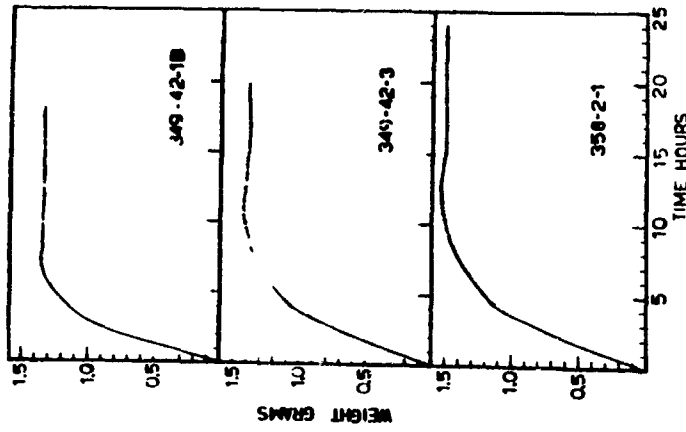


Fig. 9. Gravimetric Curves  
Samples 349-42-1B, 349-42-3, 358-2-1

larger pellets and offered no apparent compensating advantage in granule performance.

### (3) Tablets From $\text{Li}_2\text{O}_2$ Tablets

A few loose  $\text{Li}_2\text{O}$  tablets which had decomposed without sintering to the mass were obtained from the foregoing experiments. Figure 8 shows an original  $\text{Li}_2\text{O}_2$  tablet and the resulting  $\text{Li}_2\text{O}$  tablets produced at various decomposition temperatures. The tablet sizes illustrate the swelling which occurs during decomposition and the subsequent increasing shrinkage as decomposition temperature exceeds about 275 C. As shown in table VI which gives tablet characteristics and test data, the density of individual  $\text{Li}_2\text{O}$  tablets increased with decomposition temperature. The bulk density of loosely packed tablets increased similarly. Gravimetric curves are shown in figure 6 (sample 358-7-1) and figure 9 (samples 349-42-1B, 349-42-3, 358-2-1). The results parallel earlier experience with reactivity declining as tablet density increases.

### (4) Granules From Pelletized $\text{Li}_2\text{O}$ Powder

A 270 g charge of  $\text{Li}_2\text{O}_2$  powder, bulk density 0.28 g/cc was decomposed at 265 C under atmospheric pressure. On charging, the powder occupied a volume 10.4 cm in diameter by 11.8 cm deep. The sintered  $\text{Li}_2\text{O}$  cake following decomposition was 9.5 cm diameter by 13.5 cm deep, weighed 180 g, and had a bulk density of 0.188 g/cc. The  $\text{Li}_2\text{O}$  cake was pulverized and the powder was pressed into pellets 6.2 cm in diameter with a pellet density of 0.5 g/cc. The pellets were then crushed and sieved, yielding about 90 g of 4- by 10-mesh  $\text{Li}_2\text{O}$  granules.

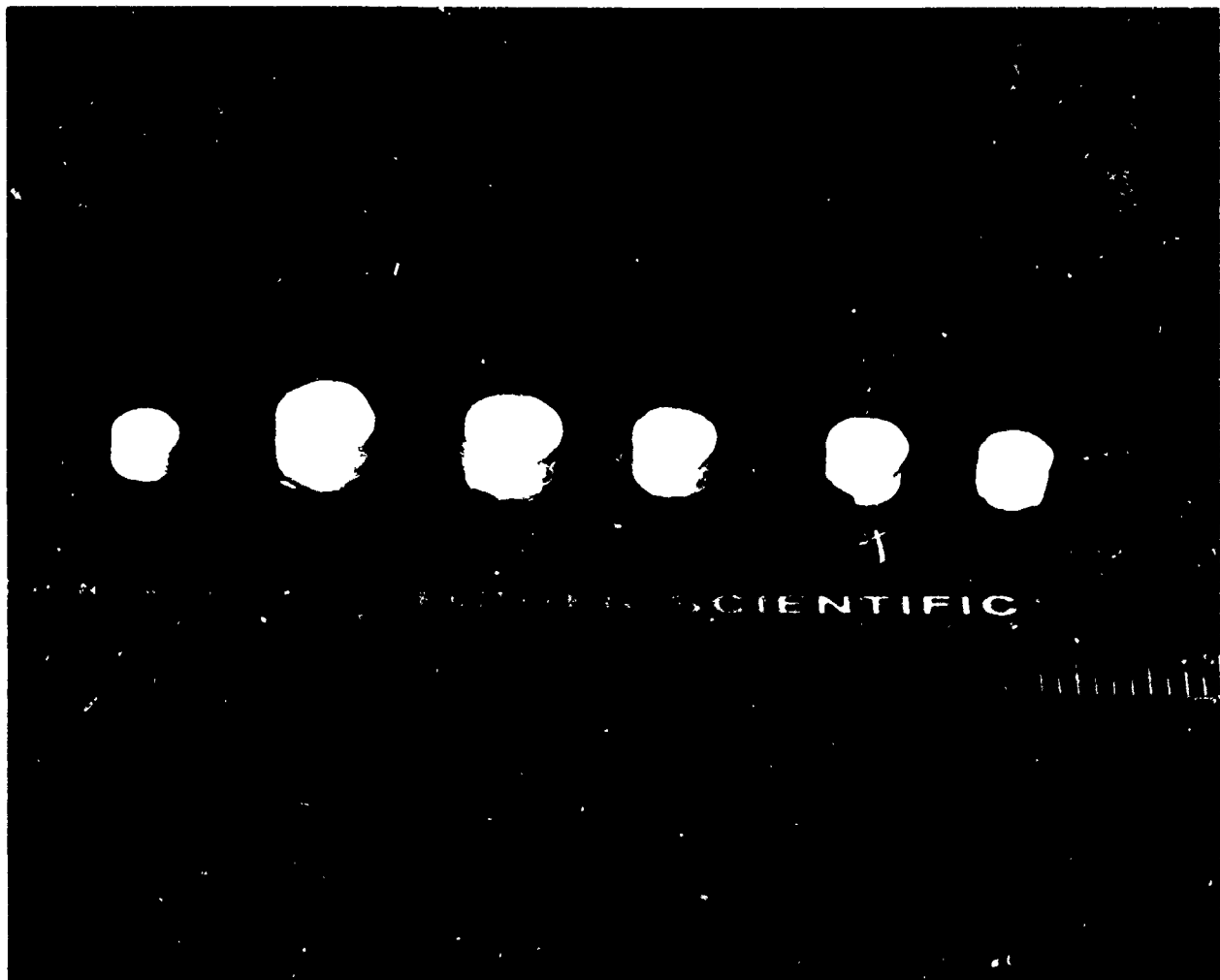


Fig. 8.  $\text{Li}_2\text{O}_2$  Tablets After Decomposition

From left to right:

<u>Tablet No.</u>	<u>Decomposition Temp. C</u>	<u>Sample No.</u>
1	original $\text{Li}_2\text{O}_2$ tablet	
2-3	250-275	349-42-1B
4	300	349-42-3
5	318	358-2-1
6	325	358-7-1

TABLE VI  
GRAVIMETRIC TEST DATA

1 Gram loosely packed  $\text{Li}_2\text{O}$  tablets exposed to Oxygen Gas, 1% (Vol)  $\text{CO}_2$ , 50% R.H.

Preparation:  $\text{Li}_2\text{O}_2$  tablets decomposed to  $\text{Li}_2\text{O}$  tablets

<u>Sample No.</u>	<u><math>\text{Li}_2\text{O}</math> Tablet Size</u>		<u>Tablet Density g/cc</u>
	<u>Diam. cm</u>	<u>Height cm</u>	
349-42-1B	0.95	0.50	0.172
349-42-3	0.78	0.44	0.260
358-2-1	0.75	0.42	0.285
358-7-1	0.63	0.37	0.372

<u>Sample No.</u>	<u>Decomp. Temp. C</u>	<u>Bulk Density g/cc</u>	<u>Reaction Times</u>		<u>Constant Wt. hr</u>	<u>Exposure Time hr</u>	<u>Product <math>\text{Li}_2\text{CO}_3</math> %</u>
			<u>(a) hr</u>	<u>(b) hr</u>			
349-42-1B	250-275	0.085	3.2	4.8	8	18	97.9
349-42-3	300	0.147	4.0	12.0	16	20	84.6
358-2-1	318	0.169	4.0	14.0	18	24	97.0
358-7-1	325	0.238	5.8	17.2	23	23	93.1

Notes: (a) For reaction  $2\text{Li}_2\text{O} + \text{CO}_2 + \text{H}_2\text{O} \rightarrow \text{Li}_2\text{CO}_3 + 2\text{LiOH}$   
 (b) For reaction  $2\text{LiOH} + \text{CO}_2 \rightarrow \text{Li}_2\text{CO}_3 + \text{H}_2\text{O}$

Results are given in table VII and figure 10 (sample 358-21-1).

(5) Granules From  $\text{Li}_2\text{O}_2$  Pellets

$\text{Li}_2\text{O}_2$  powder was pressed into pellets 6.2 cm in diameter and in thickness ranging from 3 to 4 cm to yield pellet densities of 0.77 and 0.97 g/cc. Pellets of a given density were then stacked three deep and decomposed at atmospheric pressure. During decomposition the pellets first swelled, then cracked, and finally sintered. The resulting  $\text{Li}_2\text{O}$  pellets were crushed and sieved into 4- by 10-mesh granules. Table VII (samples 358-24-1, 358-28-1, and 358-31-1) gives granule characteristics and test results. Gravimetric curves are given in figure 11. Several points are noteworthy in the data of table VII. This granular product is considerably harder than the granular material prepared by pressing  $\text{Li}_2\text{O}$  powder and crushing to size (as described in (4) above). It is also harder than granules prepared by decomposing  $\text{Li}_2\text{O}_2$  powder and crushing the resulting sintered cake (table IV, reactive low-density range). Compaction plus sintering is superior to either step alone in terms of mechanical strength. The two-step process yields hardness about equal to that of standard  $\text{LiOH}$  granules shown in table VII for comparison. The anhydrous  $\text{LiOH}$  was also subjected to  $\text{CO}_2$  absorption testing and conforms to bulk density-reactivity considerations as will be subsequently shown.

(6) Granules from Granular  $\text{LiOH}$

A sample of high density  $\text{Li}_2\text{O}$  granules, prepared by dehydrating 4- by 14-mesh  $\text{LiOH}$ , was obtained from Foote Mineral Company inventory. This material was evaluated to

TABLE VII

## GRAVIMETRIC TEST DATA, PROCESSES 2a-(4) AND 2a-(5)

1 Gram 4- by 10-mesh granular  $\text{Li}_2\text{O}$  exposed to Oxygen Gas, 1% (Vol)  $\text{CO}_2$ , 50% R.H.Preparation:  $\text{Li}_2\text{O}_2$  powder decomposed, pulverized, pressed into  $\text{Li}_2\text{O}$  pellets, pellets crushed and sieved $\text{Li}_2\text{O}_2$  powder pelletized, decomposed, sintered  $\text{Li}_2\text{O}$  pellets crushed and sieved

Sample No.	Densities			Hardness No.	Surf. Area $\text{m}^2/\text{g}$	Reaction Times		Constant Wt. hr.	Exposure Time hr.	Product % $\text{Li}_2\text{CO}_3$
	Decomp. Temp. C	Pellet g/cc	Bulk g/cc			(c) hr	(d) hr			
Pressed $\text{Li}_2\text{O}$ : 358-21-1	265	0.50	0.210	66.68	28.0	4.4	15.6	20	22	96.5
Pressed $\text{Li}_2\text{O}_2$ : 358-24-1 358-28-1 358-31-1	315 315 325	0.77 0.97 0.77	0.120 0.180 0.190	90.56 94.50 96.46	15.8 14.8 12.9	3.0 3.8 4.2	17.0 16.2 11.8	20 20 16	24 22 44	98.0 97.3 96.6
Granular $\text{LiOH}$ : 402-11-3 {a} 409-2 {b}	---	---	0.460 0.412	95 95.8	3.4 ---	---	35 26	35 26	45 26	96.5 93.7

Notes: (a) Granular anhydrous  $\text{LiOH}$ , 4 x 14 mesh, amount equivalent to 1 g  $\text{Li}_2\text{O}$   
 (b) Granular anhydrous  $\text{LiOH}$ , 10 x 30 mesh, amount equivalent to 1 g  $\text{Li}_2\text{O}$   
 (c) For reaction  $2\text{Li}_2\text{O} + \text{CO}_2 + \text{H}_2\text{O} \rightarrow \text{Li}_2\text{CO}_3 + 2\text{LiOH}$   
 (d) For reaction  $2\text{LiOH} + \text{CO}_2 / \text{Li}_2\text{CO}_3 + \text{H}_2\text{O}$

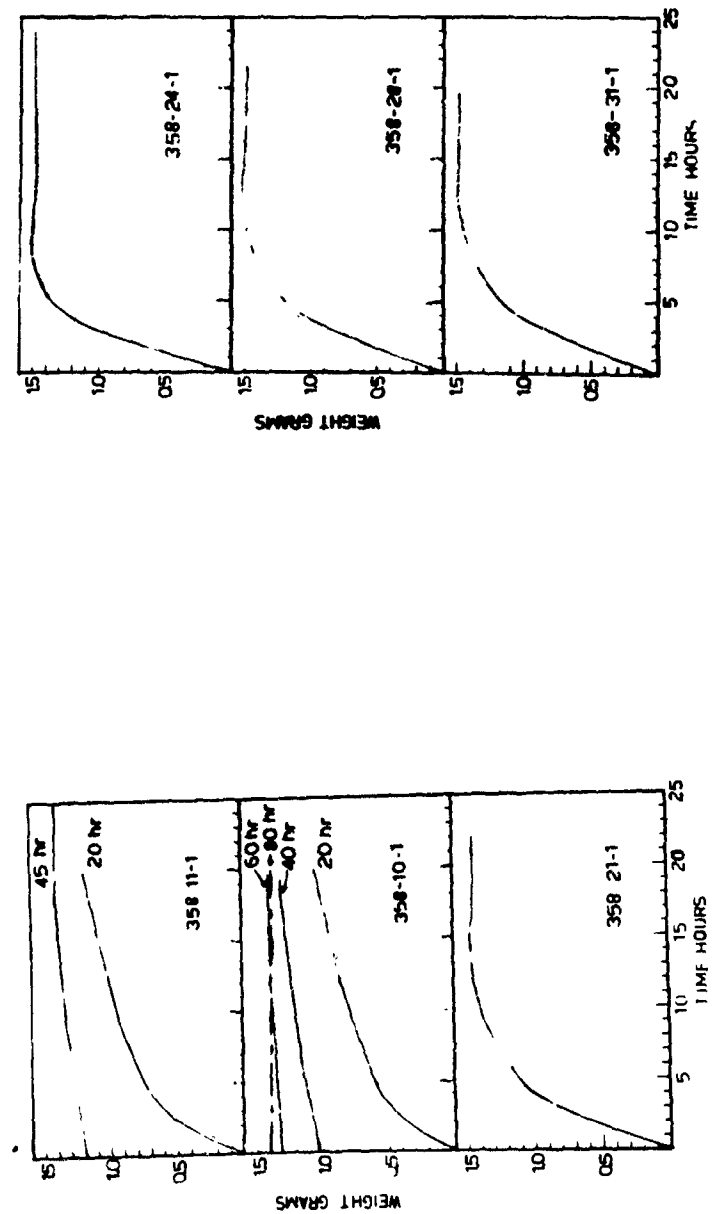


Fig. 10. Gravimetric Curves  
Samples 358-11-1, 358-10-1, 358-21-1

Fig. 11. Gravimetric Curves  
Samples 358-24-1, 358-28-1, 358-31-1

provide  $\text{Li}_2\text{O}$  density versus performance data in the high-density range. The gravimetric curve of figure 3 (sample 349-9-5) illustrates the low reactivity of this high density, low-surface-area material.

#### (7) Comparative $\text{LiOH}$ granules

Two samples of granular anhydrous  $\text{LiOH}$ , one 4- by 14-mesh and one 16- by 30-mesh, were tested to provide comparisons with  $\text{Li}_2\text{O}$ . Gravimetric curves are shown in figure 12 and in the data of table VII.

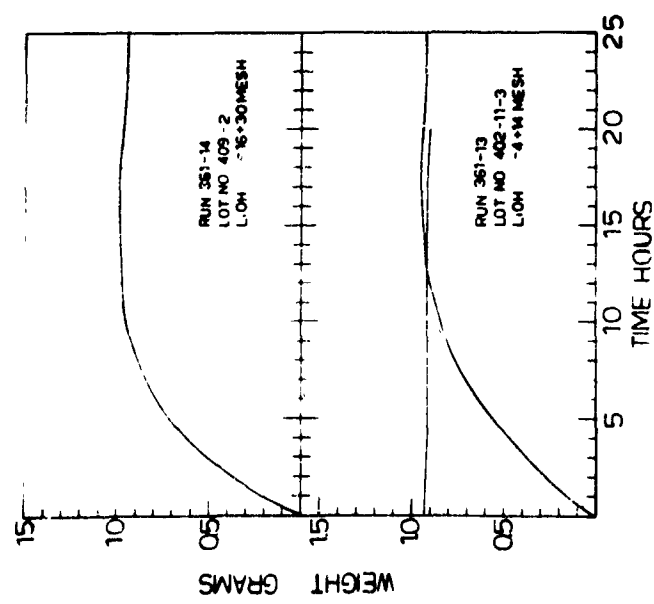
#### b. Self-supported Shapes

##### (1) From Pressed $\text{Li}_2\text{O}$ Powder

$\text{Li}_2\text{O}$  powder was prepared by decomposing  $\text{Li}_2\text{O}_2$  powder and pulverizing the sintered cake. The oxide powder was then double-end pressed into 1.27 cm diameter pellets of 1 g each. Compaction pressures of less than  $72 \text{ kg/cm}^2$  (200 psi) yielded pellets with virtually no strength. Higher pressures improved strength somewhat, but the resulting pellets tended to crack (as shown in figure 13) and remained weaker than desired. Table VIII gives characteristics of the pellets (samples 358-10-1 and 358-11-1) and shows the long reaction times encountered in absorption tests. The corresponding gravimetric curves of figure 10 reconfirm the effect of density on absorption rate. While the direct compaction of  $\text{Li}_2\text{O}$  powder offers process simplicity, the conflicting requirements of high density for strength and low density for reactivity probably cannot be compromised by mechanical pressing alone.



Fig. 13. Porous Solid Li<sub>2</sub>O Shapes  
 Left: Compressed Li<sub>2</sub>O powder  
 Right: Decomposed, sintered Li<sub>2</sub>O<sub>2</sub> powder



GRAVIMETRIC TEST DATA, POROUS SOLID Li<sub>2</sub>O  
 1 Gram Cylindrical Li<sub>2</sub>O Shape exposed to Oxygen Gas, 1% (Vol) CO<sub>2</sub>, 50% R.H.  
 Preparation: Pressed Li<sub>2</sub>O-Li<sub>2</sub>O<sub>2</sub> Powder decomposed, pulverized, mechanically pressed  
 Sintered Li<sub>2</sub>O-Li<sub>2</sub>O<sub>2</sub> Powder decomposed, sintered cake carved into cylinders

Sample No.	Press Load		Shape Size		Constant Wt.	Exposure Time hr	Product Li <sub>2</sub> CO <sub>3</sub> %
	Diam. cm	Height cm	Diam. cm	Height cm			
<b>Pressed:</b>							
358-11-1	72	1.27	1.27	1.72			
358-10-1	144	1.27		1.60			
<b>Sintered:</b>							
349-11-1	--	1.53	1.53	3.43			
349-13-1	--	1.20		2.82			
349-18-1	--	1.50		1.00			
<b>Decomp. Temp.</b>							
Sample No.	Shape Density	Time (a) hr	Time (b) hr				
	gm/cc						
Pressed:	0.475	15	25				
358-11-1	285	20	70				
358-10-1	285	0.487					
<b>Sintered:</b>							
349-11-1	285	0.165	4	12	16	18	97.0
349-13-1	325	0.220	4	14	18	18	97.0
349-18-1	350	0.548	67	--	No	105	85.2
Notes: (a)	For reaction 2Li <sub>2</sub> O + CO <sub>2</sub> + H <sub>2</sub> O $\rightarrow$ Li <sub>2</sub> CO <sub>3</sub> + 2LiOH						
(b)	For reaction 2LiOH + CO <sub>2</sub> $\rightarrow$ Li <sub>2</sub> CO <sub>3</sub> + H <sub>2</sub> O						

### (2) Sintered Shapes From $\text{Li}_2\text{O}_2$ Powder

$\text{Li}_2\text{O}$  shapes were prepared by carving cylinders from the lightly sintered cakes of oxide resulting from the decomposition of loosely packed  $\text{Li}_2\text{O}_2$  powder. The cylinders (see figure 13) were fragile but appeared stronger than the mechanically compacted pellets reported above. Table VIII (samples 349-11-1, 349-13-1, and 349-18-1) gives characteristics of the sintered shapes. The first two samples demonstrated that porous, low-density shapes would allow active diffusion of  $\text{CO}_2$  through depths of at least 7 mm. The low reactivity of high-density (0.548 g/cc) sample 349-18-1 conforms to earlier findings. Figure 14 shows the corresponding gravimetric curves.

### (3) Sintered Shapes From Granular $\text{Li}_2\text{O}_2$

$\text{Li}_2\text{O}_2$  powder was pressed into large pellets which were then crushed and sieved to yield granules. The granules were decomposed in molds at normal packing density and atmospheric pressure. Swelling was observed at low decomposition temperatures (about 285 C), and the material filled the mold shape as decomposition proceeded. The swelling was more pronounced than in process (2) above, and the shapes were harder and more substantial. The process, considered the best of the alternates studied, is further reported in section III.

#### c. Gas Velocity Effect

In the foregoing screening tests, atmospheric conditions were held constant, and all samples were exposed to a nominally passive (81 cm/min velocity) gas. Only the oxide sample form and density were varied. To explore the effect of

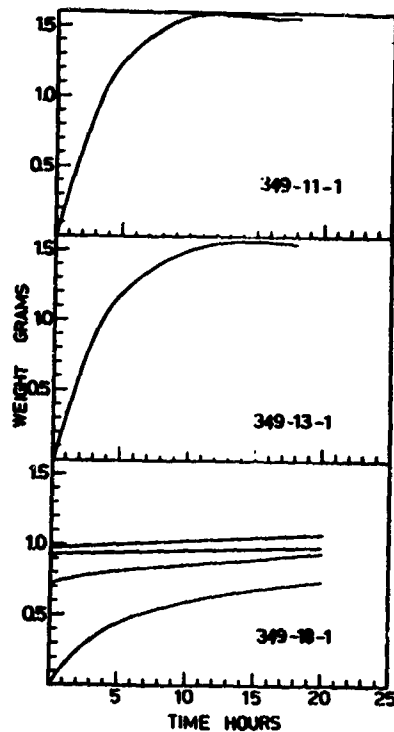


Fig. 14. Gravimetric Curves  
Samples 349-11-1, 349-13-1, 349-18-1

gas velocity, granules and tablets were tested in the gravimetric apparatus at double the standard velocity. Table IX, which compares corresponding samples at standard and higher velocity, indicates  $\text{CO}_2$  absorption rate increased significantly. The higher velocity apparently induced some circulation within the sample bed and increased  $\text{CO}_2$  partial pressure at its face.

TABLE IX  
GRAVIMETRIC TESTS, GAS VELOCITY EFFECT

1 Gram 4- by 10-Mesh Granular  $\text{Li}_2\text{O}$  exposed to Oxygen Gas, 1% (Vol)  $\text{CO}_2$ , 50% R.H.

Preparation: 349-42-1b:  $\text{Li}_2\text{O}_2$  Tablets decomposed to  $\text{Li}_2\text{O}$  tablets  
 358-24-1:  $\text{Li}_2\text{O}_2$  powder pelletized, decomposed, sintered  $\text{Li}_2\text{O}$   
 crushed and sieved  
 358-31-1: As above

Sample No.	Bulk Density g/cc(1)	Gas Velocity cm/min	Reaction Time (2) hr	Exposure Time hr	Product $\text{Li}_2\text{CO}_3$ %
Tabletted $\text{Li}_2\text{O}_2$					
349-42-1B	0.085	81	3.2	18	97.9
349-42-1B	0.107	162	2.5	7	96.0
Pressed $\text{Li}_2\text{O}_2$					
358-24-1	0.120	81	3.0	24	98.0
358-24-1	0.127	162	2.3	7	91.4
Pressed $\text{Li}_2\text{O}_2$					
358-31-1	0.199	81	4.2	44	96.6
358-31-1	0.199	162	3.3	7	85.6

Notes: (1) Bulk densities are approximate, being based on 1 g samples

(2) For reaction  $2\text{Li}_2\text{O} + \text{CO}_2 + \text{H}_2\text{O} \rightarrow \text{Li}_2\text{CO}_3 + 2\text{LiOH}$

#### d. Reaction Product Composition

All reacted samples from the gravimetric runs were analyzed by the procedures outlined in section I. Reported total alkalinity was mathematically translated into the compound pairs which are theoretically in equilibrium with each other (i.e.--  $\text{Li}_2\text{O}$  and  $\text{LiOH}$ ;  $\text{LiOH}$  and  $\text{LiOH}\cdot\text{H}_2\text{O}$ ;  $\text{LiOH}\cdot\text{H}_2\text{O}$  and  $\text{H}_2\text{O}$ ). Kinetically a  $\text{Li}_2\text{O}-\text{LiOH}-\text{LiOH}\cdot\text{H}_2\text{O}$  mixture is possible and was detected by x-ray diffraction. Reaction product compositions, based on the equilibrium pairs, are given in table X.

#### e. Analysis of Results

In figure 15, the density of the various  $\text{Li}_2\text{O}$  samples is plotted against the corresponding time required for each to attain constant weight during passive gravimetric testing. Two curves are shown, one represents supported bed samples (granules or loose tablets) and one represents self-supported samples. Also shown are calculated limiting densities for 4- by 10-mesh granules and for self-supported shapes, based on formation of a nonporous protective coating of  $\text{LiOH}\cdot\text{H}_2\text{O}$  on the  $\text{Li}_2\text{O}$ . In both cases, the experimental data substantiate the density limitations (0.32 g/cc bulk density for 4- by 10-mesh granules and 0.54 g/cc for self-supported shapes) estimated from the molar volume relations of section I. The curves also provide a more rational basis for performance prediction and absorbent design than heretofore available.

The curves intersect, indicating equivalent  $\text{CO}_2$  absorption rate; at about 0.16 g/cc density. For the 4- by 10-mesh granular bed, this value represents bulk density; whereas the

TABLE X  
GRAVIMETRIC TESTS, REACTION PRODUCT ANALYSES

Table No.	Sample No.	% Li <sub>2</sub> O	% Li <sub>2</sub> CO <sub>3</sub>	% LiOH	% LiOH·H <sub>2</sub> O	% H <sub>2</sub> O
IV	349-11-2	0	99.9	0	0	0
	349-13-2	0	97.7	0	0	2.2
	349-16-2	0	97.6	0	0	2.3
	349-18-2	0	85.1	14.9	0	0
	349-21-2	52.0	22.9	25.2	0	0
	349-23-2	63.1	26.6	10.3	0	0
	349-9-5	0	90.0	2.6	7.4	0
VIII	349-11-1	0	97.0	0	2.9	0
	349-13-1	0	97.0	0	2.1	0.8
	349-18-1	2.7	85.2	12.1	0	0
	358-11-1	0	90.05	0	8.5	1.5
	358-10-1	0	97.96	0	0.5	1.5
V	349-35-3	0	96.50	0	1.0	2.5
	349-42-1C	0	97.98	0	0	2.0
	349-42-4	0	97.20	0	1.0	1.8
	358-2-3	0	96.66	0	1.3	2.0
	358-7-3	0	95.07	0	3.7	1.2
VI	349-42-1B	0	97.90	0	0.2	1.9
	349-42-3	0	84.60	1.8	13.6	0
	358-2-1	0	97.0	0	0.4	2.6
	358-7-1	0	93.1	0	6.1	0.8
VII	358-21-1	0	96.49	0	1.6	1.9
	358-24-1	0	98.04	0	0.3	1.7
	358-28-1	0	97.37	0	0.8	1.8
	358-31-1	0	96.6	0	2.0	1.4
	402-11-3	0	96.5	0	2.4	1.1
	409-2	0	93.7	0	4.5	1.8
IX	349-42-1B(a)	0	96.0	0	2.1	1.9
	358-24-1(a)	0	91.4	0	6.6	2.0
	358-31-1(a)	0	85.6	4.5	9.9	0

(a) at 162 cm/min gas velocity

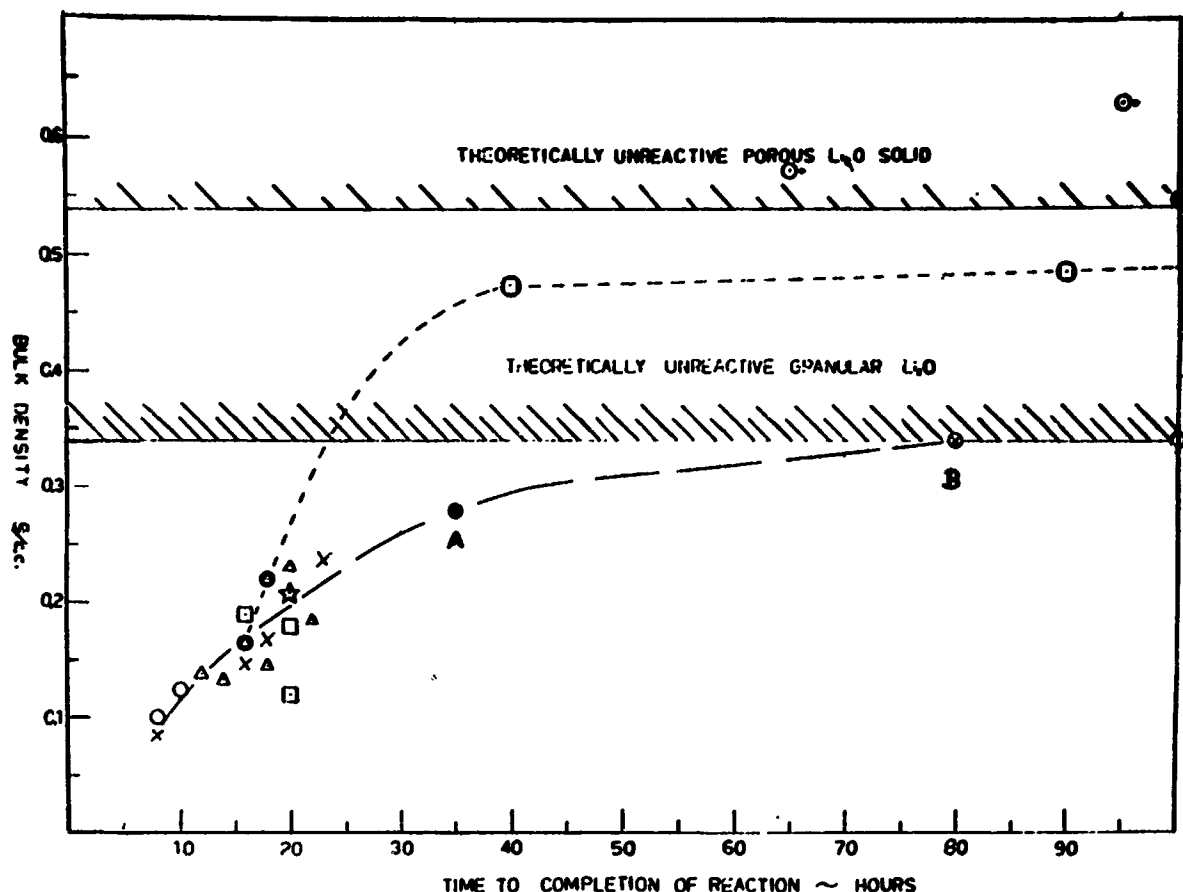


Fig. 15. Bulk Density of Li<sub>2</sub>O versus Time for Complete Carbonation

Symbol      Li<sub>2</sub>O Preparation Process No.

○	2a - (1)	granular
△	2a - (2)	granular
×	2a - (3)	granular
★	2a - (4)	granular
□	2a - (5)	granular
●	2a - (6)	granular
○	2b - (1)	self-supported
○	2b - (2)	self-supported
●	4- by 14-mesh, granular LiOH	
→	reaction incomplete	

Notes: (1) Processes are described in tables II and III  
 (2) Plotted LiOH bulk density adjusted to equivalent Li<sub>2</sub>O basis  
 (3) Atmosphere 1% CO<sub>2</sub> in oxygen, 50% R.H., 81 cm/min gas velocity.

density of a single granule itself would be on the order of 0.26 g/cc (i.e., bulk voids between granules occupy about 38.5% of the bed volume). Several other points on the supported bed curve illustrate the general utility of the density-reactivity relation. Point A designates the reaction time for 4- by 14-mesh granular LiOH (sample 402-11-3) with the hydroxide density expressed on a Li<sub>2</sub>O basis (i.e., LiOH bulk density  $\times$  Li<sub>2</sub>O/2LiOH). This represents a theoretical LiOH dehydration to Li<sub>2</sub>O. The point conforms with other experimental points for Li<sub>2</sub>O. Point B designates results obtained with Li<sub>2</sub>O granules prepared by actually dehydrating 4- by 14-mesh LiOH. The sintering and volume shrinkage that occur in this dehydration increases bulk density and causes long reaction time.

### 3. DYNAMIC TESTS

#### a. Apparatus and Procedure

For screening tests under dynamic conditions, gas was passed directly through beds of Li<sub>2</sub>O, using the apparatus shown in figure 16. The test was based on measuring per cent of CO<sub>2</sub> input absorbed by the sample in a single gas pass over a period of about one-half hour. Feed gas composition and flow rate and sample charge weights were held constant. The only pertinent variables were sample bulk density and bed depth. Gas flow rate was 28.9 liters/min, the gas being oxygen containing 1% (vol) CO<sub>2</sub> and water vapor equivalent to 50% relative humidity at 22 C. Relative humidity was controlled by bubbling the gas through a series of sulfuric acid solutions. A direct-reading, calibrated

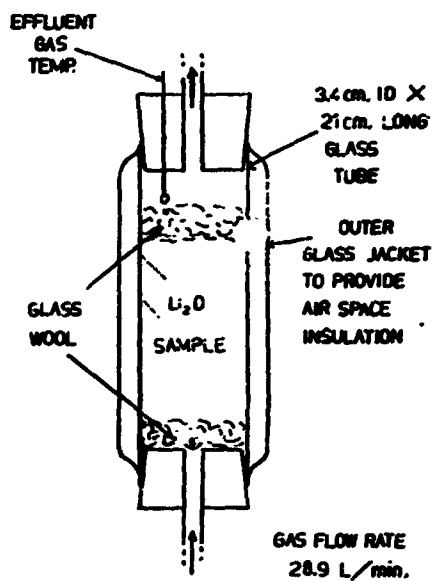


Fig. 16. Dynamic Screening Test Apparatus

hygrometer was used to check relative humidity before, during, and after each test run. Checks indicated the moisture input consistently ranged between 48 and 52% R.H.  $\text{CO}_2$  flow was measured by a dry test gas meter with volume being adjusted to fix  $\text{CO}_2$  input rate at 17 grams per half-hour. Sample quantities were fixed at 12.6 g  $\text{Li}_2\text{O}$ , which were larger than actually required (it required only 11.54 g pure  $\text{Li}_2\text{O}$  to absorb 17.02 g  $\text{CO}_2$ ), to allow for impurity and moisture content.

b. Test Data

Granular samples were drawn from the same lots of material used in gravimetric testing and bear identical sample numbers for comparison. Information gathered in dynamic testing is listed below, and corresponding data are given in table XI. Sample characteristics - analysis, bulk density, surface area, hardness, and decomposition temperature in preparation

Bed characteristics - depth and average pressure loss

Absorption performance - product analysis, fraction of input CO<sub>2</sub> absorbed, effluent gas temperature

c. Analysis of Results

In figure 17, sample bulk density is plotted against per cent of CO<sub>2</sub> input absorbed. Samples at a number of points, designated by identical symbols, were prepared by the same general process steps but with conditions varied to change density. As shown by the curve, bulk density was the prime factor in determining diffusion rate and CO<sub>2</sub> absorption regardless of preparation method. Point A (sample 402-11-3) designating granular LiOH with its density expressed on a Li<sub>2</sub>O basis conforms with the other experimental points for Li<sub>2</sub>O. This was also true in gravimetric testing. Point B (sample 349-9-5) designating Li<sub>2</sub>O actually prepared by dehydrating LiOH is well off the experimental curve.

The granule volume shrinkage accompanying dehydration is illustrated by the bulk density change from point A to point B. However, the low CO<sub>2</sub> absorption at point B cannot be

TABLE XI  
DYNAMIC TEST DATA AT 50% R.H. INPUT

Exposure of 4- by 10-mesh Li<sub>2</sub>O to equivalent amount of 1% CO<sub>2</sub> in Oxygen at 50% relative humidity with 28.9 liters-per-minute gas flow.

Sample No.	Decomp. Temp. C	Bulk Den-sity g/cc	Sur-face Area m <sup>2</sup> /g	Hard-ness No.	Analysis Before Exposure			
					Li <sub>2</sub> O %	LiClO <sub>3</sub> %	LiOH %	Li <sub>2</sub> O <sub>2</sub> %
349-11-2	285	0.10	14.70	66.3	88.9	2.7	8.4	0.2
349-13-2	325	0.12	13.35	59.3	89.5	0.6	9.8	0.1
349-16-2	325	0.12	13.80	54.6	92.5	2.2	5.3	0.1
349-18-2	350	0.34	3.85	93.1	94.6	5.1	0.3	0.02
349-21-2	385	0.57	0.28	98.2	94.4	2.4	3.2	0.005
349-23-2	430	0.63	---	92.6	94.8	4.7	0.5	0.004
349-9-5	644	0.34	0.91	89.2	97.1	2.6	0.3	0.00
349-35-3	250	0.13	12.65	---	85.3	1.1	10.8	2.8
349-42-1C	275	0.13	12.85	---	93.9	3.0	2.6	0.5
349-42-4	300	0.16	13.84	---	92.7	1.5	5.8	0.1
358-2-3	318	0.18	13.34	---	89.6	2.0	8.4	0.08
358-7-3	325	0.23	12.75	---	93.1	1.8	5.1	0.06
358-21-1	265	0.21	28.03	66.6	91.0	2.5	6.5	0.13
358-24-1	315	0.13	15.77	90.56	93.1	1.2	5.7	0.09
358-28-1	315	0.15	14.82	94.5	91.4	1.6	7.0	0.07
358-31-1	325	0.20	12.97	96.4	93.5	1.3	5.2	0.05
402-11-3	---	0.47	3.44	95	---	---	99.5	---

TABLE XI (Continued)

Bed Depth (d) cm	Press. Loss (c) Mm Hg	Analysis After Exposure				Input CO <sub>2</sub> Absorbed %	Gas Temp. (e) C
		Li <sub>2</sub> O %	LiOH %	LiOH·H <sub>2</sub> O %	Li <sub>2</sub> CO <sub>3</sub> %		
13.8	11.8	0	8.0	5.1	86.8	86.0	136
10.8	6.2	0	26.8	1.5	71.7	65.8	105
11.4	8.4	0	24.5	0.6	74.9	68.5	140
4.2	2.8	35.2	27.48	0	37.3	21.7	80
2.5	2.25	87.2	5.4	0	7.4	2.35	34
2.2	1.87	91.8	2.6	0	5.5	0.51	31
3.7	2.8	87.2	3.8	0	9.1	3.12	37
10.0	5.6	14.0	24.1	0	60.3	46.6	94
10.8	4.7	5.2	23.0	0	71.8	60.4	114
9.4	3.4	2.5	36.2	0	61.4	51.4	131
7.6	---	9.1	26.1	0	64.8	51.0	124
5.6	1.8	20.2	22.0	0	57.6	41.7	94
6.1	1.87	10.3	30.6	0	59.1	45.5	107
10.3	3.0	4.4	42.6	0	53.0	45.1	96
9.0	2.4	6.1	30.5	0	63.4	52.7	115
6.5	2.2	14.1	32.9	0	53.0	39.7	78
3.9	1.31	0	50.0	13.3	36.7	28.65	42

Notes: (a) Li<sub>2</sub>O preparation processes described in table II.  
 (b) Sample 402-11-3 is 4- by 14-mesh granular LiOH and weighed 18.5 grams.  
 (c) Pressure loss through bed is average value at 28.9 liters/min. gas flow.  
 (d) Bed diameter 3.4 cm in all cases.  
 (e) Gas temperatures listed are maximum temperature of gas leaving bed.

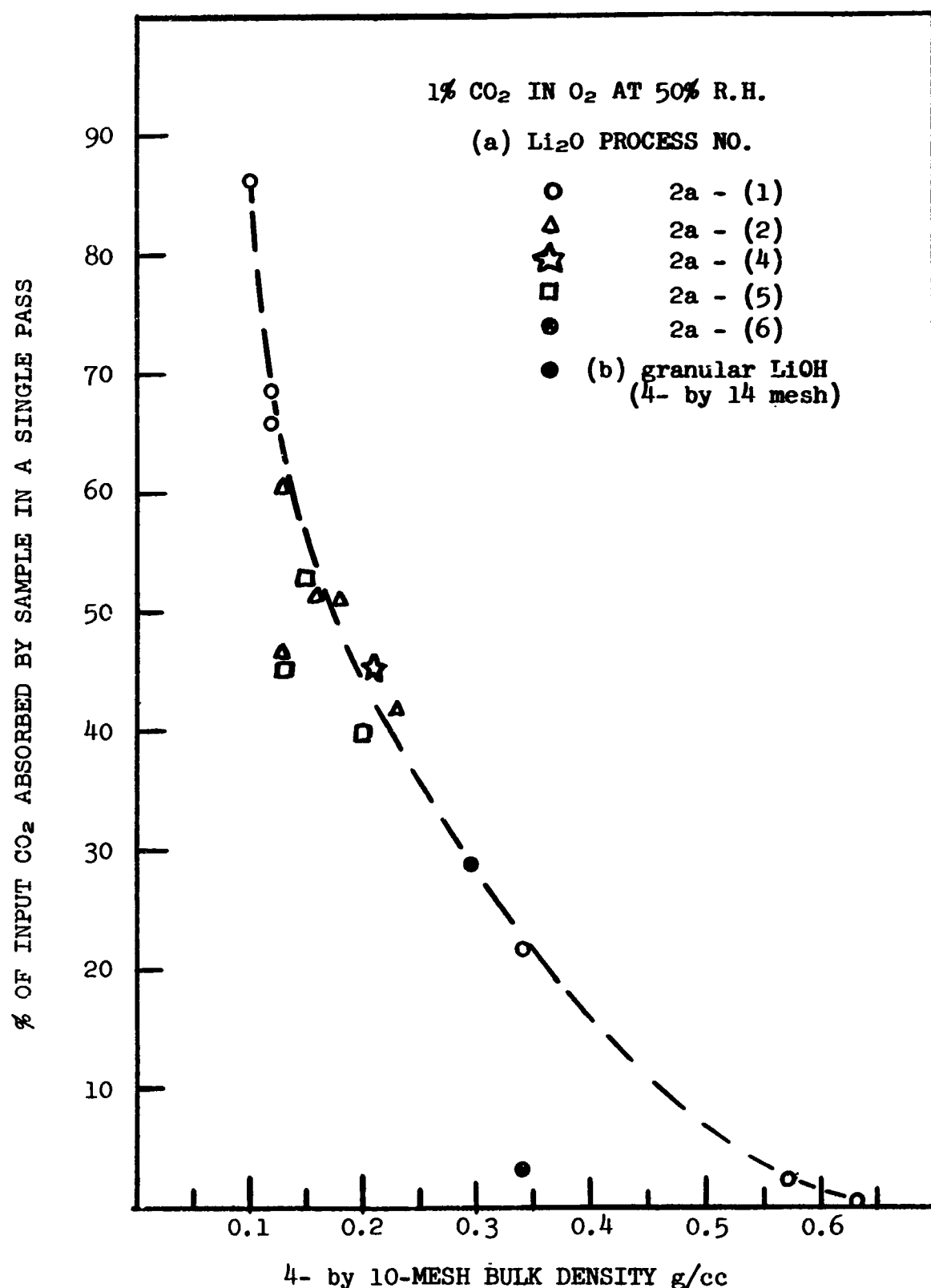


Fig. 17. Bulk Density of Granular Li<sub>2</sub>O versus CO<sub>2</sub> Absorption in a Single Pass

Notes: (a) Processes are described in table II  
 (b) Plotted LiOH bulk density adjusted to equivalent Li<sub>2</sub>O basis  
 (c) Atmosphere 1% CO<sub>2</sub> in oxygen, 50% R.H.

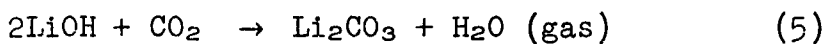
attributed to density increase alone. Very probably, a  $\text{Li}_2\text{O}$  granule prepared under the relatively high temperatures required for dehydration has a sintered surface and nonuniform density which greatly affects  $\text{CO}_2$  diffusion in a short-run test.

A semi-logarithmic plot of the preceding results (figure 18) yields the following relation applicable to granular  $\text{Li}_2\text{O}$  under the stated test conditions--

$$\% \text{ Input } \text{CO}_2 \text{ absorbed} = \frac{\log 0.5968 - \log \text{bulk density}}{0.010671}$$

The zero intercept at 0.59 g/cc bulk density is of interest since the molar volume relations (table I) indicate formation of a nonporous  $\text{LiOH}$  coating on 4- by 10-mesh  $\text{Li}_2\text{O}$  at 0.54 g/cc bulk density. If  $\text{LiOH}$  is formed as a nonporous coating on the  $\text{Li}_2\text{O}$ , any subsequent reaction products (i.e.  $\text{Li}_2\text{CO}_3$  or  $\text{LiOH}\cdot\text{H}_2\text{O}$ ) amplify its protectiveness, since these products are protective on  $\text{LiOH}$ . In contrast, a  $\text{LiOH}\cdot\text{H}_2\text{O}$  coating on  $\text{Li}_2\text{O}$  does not produce this double-barrier effect, since the  $\text{Li}_2\text{CO}_3$  reaction product is porous relative to  $\text{LiOH}\cdot\text{H}_2\text{O}$ .

Figure 19 shows effluent gas relative humidity and temperature profiles for a number of samples. The correspondence between  $\text{CO}_2$  removal ability and initial absorption of moisture is evident. The profile of sample 349-11-2 is noteworthy since it demonstrates that reaction



is proceeding toward the end of this run as evidenced by effluent humidity rising above feed moisture level.

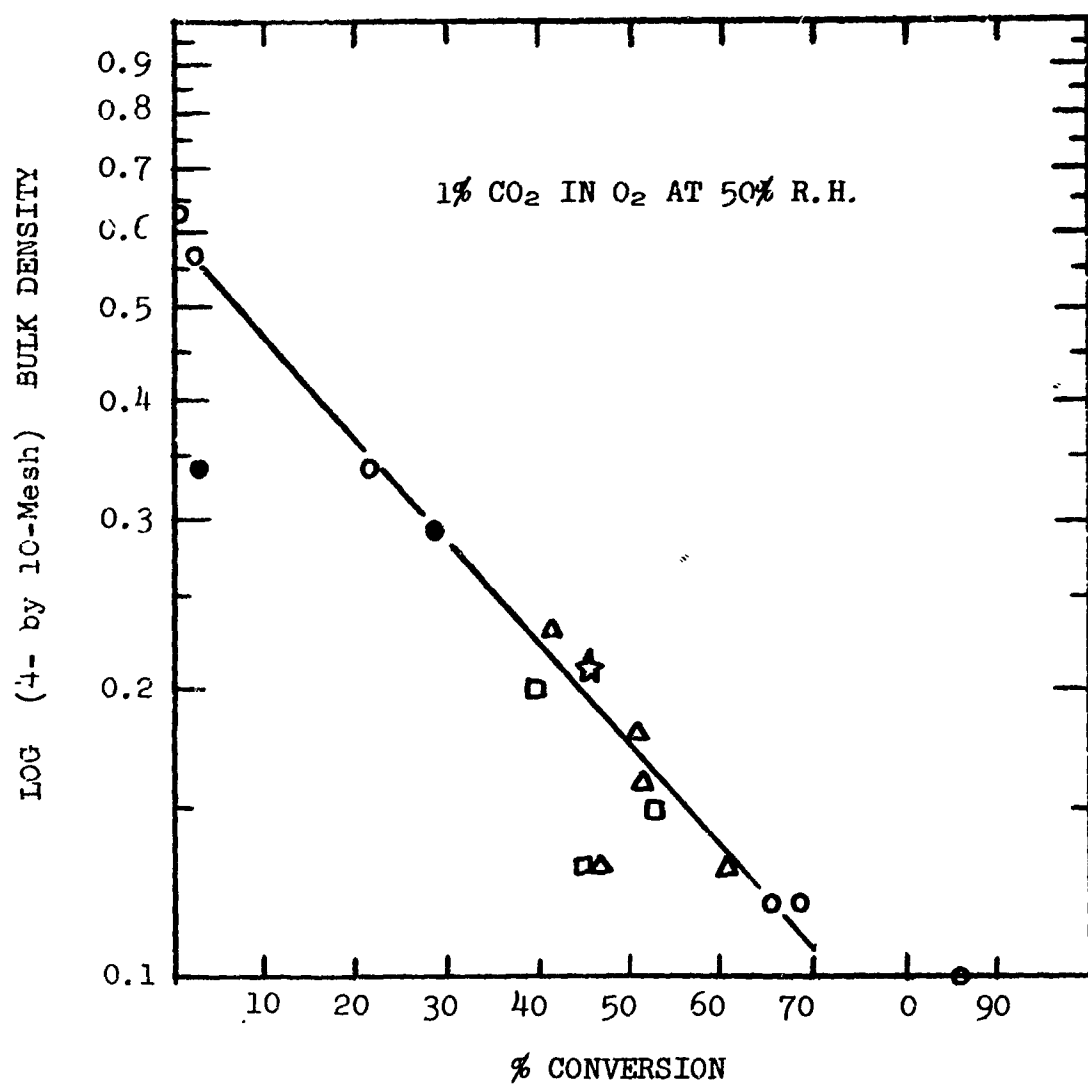


Figure 18

Log 4- by 10-mesh Bulk Density vs. % of CO<sub>2</sub> Input  
(1% CO<sub>2</sub> in Oxygen at 50% R.H.) Absorbed during a single pass.

Key same as in figure 16.

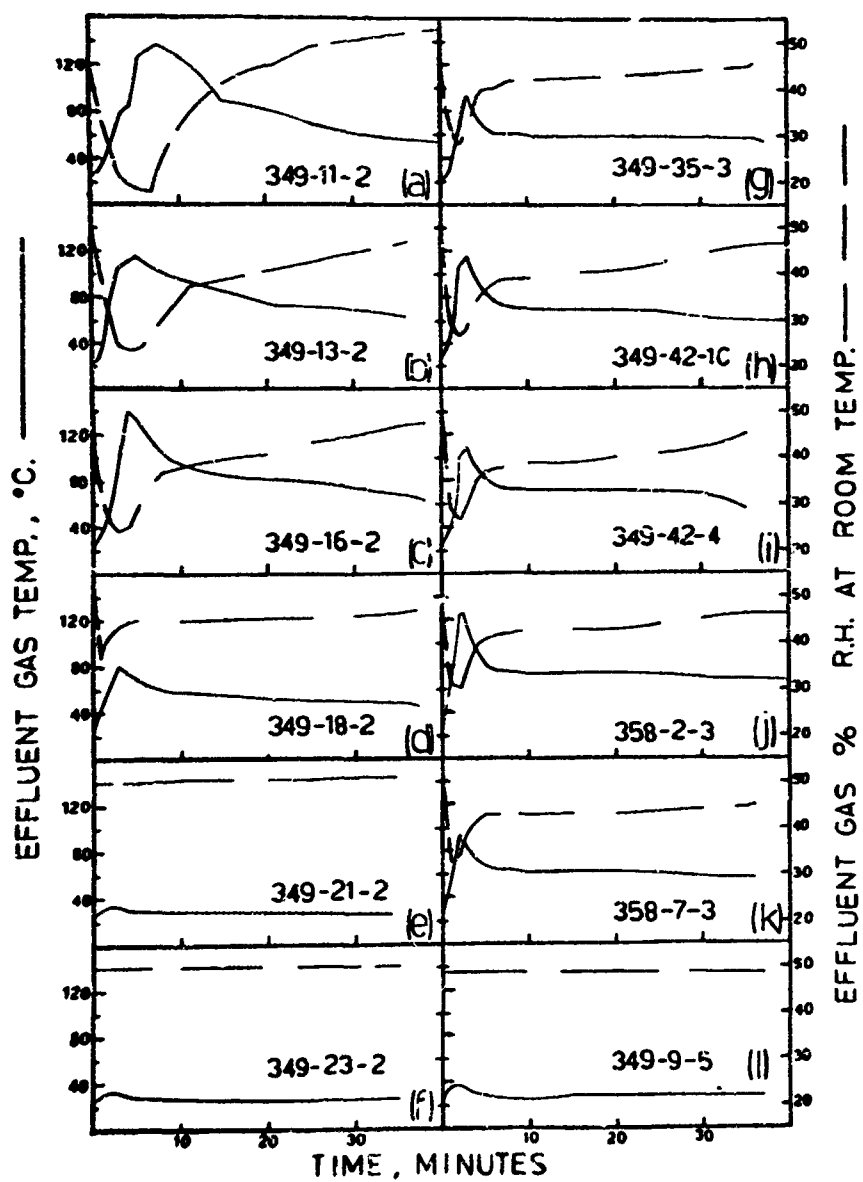
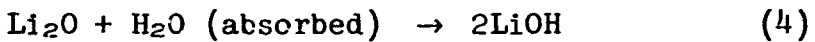
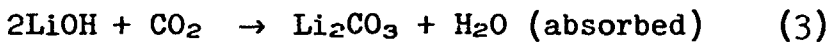
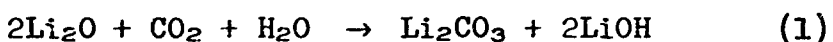


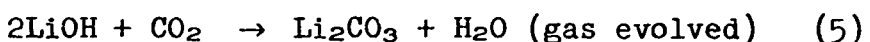
Fig. 19. Dynamic Test

Effluent gas temperature and Relative Humidity (at 25 °C)  
with 1%  $\text{CO}_2$  and 50% Relative Humidity Input.

$\text{CO}_2$  absorption by overall reaction (1) resulting from reactions (2), (3), and (4) requires that the molar ratio  $\text{H}_2\text{O}/\text{CO}_2$  absorbed be unity. If this occurs, the molar ratio of  $2\text{LiOH}/\text{Li}_2\text{CO}_3$  found in the product should be unity for samples still containing unreacted  $\text{Li}_2\text{O}$ :



In testing, a feed gas  $\text{H}_2\text{O}/\text{CO}_2$  molar ratio of about 1.4 was maintained. However, as shown in table XII which lists the  $2\text{LiOH}/\text{Li}_2\text{CO}_3$  molar ratio for all samples containing residual  $\text{Li}_2\text{O}$  on test completion, only some of the samples have a ratio near or exceeding unity in accordance with reaction (1) with the excess moisture provided. This indicates that reaction (5)



as well as reactions (3) and (4) is occurring with  $\text{Li}_2\text{O}$  present. Therefore, the reaction mechanism may vary as it is influenced by sample porosity, bed temperature, and gas flow rate.

The effect of higher moisture input was studied by increasing feed gas  $\text{H}_2\text{O}/\text{CO}_2$  molar ratio to 2.43 with other test conditions remaining the same. The increase, from 50% to 88% R.H., yielded complete  $\text{Li}_2\text{O}$  consumption and increased conversion to  $\text{Li}_2\text{CO}_3$  as shown by comparing tables XI and XIII. The initial effluent gas temperature almost doubled as shown in figure 20. The higher humidity did not affect  $\text{CO}_2$  absorption rate of the  $\text{LiOH}$  sample (tables XI and XIII, sample 402-11-3). In this case,

CO<sub>2</sub> absorption is evidently controlled by diffusion and is unaffected by the additional LiOH·H<sub>2</sub>O resulting from higher humidity.

TABLE XII  
REACTION PRODUCT MOLAR RATIOS

<u>Sample No.</u>	<u>Residual Li<sub>2</sub>O</u> <u>%</u>	<u>Molar Ratio</u> <u>2LiOH/Li<sub>2</sub>CO<sub>3</sub></u>
349-18-2	35.2	1.13
-21-2	87.2	1.12
-23-2	91.8	0.72
-9-5	87.2	0.64
-35-3	14.0	0.61
-42-1C	5.2	0.49
-42-4	2.5	0.91
358-2-3	9.1	0.62
-7-3	20.2	0.59
-21-1	10.3	0.80
-24-1	4.4	1.24
-28-1	6.1	0.74
-31-1	14.1	0.96

TABLE XIII  
DYNAMIC TEST RESULTS

Exposure of 4- by 10-Mesh  $\text{Li}_2\text{O}$  to equivalent amount of 1%  $\text{CO}_2$  in Oxygen at 88% relative humidity with 28.9 liters per minute gas flow rate.

<u>Sample No.</u>	<u>(Note)</u>	<u>Sample Weight Grams</u>	<u>Bulk Density g/cc</u>	<u>Granular Bed</u>		<u>Average Pressure Drop mm Hg</u>
				<u>dia. cm</u>	<u>depth cm</u>	
358-24-1	(a)	12.6	0.13	3.4	11.2	3.0
358-28-1	(a)	12.6	0.15	3.4	9.3	2.6
358-31-1	(a)	12.6	0.19	3.4	6.5	2.2
402-11-3	(b)	18.5	0.47	3.4	4.5	1.12

Note: (a)  $\text{Li}_2\text{O}_2$  powder compressed, decomposed and granulated  
(b)  $\text{LiOH}$ , 4- by 14-mesh

TABLE XIII (Continued)

Analysis of Product After Dynamic Test					% of Input CO <sub>2</sub> Absorbed	Peak temp. of Effluent Gas C
Li <sub>2</sub> O	LiOH	LiOH·H <sub>2</sub> O	Li <sub>2</sub> CO <sub>3</sub>	H <sub>2</sub> O		
0	6.3	11.1	82.6	0	85.6	193
0	12.1	11.0	76.9	0	76.8	192
0	19.6	6.8	73.6	0	69.1	178
0	39.0	28.6	32.4	0	28.93	47

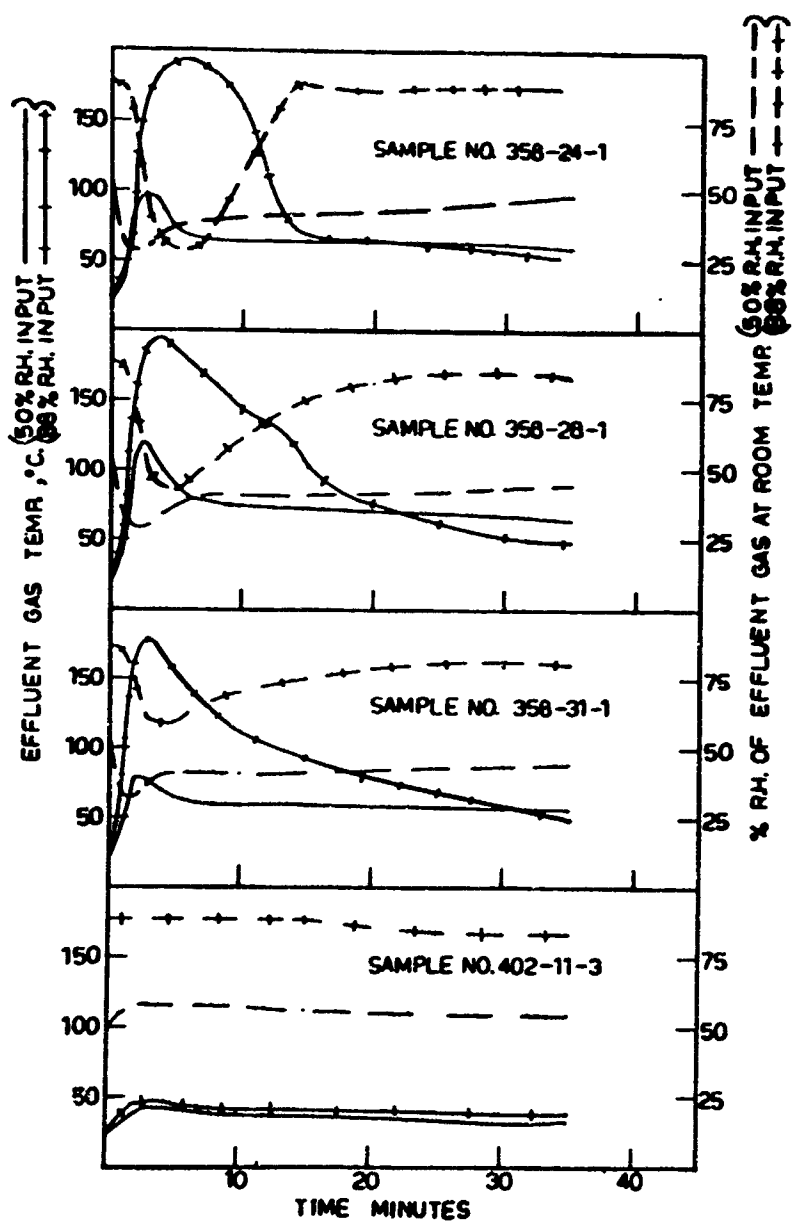


Fig. 20. Dynamic Test.

Effluent Gas Temperature and Relative Humidity at 50 and 88% Relative Humidity Input.

## SECTION III

### CONFIGURATION TESTS WITH LOW MOISTURE AVAILABILITY

#### 1. APPARATUS AND PROCEDURES

The test apparatus consisted of a bell jar environmental chamber, recirculating gas lines, and appropriate auxiliaries, controls, and instruments as illustrated in figure 21. Apparatus details were as follows --

Bell jar volume                    12.7 liters; 2.14 cm ID

Total system volume                17.0 liters

Electric hygrometer: Cat. No. 15-3000, Hygrodynamics Inc.  
Silver Springs, Md.

CO<sub>2</sub> analyzer                    : Model 405-C1, Gow-Mack Instrument  
                                      Co., Madison, N. J.

Air was used as the carrier gas. The thermoconductivity cell was calibrated at 0, 1, and 4% CO<sub>2</sub> before each run with preanalyzed gas mixtures and was rechecked after each run. CO<sub>2</sub> readout was not affected by flow rate but varied slightly with pressure changes. Gas temperature, relative humidity, and CO<sub>2</sub> concentration were logged by a strip chart recorder. CO<sub>2</sub> volume, temperature, and pressure at the gas meter were periodically noted and recorded.

Granular Li<sub>2</sub>O was used in all tests. Except as noted, all samples were prepared by pelletizing Li<sub>2</sub>O<sub>2</sub> powder, decomposing at various temperatures to yield desired density, crushing the sintered Li<sub>2</sub>O pellet, and sieving to 4- by 10-mesh size (i.e., process 2a-(5), section II). Tests were conducted under both passive and dynamic conditions.

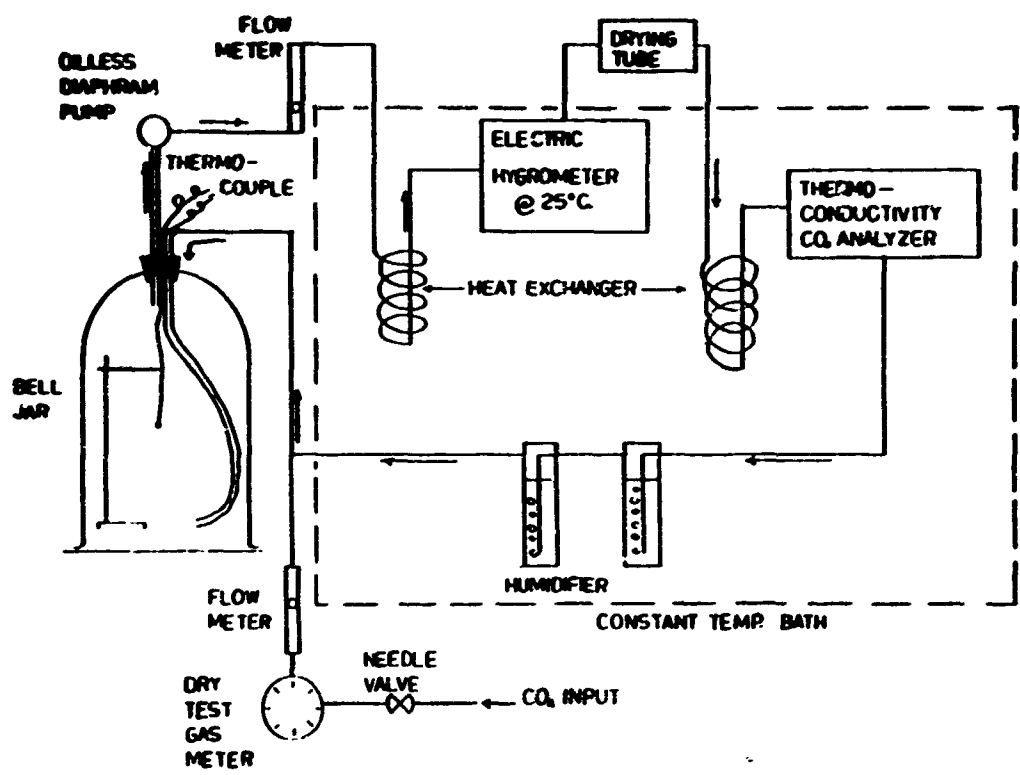


Fig. 21. Apparatus For 1-Atmosphere Tests

## 2. EXPLORATORY RUNS

Four exploratory runs were made to check the apparatus and evaluate the use of polypropylene for supporting granular beds. In each run granular  $\text{Li}_2\text{O}$ , bulk density 0.1 g/cc, was displayed in a single rectangular bed 12.2 cm wide, 16.5 cm high, and 1.5 cm thick containing about 41 grams  $\text{Li}_2\text{O}$ . The granules were enclosed and supported by 12-mesh, polypropylene netting (0.5 mm strand diameter, about 55% open area). Polypropylene spacer wires were run through the bed and fused to the netting to prevent wall sagging. Gas flow to the chamber was 6.6 liter/min, yielding a nominal velocity of 18 cm/min (based on chamber cross-section) for passive runs. Two runs were made under passive conditions and with 50% and 100% input relative humidity respectively. Two runs were made with the gas stream directed at the bed face. As shown in table XIV, chamber humidity could not be maintained and fell below the hygrometer range. Chamber  $\text{CO}_2$  concentration rose rapidly. In one case, directing 100% R.H. gas at the bed face raised temperature sufficiently to sinter the sample and melt the polypropylene (melting point 160 to 177 C).

## 3. PASSIVE TESTS

### Run 368-39

Further data were obtained on the effect of low moisture availability by making a passive run with three rectangular beds (identical to those described above) suspended in the chamber with nominal gas velocity at 18 cm/min. Figure 22 gives  $\text{CO}_2$ , temperature, and humidity (within the 40% to 60% R.H. range

TABLE XIV  
PASSIVE TEST DATA, GRANULE RECTANGULAR BED

Run	Time Min.	Chamber Temp. C	Chamber % R.H. at 25 C	Vol.% CO <sub>2</sub>	Accumulative g CO <sub>2</sub> Input	Remarks
(a)	0	23	50	0	0	4.6 g H <sub>2</sub> O/hr
	1	26	≤ 40	trace		
	2	28	≤ 40	0.15		
	3	31	≤ 40	0.30		
	4	34	≤ 40	0.68		
	5	35	≤ 40	1.40		
	6	37	≤ 40	2.0		
	7	38	≤ 40	2.6		
	8	39	≤ 40	3.1		
	9	39	≤ 40	3.7		
	10	39	≤ 40	4.3	4.5	
(b)	0	23	50	0	0	4.6 g H <sub>2</sub> O/hr
	1	23	≤ 40	trace		
	2	24	≤ 40	trace		
	3	25	≤ 40	0.1		
	4	26	≤ 40	0.3		
	5	26	≤ 40	0.95		
	6	26	≤ 40	2.0		
	7	26	≤ 40	3.2		
	8	26	≤ 40	4.8		
	10	26	≤ 40	off scale	4.5	
(c)	Same results as (a) and (b)					
(d)	100% R.H. input 0.5 cm from the bed caused excessive localized heating sintering the sample and melting the polypropylene netting					

Notes:

Run (a) Single rectangular bed mounted vertically in the center of the chamber; 50% relative humidity input

(b) Single rectangular bed mounted horizontally on the bottom of the chamber with input gas recirculating lines 0.5 cm above the face of the bed; 50% relative humidity input

(c) As with (a) but at 100% relative humidity input

(d) As with (b) but at 100% relative humidity input

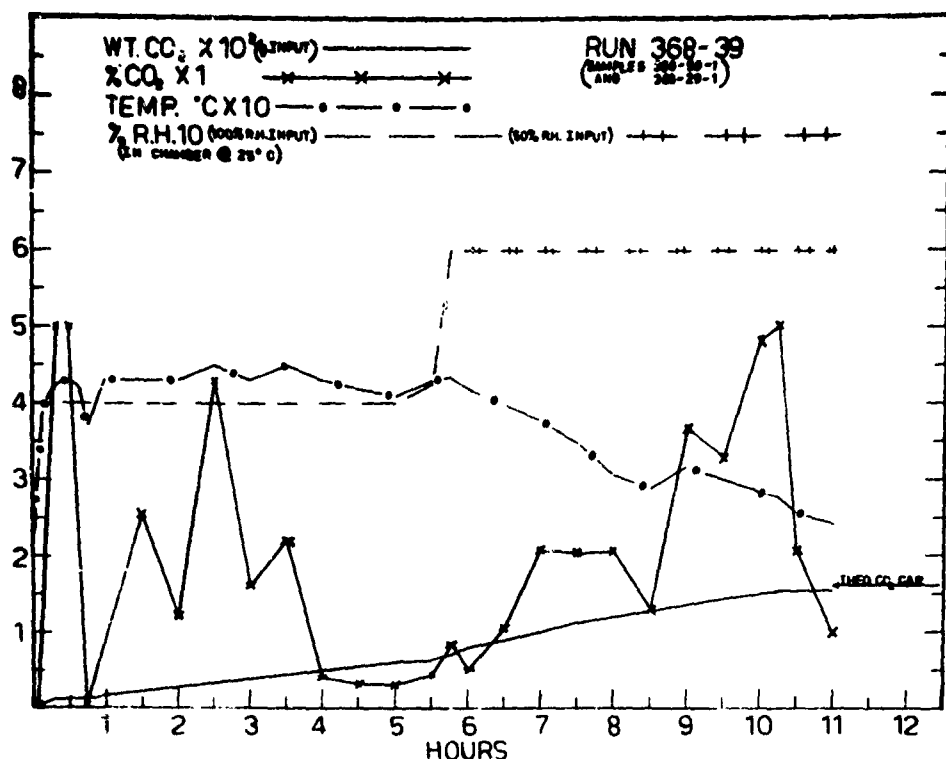


Fig. 22. Passive Test Profiles, Granule Rectangular Bed.

Run 368-39

of the available hygrometer) profiles. Test data are given in table XV. On starting, gas feed to the chamber was held at 100% R.H. introducing 9.22 g H<sub>2</sub>O/hr. Relative humidity in the chamber was beyond instrument range but was less than 40%. When chamber CO<sub>2</sub> concentration rose to 5%, the CO<sub>2</sub> feed was

TABLE XV  
TEST DATA AT ONE ATMOSPHERE

Run No.	Configuration	Lithium Oxide			Chamber Gas		Avg. CO <sub>2</sub> Absorp. Rate (b) g/hr
		Wt. g	Bulk Dens. g/cc	Hardness No.	Run Time hr	Average Velocity cm/min	
368-39	Rect. Beds	109.9	0.10	52.0	11.0	18.0	1.94
368-45	Cyl. Bed	103.3	0.10	52.0	7.5	18.0	2.59
376-11	Cyl. Bed	92.2	0.10	52.0	5.5	38.7	1.88
376-13	Cyl. Bed	306.7	0.34	79.2	12.8	38.7	2.18
376-15	Cyl. Bed	242.3	0.24	66.9	10.5	38.7	2.79
376-16	Belt	134.5	0.11	---	6.0	38.7	2.02
376-17	Belt	263.0	0.18	---	10.5	38.7	2.36
376-19	Dynamic Bed	139.8	0.10	53.0	5.0	---	0.93
376-38	Dynamic Bed	272.0	0.31	66.6	8.8	---	1.61
							33.9

Notes: (a) 10- by 30-mesh granular Li<sub>2</sub>O in Run No. 376-17; all other runs

(b) 4- by 10-mesh granules  
(b) Based on cumulative g CO<sub>2</sub> feed up to run termination at 1% CO<sub>2</sub> in chamber gas

TABLE XV (Continued)

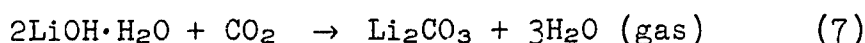
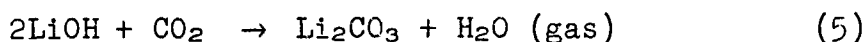
Run No.	Li <sub>2</sub> O Used %(c)	Analysis of Reaction Product						
		Li <sub>2</sub> O	LiOH	Li <sub>2</sub> CO <sub>3</sub>	Li <sub>2</sub> O <sub>2</sub>	Li <sub>2</sub> O	LiOH·H <sub>2</sub> O	Li <sub>2</sub> CO <sub>3</sub>
368-39	95.2	89.5	8.9	1.5	0.1	0	0	0.7
368-45	85.2	92.4	4.5	3.0	0.1	0	0.3	5.9
376-11	96.3	94.5	0.0	5.8	0.1	0	0	93.8
376-13	52.1	90.4	4.6	5.0	0.1	6.3	24.4	0
376-15	80.4	85.0	12.3	2.7	0.01	1.3	7.8	0
376-16	86.9	91.2	6.8	2.0	0.14	0	2.7	5.7
376-17	81.2	90.5	7.5	1.9	0.05	0	9.5	4.3
376-19	98.6	90.7	8.5	0.7	0.08	0	0	86.3
376-38	74.1	92.7	5.4	2.0	0.0	0	8.6	11.3

Note: (c) Based on treating absorbent charge as 100% Li<sub>2</sub>O

cutoff and water feed was continued. Up to  $\text{CO}_2$  cutoff the cumulative input  $\text{H}_2\text{O}/\text{CO}_2$  molar ratio was 0.7 (note: all cumulative  $\text{H}_2\text{O}/\text{CO}_2$  molar ratios are calculated from time zero and represent input to the chamber, not molar ratio actually absorbed by the sample). With continued moisture addition and no  $\text{CO}_2$  feed, chamber  $\text{CO}_2$  concentration declined and the cumulative molar ratio had increased to 1.84 when  $\text{CO}_2$  concentration reached zero.  $\text{CO}_2$  feed was then resumed on a demand, rather than fixed rate, basis.

The feed adjustments are not obvious from the input  $\text{CO}_2$  profile but are magnified in the  $\text{CO}_2$  concentration profile because of the small chamber volume. A fairly steady and low concentration of 0.4%  $\text{CO}_2$  was maintained during the 4th and 5th hours. The cumulative molar ratio had attained 1.9 at the end of this period. The correspondence between  $\text{CO}_2$  removal and the  $\text{H}_2\text{O}/\text{CO}_2$  molar ratio agrees with earlier research (references 2, 3) indicating poor absorption rate when the gas  $\text{H}_2\text{O}/\text{CO}_2$  molar ratio is below unity.

Figure 22 also illustrates the rapid humidity increase occurring after the  $\text{Li}_2\text{O}$  has been converted to  $\text{Li}_2\text{CO}_3$  and  $\text{LiOH}$  and absorption proceeds via reactions (5) and (7). Chamber humidity reached 100% at 6 hours as evidenced by condensation.



Run 368-45

A thin-walled, cylindrical configuration (see figure 23) was tested. The unit, fashioned from polypropylene netting

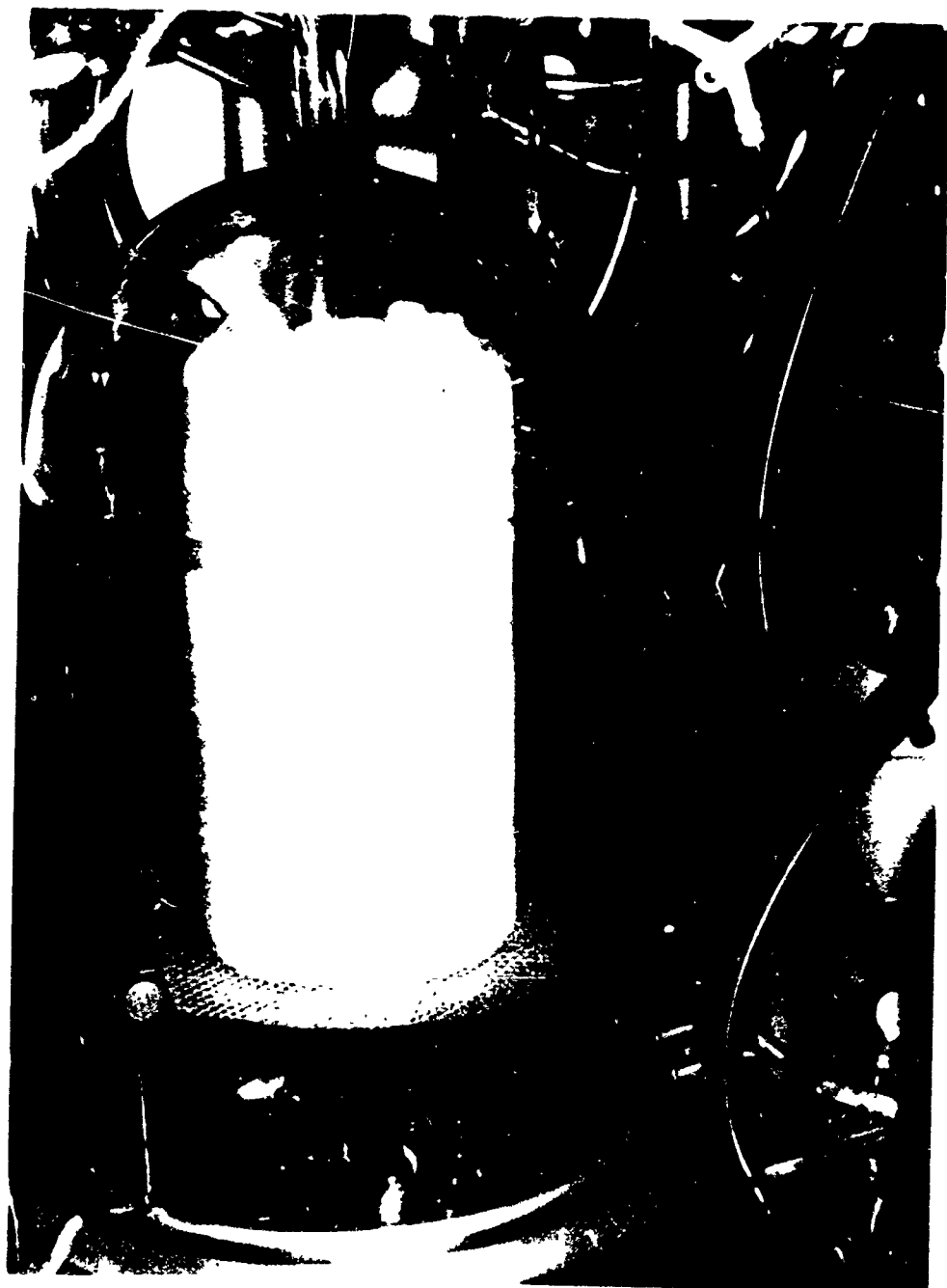
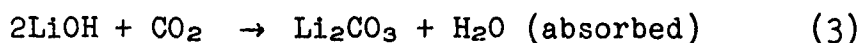


Fig. 23. Passive Cylindrical Bed Configuration

as previously described, had an 11.6-cm outer diameter, 1.3-cm thick bed walls, and was 20 cm in height.  $\text{Li}_2\text{O}$  charge weight and test conditions were similar to the previous run, but a higher  $\text{CO}_2$  concentration was maintained throughout the run, with input  $\text{CO}_2$  controlled on a demand basis. Profiles (humidity again limited by hygrometer range) are given in figure 24, data in table XV. Cumulative  $\text{H}_2\text{O}/\text{CO}_2$  molar ratio was 1.7 at the 4-hour point.

Run 376-11

The previous results suggested that performance of the passive displays might be improved by increased gas recirculation rate. Higher flow would increase moisture input rate to the chamber and, hence, raise ambient humidity. Chamber superficial gas velocity was increased to 38.7 cm/min versus 18 cm/min previously used, thus increasing moisture input to 19.5 g/hr. A wider range (5% to 95% R.H.) electric hygrometer was installed to allow calculation of the  $\text{H}_2\text{O}$  (absorbed)/ $\text{CO}_2$  (absorbed) molar ratio as well as the  $\text{H}_2\text{O}$  (input)/ $\text{CO}_2$  (input) ratio. A cylindrical configuration and granular  $\text{Li}_2\text{O}$  were used, both identical to the previous run.  $\text{CO}_2$  feed was controlled on a demand basis. In the first 45 minutes of test, the input ratio was 1.33, whereas the molar ratio  $\text{H}_2\text{O}$  (absorbed)/ $\text{CO}_2$  (input) was only 0.86 which explains the steady  $\text{CO}_2$  concentration rise shown in the profiles of figure 25. The rate of initial  $\text{CO}_2$  absorption via reaction (3) was limited by the rate of reaction (2).



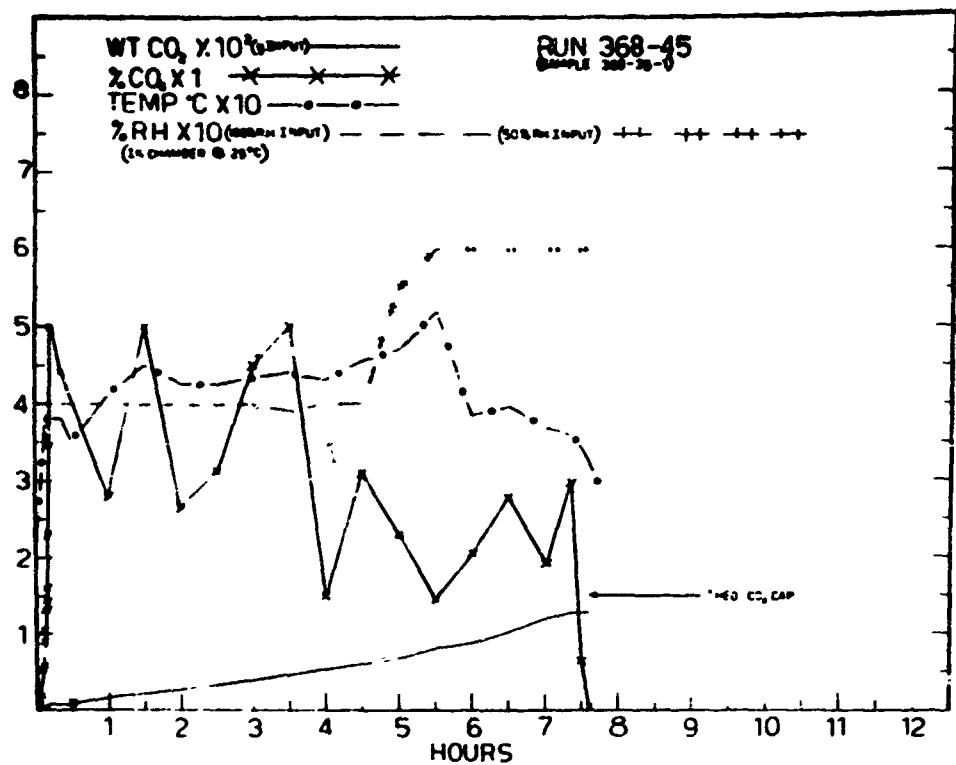


Fig. 24. Passive Test Profiles, Granule Cylindrical Bed  
Run 368-45

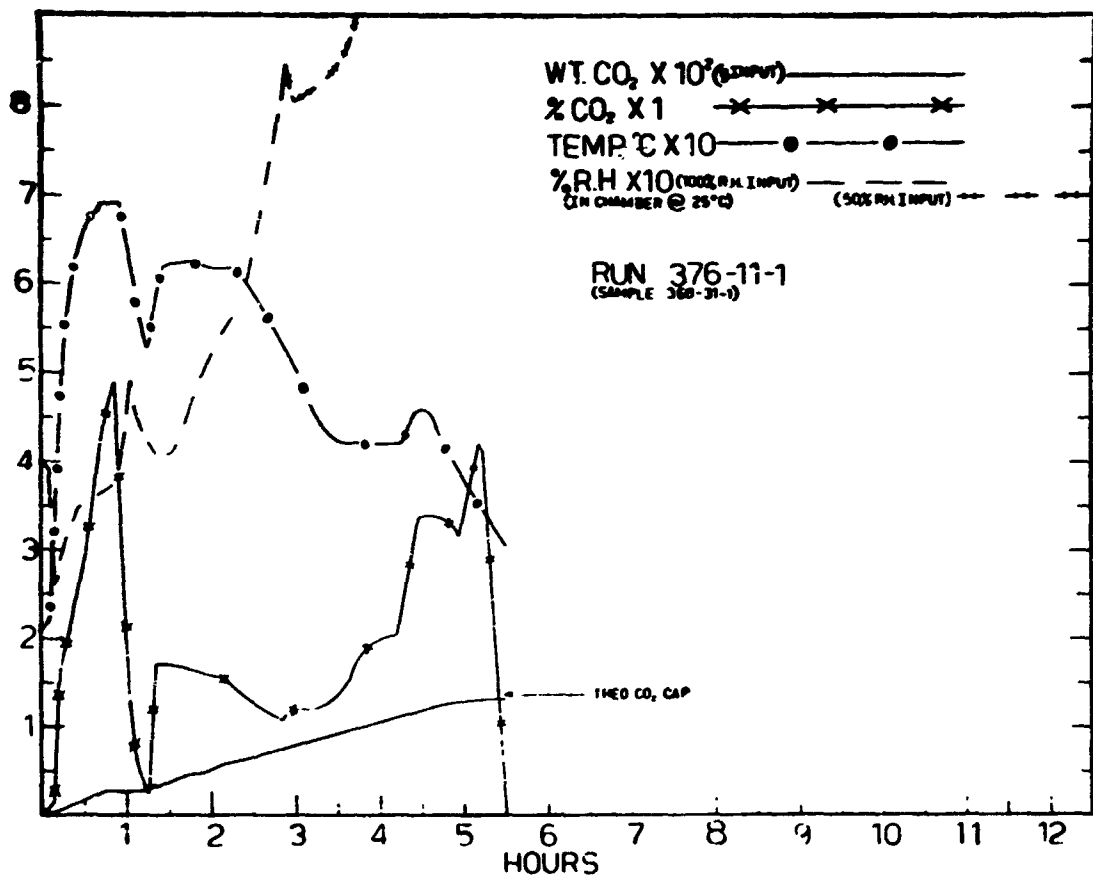


Fig. 25. Passive Test Profiles, Granule Cylindrical Bed  
Run 376-11

$\text{CO}_2$  input was cutoff and moisture feed continued until chamber concentration had dropped to 0.45%  $\text{CO}_2$ . At this point, cumulative  $\text{H}_2\text{O}$  (input)/ $\text{CO}_2$  (input) ratio was 2.04 and the cumulative  $\text{H}_2\text{O}$  (absorbed)/ $\text{CO}_2$  (input) ratio was 1.3. These results indicated the passive array could maintain a low ambient  $\text{CO}_2$  concentration, provided  $\text{H}_2\text{O}$  (input)/ $\text{CO}_2$  (input) ratio was near 2. Test data are given in table XV.

Runs 376-13 and 376-15

Cylindrical configurations, demand basis  $\text{CO}_2$  feed, and test conditions were similar to the previous run. However bulk density of the granular  $\text{Li}_2\text{O}$  was increased to 0.34 g/cc in Run 376-13 and 0.24 g/cc in Run 376-15. Figures 26 and 27 and table XV give results.

Runs 376-16 and 376-17

The need for a high percentage of open area in granular bed supports was studied by testing beds enclosed in tightly woven monofilament polypropylene fabric. Belt-type configurations, shown in figure 28 and 29, were fabricated by folding 42-cm-wide fabric in half and sewing or stapling seams to form a series of pouches for the granular  $\text{Li}_2\text{O}$  charge. The fabric (6-mil yarn, 148 by 74 filaments per inch, weight 116 g/m<sup>2</sup>) had only about 6.2% open area. Test profiles for Run 376-16, made with 4- by 10-mesh granules at 0.11 g/cc bulk density, are given in figure 30. Profiles for Run 376-17, 10- by 30-mesh granules at 0.18 g/cc bulk density, are shown in figure 31. Table XV gives test data. Results indicated the low open area fabric did not significantly hinder  $\text{CO}_2$  and moisture access to the bed.

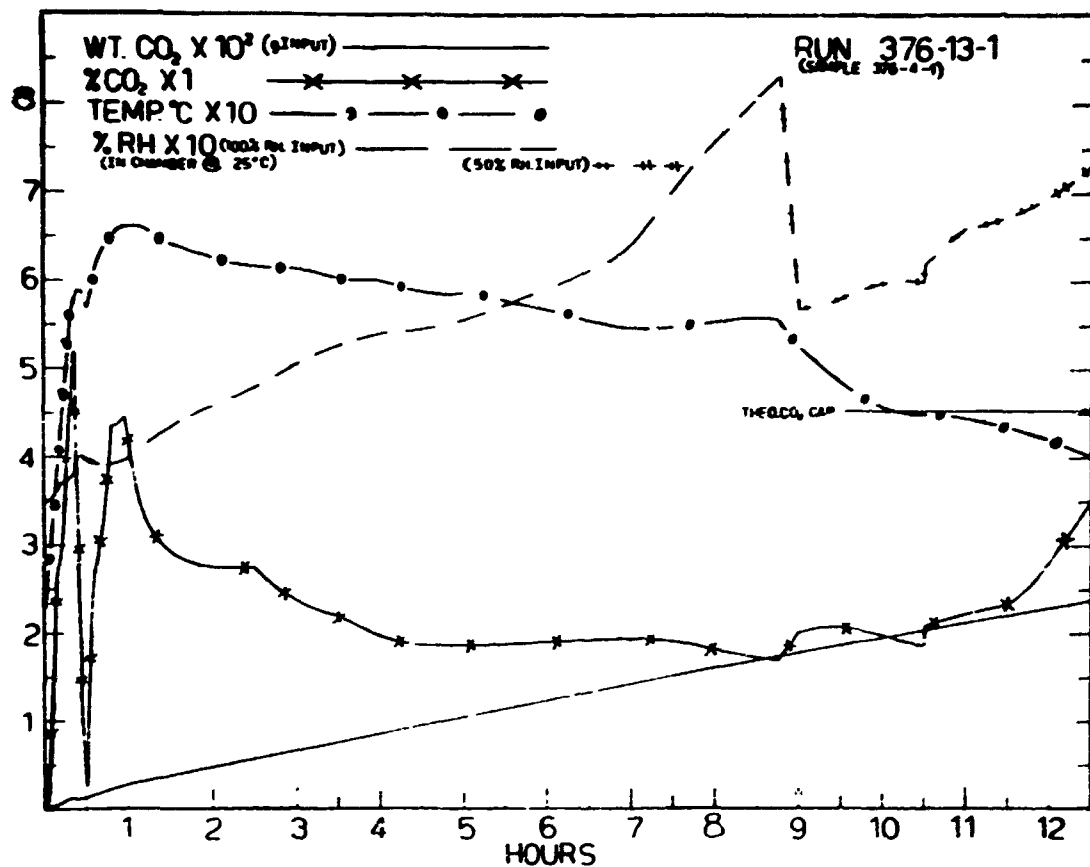


Fig. 26. Passive Test Profiles, Granule Cylindrical Bed  
Run 376-13

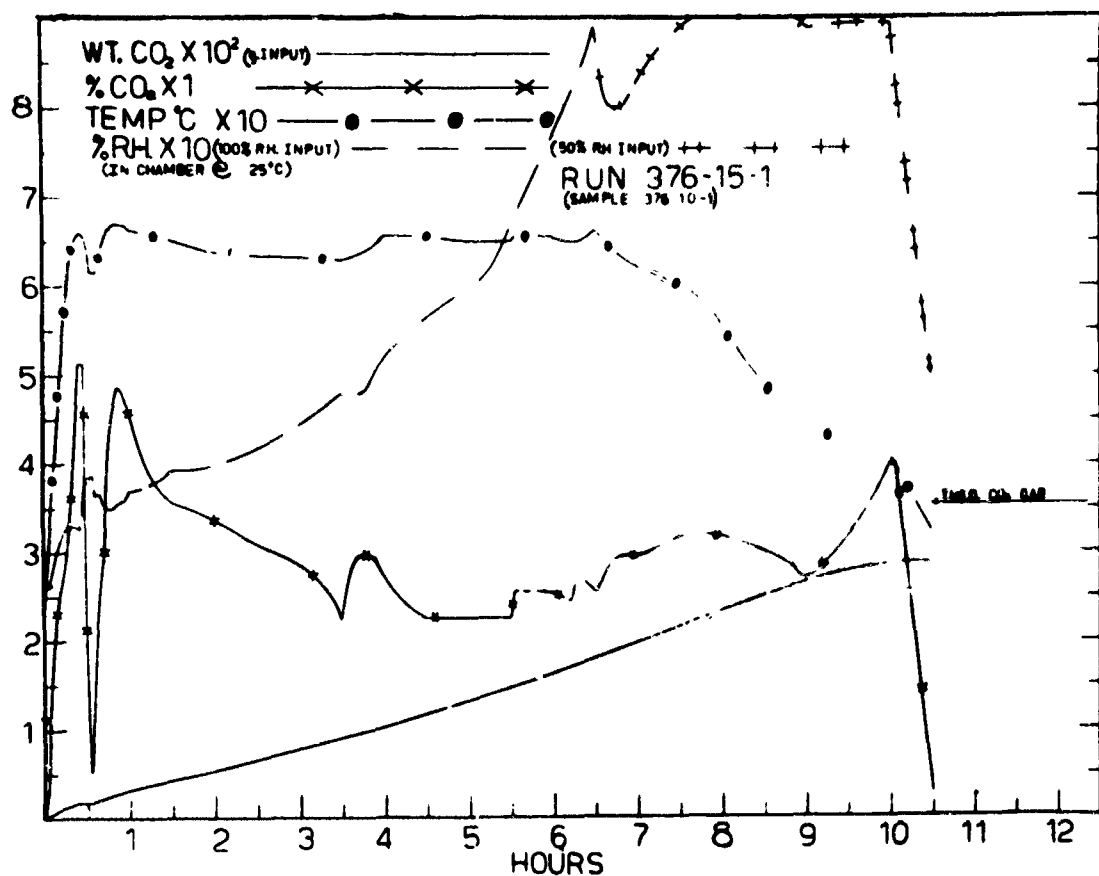
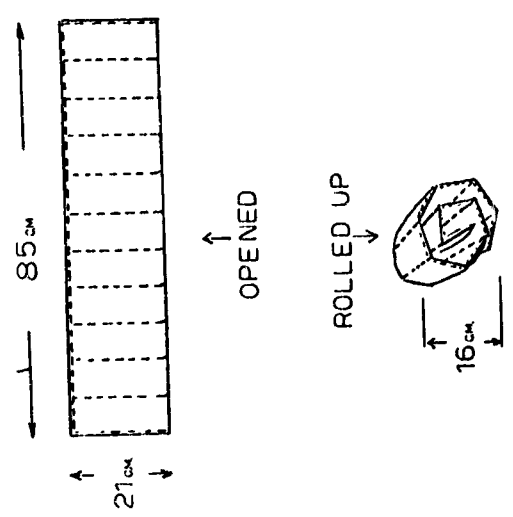


Fig. 27. Passive Test Profiles, Granule Cylindrical Bed

Run 376-15



Fig. 29. Granule Belt Configuration  
In Test Apparatus



POUCHES MADE FROM POLYPROPYLENE CLOTH

Fig. 28. Granule Belt Configuration

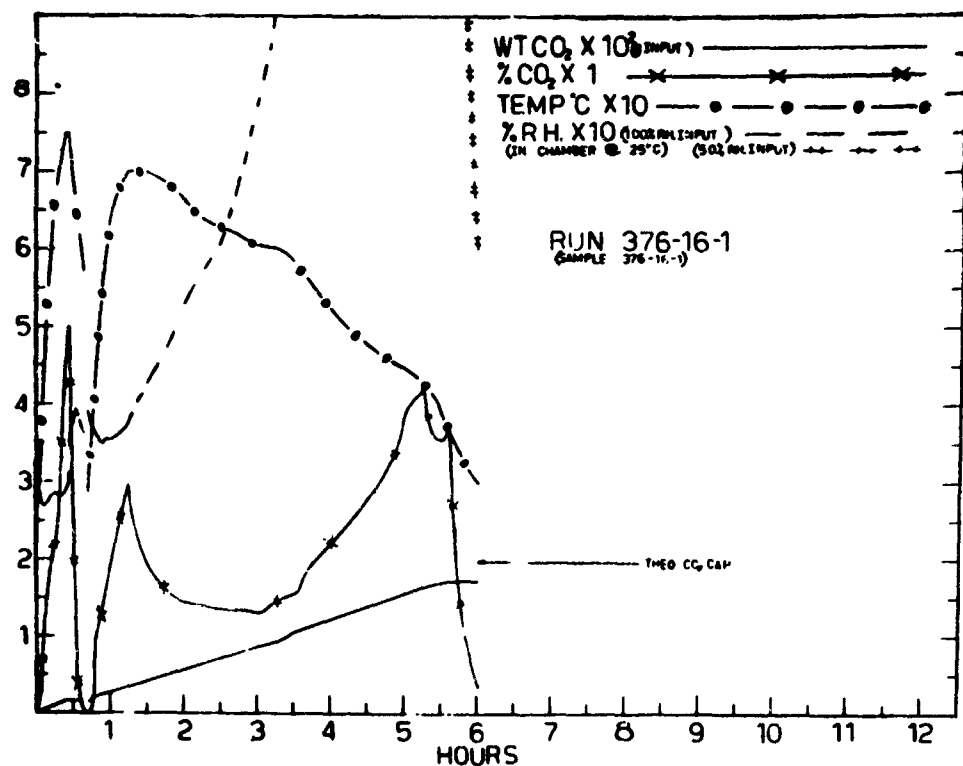


Fig. 30. Passive Test Profiles, Granule Belt  
Run 376-16-1

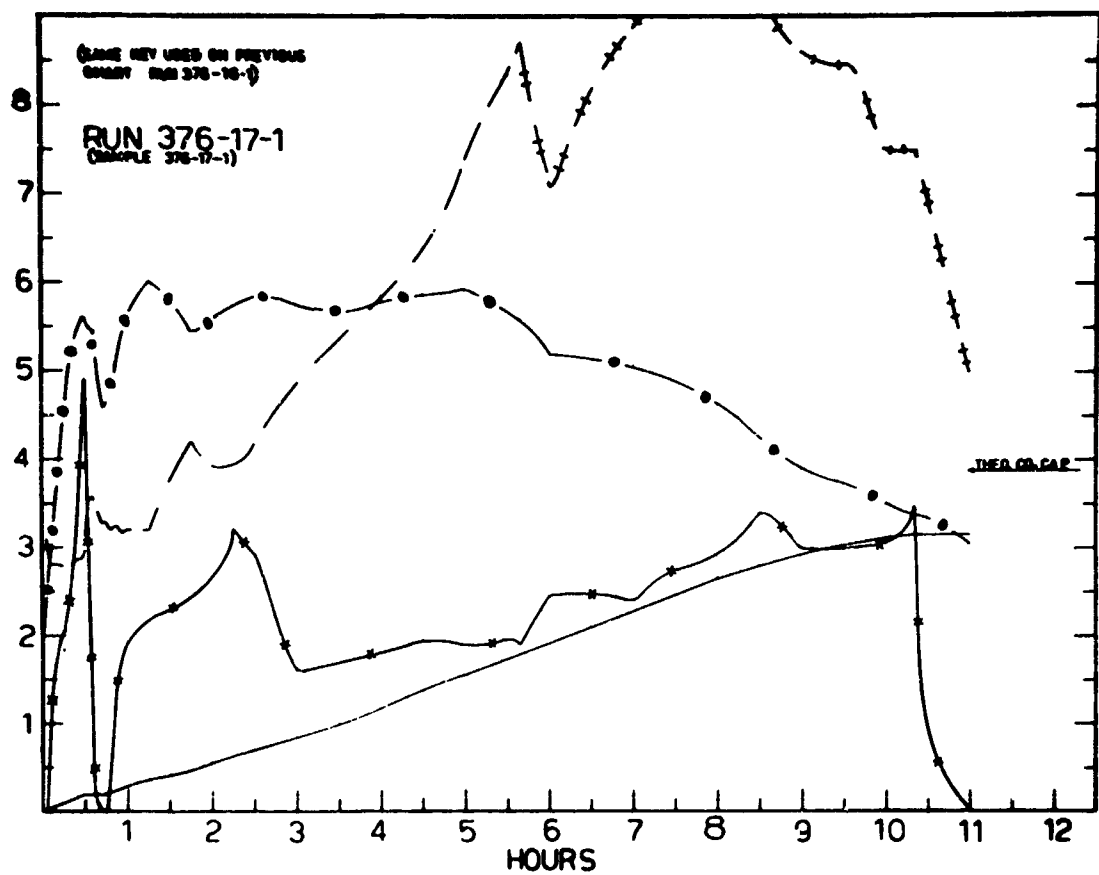


Fig. 31. Passive Test Profiles, Granule Belt

Run 376-17-1

#### 4. DYNAMIC TESTS

##### a. Dynamic Test Unit

A supported bed, forced circulation, type CO<sub>2</sub> absorber was fabricated and mounted within the test chamber as shown in figures 32 and 33. Operating characteristics with the motor-blower at 24 to 27 volts and a 4- by 10-mesh granular Li<sub>2</sub>O bed in place were as follows--

Gas rate through bed	214 liters/min
Average velocity across bed face plate	15 m/min
Blower exhaust velocity	780 m/min
Pressure loss across granule bed	0.16 mm Hg
Bed - diameter	13.5 cm
depth	9.0 cm
volume	1.29 liters
Weights - blower	79 g
- unit, less Li <sub>2</sub> O	623 g

##### b. Tests

###### Run 376-19

Bulk density of the granular charge was 0.10 g/cc. The test profile given in figure 34 was similar to the passive test experience in demonstrating that hydrolysis must proceed carbonation. As before, the CO<sub>2</sub> feed was cutoff to increase the H<sub>2</sub>O (input)/CO<sub>2</sub> (input) molar ratio, and subsequent CO<sub>2</sub> feed was on a demand basis. At 2 hours, a sharp increase in absorption occurred, followed by falling chamber CO<sub>2</sub> concentration and rising relative humidity. At the 2-hour point, 69.3 g CO<sub>2</sub> and 39 g H<sub>2</sub>O had been fed to the chamber. The corresponding

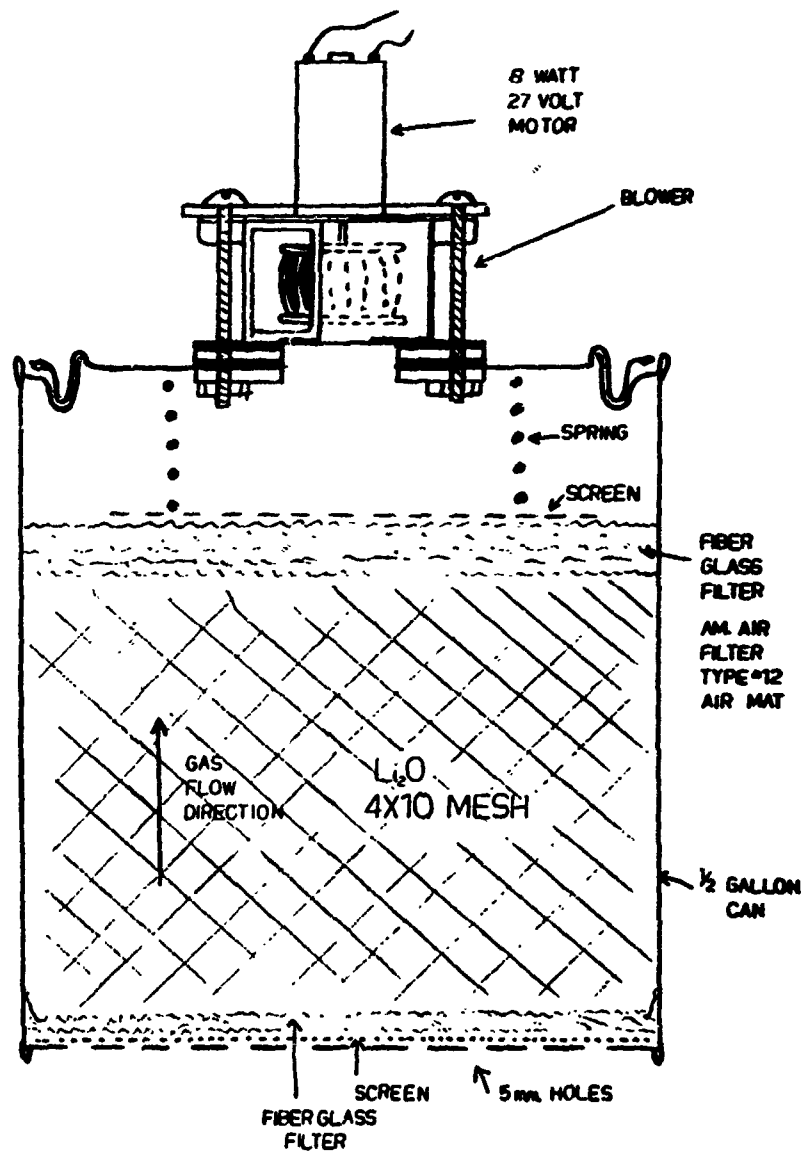


Fig. 32. Dynamic Absorber



Fig. 33. Dynamic Absorber In Test Apparatus

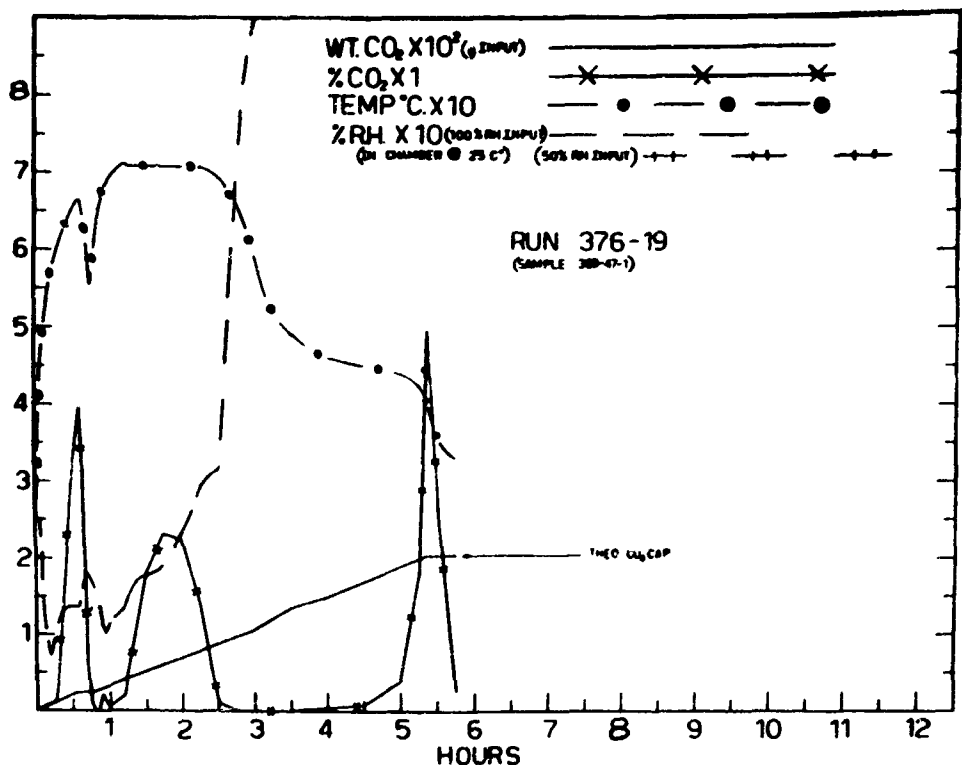
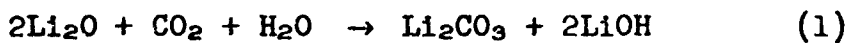


Fig. 34. Dynamic Test Profiles

Run 376-19

cumulative molar ratios were 1.3 H<sub>2</sub>O (input)/CO<sub>2</sub> (input) and 1.1 H<sub>2</sub>O (absorbed)/CO<sub>2</sub> (input). At the 2.5-hour point, calculations indicate 112 g Li<sub>2</sub>O had been carbonated and hydrated via reaction (1).



Since the initial sample charge was 126.4 g Li<sub>2</sub>O, little oxide remained at this time and a sharp rise in humidity signaled the occurrence of reaction (5):



Absorption after 2.5 hours proceeded at a high and steady rate, maintaining low chamber CO<sub>2</sub> concentration. Test data are given in table XV.

#### Run 376-38

Test conditions were identical with the previous run, except that the bulk density of the charge was 0.31 g/cc and charge weight was correspondingly greater. Profiles are given in figure 35 (notation "a" indicates interruption of the run with the absorbent removed from the chamber, stored overnight, and restarted the next day). Table XV gives test data.

#### c. Analysis of Results

Results with granular Li<sub>2</sub>O arrays, whether under passive or dynamic conditions, indicate the cumulative H<sub>2</sub>O (input)/CO<sub>2</sub> (input) must be well above unity to initiate absorption and maintain low chamber CO<sub>2</sub> concentration during initial operation. Experience suggests this ratio should be no less than 2 for passive displays (at 38 cm/min gas velocity) and no less than 1.44 for granular dynamic beds. Product analyses

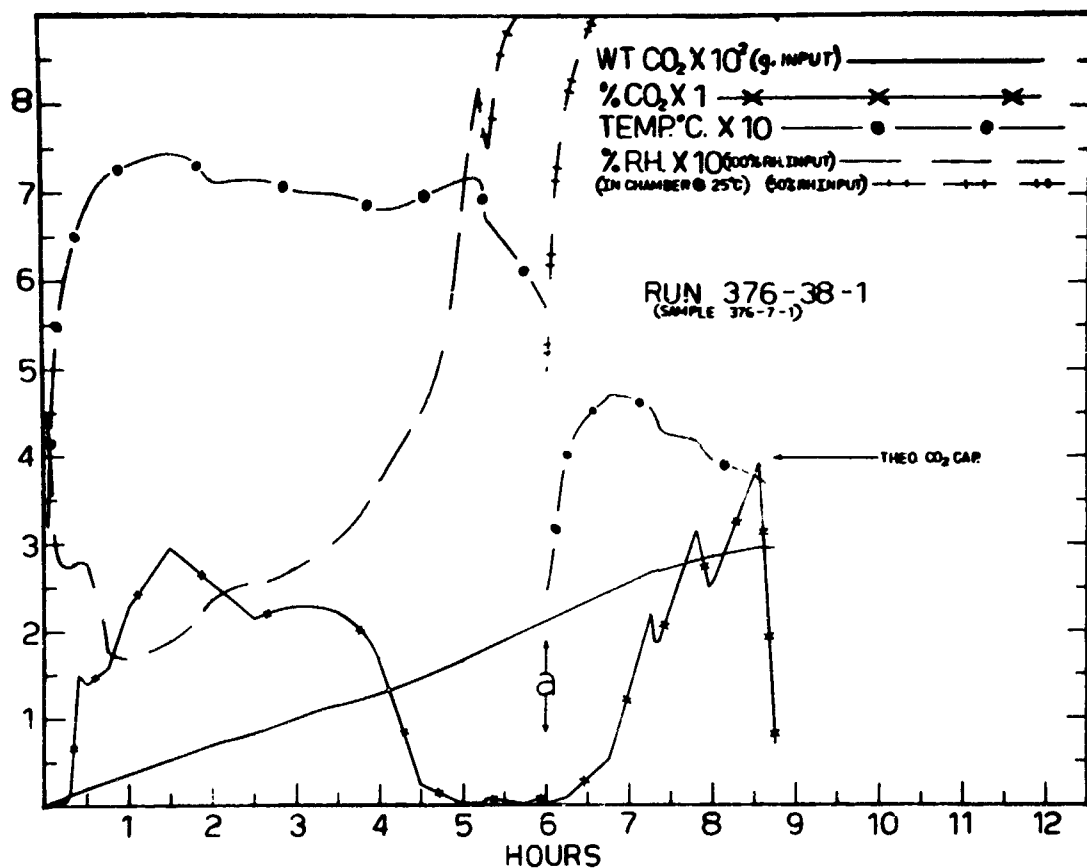


Fig. 35. Dynamic Test Profiles

Run 376-38-1

indicate that reactions (1) and (5)



can proceed concurrently in passive operation even while a relatively large amount of unreacted  $\text{Li}_2\text{O}$  is available. Under dynamic operation, the consumption of  $\text{Li}_2\text{O}$  via reaction (1) is more complete before reaction (5) proceeds. Therefore, reaction mechanism in the absorption process is influenced by the design of the system.

## SECTION IV

### ABSORBER DEVELOPMENT AND TESTING AT ONE ATMOSPHERE

#### 1. APPARATUS

Tests were conducted in a large (118.3 cm long, 60.6 cm wide, 58.7 cm high) environmental chamber fabricated of "Plexiglass" and fitted with glove ports, gas expansion bag, and electrical power, gas, and instation connections. Samples were introduced through an airlock chamber extending (35 cm diameter, 44 cm long) from one end of the main chamber. In operation the main and airlock chambers were connected making total chamber volume about 463 liters (16.3 ft<sup>3</sup>). A blower mounted within the chamber circulated the chamber gas through a humidity control circuit at the rate of 168 liters/min. A 2-liter flask in this circuit, filled with crumpled absorbent paper to provide high surface area, was heated or cooled to evaporate or condense water as required. The evaporation or condensation rate was manually controlled to maintain 50% R.H. in the main chamber.

With the chamber atmosphere at design conditions for absorption, i.e. 25 C, 50% R.H. (11.8 mm Hg partial pressure H<sub>2</sub>O), and 1% CO<sub>2</sub> (7.6 mm Hg partial pressure CO<sub>2</sub>) the ambient H<sub>2</sub>O/CO<sub>2</sub> molar ratio would exceed unity, a condition suitable for CO<sub>2</sub> absorption as established in section III. Gas returning to the main chamber from the humidity control circuit was introduced through a porous dispersing tube. Measurements indicated the return gas did not impart a detectable velocity to the gas volume within the main chamber. Gas velocities within the chamber itself were produced by a 40-watt fan mounted in the chamber and controlled

by a "Powerstat". The chamber gas velocities were measured by an anemometer located within the chamber and manipulated through the glove ports. With the fan operating, gas circulation within the chamber, viewed from above, was counterclockwise. Table XVI gives gas velocity, parallel and perpendicular to this general circulatory movement, for various locations within the chamber. Chamber gas temperature, humidity, and  $\text{CO}_2$  concentration were continuously recorded. To insure collection of representative mixed samples of chamber gas, samples were simultaneously pumped from each corner of the chamber via sampling tubes of identical length. Temperature measurements were taken at the downstream gas end of dynamic and semi-dynamic configurations. For passive configurations, temperature was measured on the center surface of the absorbent. A diagram of the apparatus showing gas sampling points, humidity control circuit,  $\text{CO}_2$  feed, and location of the blower and fan, is given in figure 36.

TABLE XVI  
CHAMBER GAS VELOCITIES WITH FAN OPERATING

Direction--	Parallel To Main Gas Flow		Perpendicular To Main Gas Flow
Fan Voltage--	<u>55v</u>	<u>110v</u>	<u>55v</u>
Gas Velocity--	m/min	m/min	m/min
Probe Location:			
Above, Behind Fan	6.1	13.7	---
Corner No. 1	8.5	18.3	3.1
Corner No. 2	7.0	13.7	6.1
Position A	10.6	---	3.1
Corner No. 3	8.5	12.8	6.7

The chamber, without absorbent chemical in place but with blower and fan operating, was fed with 46.7 g  $\text{CO}_2$ /hr. Average

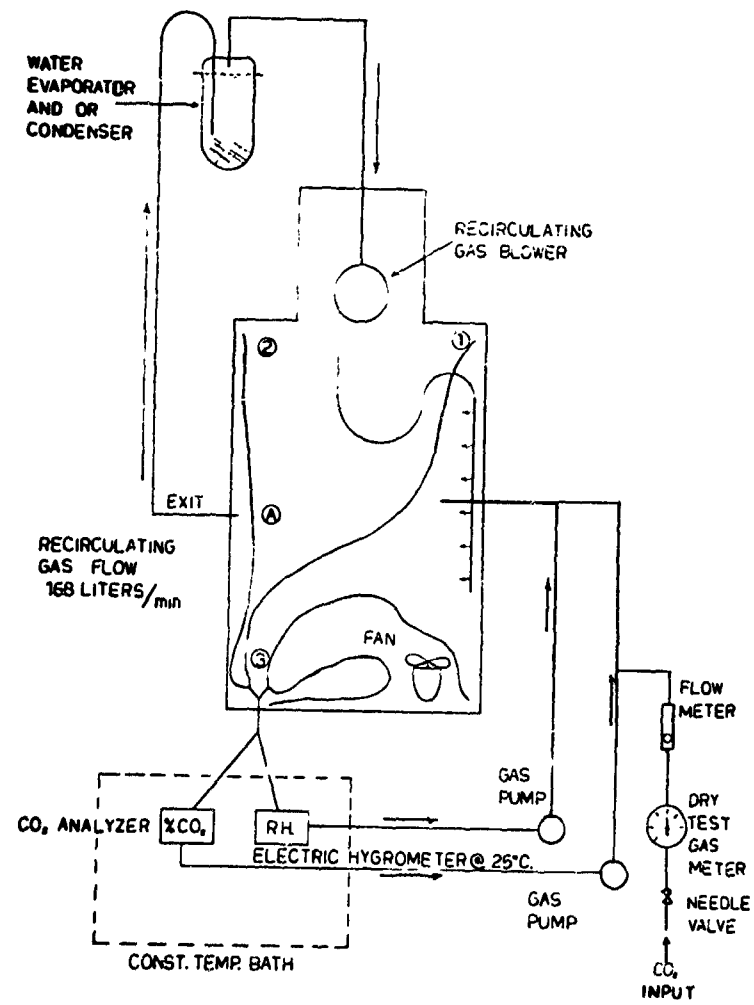


Fig. 36. Apparatus For 1-Atmosphere Tests

human  $\text{CO}_2$  production during intense activity is 41.3 g/manhour (reference 10). Table XVII gives the resulting  $\text{CO}_2$  concentration buildup with time.

TABLE XVII  
CHAMBER  $\text{CO}_2$  CONCENTRATION WITH ZERO ABSORPTION

Time Min	Cumulative $\text{CO}_2$ Feed g	Chamber $\text{CO}_2$ Concentration % (Vol)
15	11.2	1.12
30	22.9	2.45
45	35.1	3.60

## 2. GRANULAR $\text{Li}_2\text{O}$ DEVELOPMENT

Previous experience had suggested the best process for reactive  $\text{Li}_2\text{O}$  granules was pelletizing high surface area  $\text{Li}_2\text{O}_2$  powder, decomposing at temperatures consistent with desired bulk density, and crushing and sieving the resulting  $\text{Li}_2\text{O}$  pellets to the appropriate, granule size. Therefore, efforts at improving the dusting characteristics of granular  $\text{Li}_2\text{O}$  were concentrated on this product. Three methods--granule coating, dedusting, and fabric encasement, were investigated as outlined below.

### a. Granule Coating

The general technique visualized was that of spraying a light porous film of nonreactive material on the granules, which coated their surface and bounded any dust particles to the surface. Polyethylene and polypropylene, although unreactive with strong bases, proved unsuitable since they are insoluble in suitable solvents. A hydroscopic poly vinyl-

pyrrolidone-vinylacetate copolymer solution (PVP/VA, 70/30 ratio, 50% ethanol solution) appeared suitable and was diluted further with ethanol for spraying. Copolymer to the extent of 5% of the Li<sub>2</sub>O weight was applied, and the sprayed granules were heated at 100 C under vacuum until they appeared dry. The treatment did not improve dusting, and the granules had a strong sweet odor.

b. Dedusting

Observations during hardness testing (basically a measure of attrition during sieving) suggested that granule hardness and dusting might be improved by controlled attrition. The principle was confirmed when a mixture of three granular samples (Nos. 376-10, 376-7, 376-4) with hardness values of 67, 66, and 79 yielded a value of 99.8 on retesting. The technique was studied further by devising a deduster consisting of an inclined rotating (60 rpm) container fitted with a 20-mesh, metal screen at the bottom and a gas inlet at the top. Dry gas at 5 to 15 liters/min was passed through the rotating Li<sub>2</sub>O charge, and it exited with entrained dust particles through the screen bottom. The apparatus is shown in figure 37.

As shown in table XVIII, the dedusting procedure improved both the hardness and bulk density of granular oxide prepared from pelletized Li<sub>2</sub>O<sub>2</sub> (i.e., process 2a-5 of table II). Granules prepared by decomposing Li<sub>2</sub>O<sub>2</sub> powder (process 2a-1) were merely reduced to smaller size during dedusting, with no improvement in hardness. Microphotographs of a Li<sub>2</sub>O granule before and after dedusting, figures 38 and 39, show a distinct change in



Fig. 37. Dedusting Apparatus

TABLE XVIII  
DEDUSTING OF 4- by 10-MESH GRANULAR  $\text{Li}_2\text{O}$

Sample No.	Tumbling Time hr	Bulk Density Before g/cc	Bulk Density After g/cc	Wt Loss -20 Mesh %	Hardness No.
361-20-1(a)	24.0	0.21	0.25	7.9	97
361-40-1(b)	2.5	0.12	0.14	14.3	61

Notes: (a) Prepared from compressed  $\text{Li}_2\text{O}_2$   
(b) Prepared from  $\text{Li}_2\text{O}_2$  powder

the surface and periphery of the granule indicating fine particles and fragile projections have been removed.

c. Fabric Encasement

The dust-retention capability of various support fabrics for granular beds was studied. A dusting test was devised similar to the  $\text{KO}_2$  dusting test of McGoff (reference 11). Fabric envelopes were filled with 10 g charges of  $\text{Li}_2\text{O}$ , the open ends were folded over twice and stapled, and each envelope was enclosed in a polyethylene bag. The samples were vibrated in a Rotap machine at 150 cycles/min for 30 minutes. Following vibration, dust collected in the plastic bag was washed out with water and the solution was titrated with standard acid to the methyl orange end point. Table XIX gives results. The data confirm the benefit of rotary dedusting by showing that 4- by 10-mesh granule is less dusty than the 10- by 30-mesh size. The data also indicate that closely woven fabric supports retard dusting. In future work, substituting multifilament fiber glass



Fig. 38. Microphotograph, Li<sub>2</sub>O Granule Before Dedusting

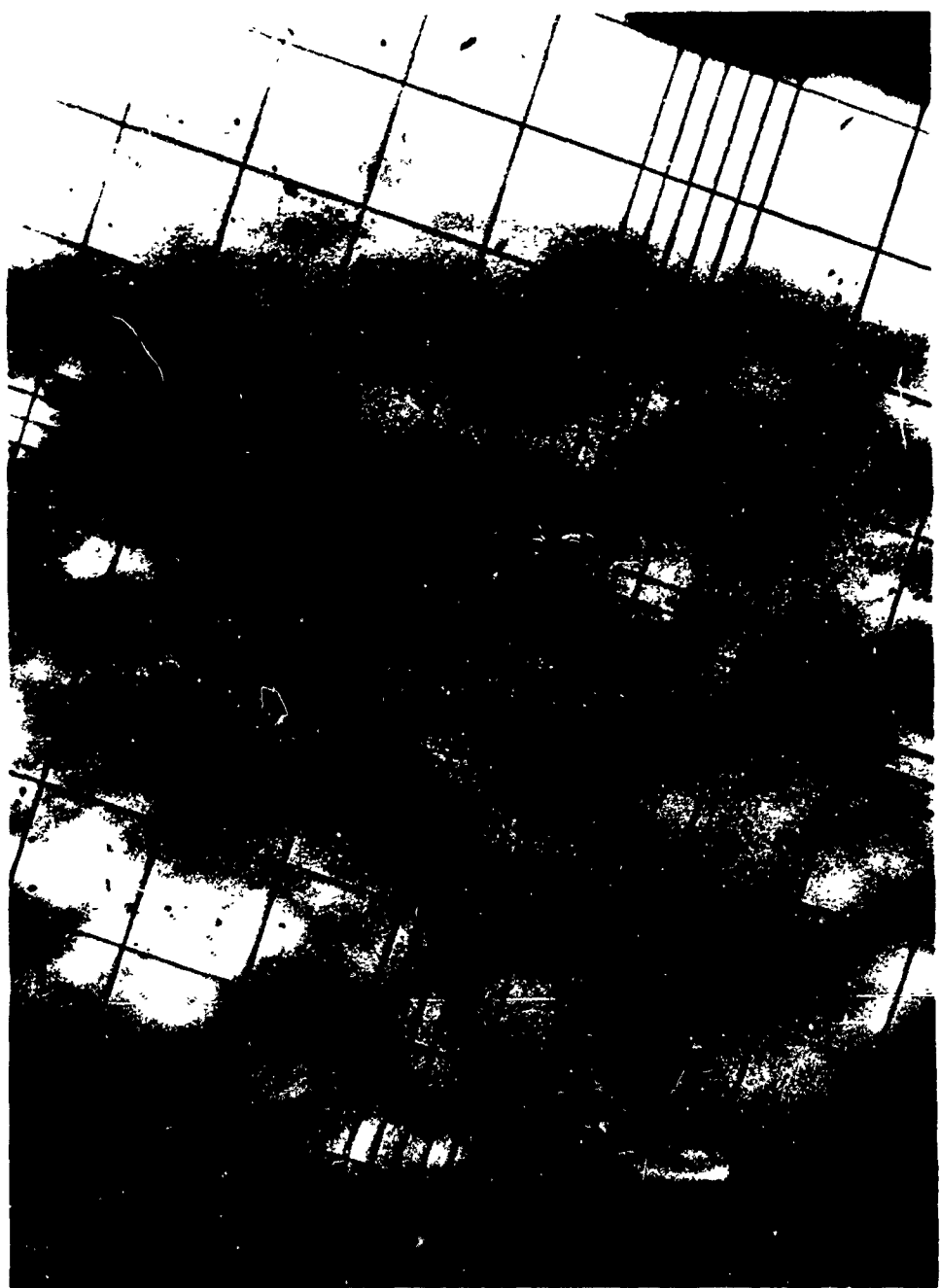


Fig. 39. Microphotograph, Li<sub>2</sub>O Granule After Dedusting

TABLE XIX  
DUSTING TESTS WITH FABRIC ENCASEMENT

<u>Fabric Type</u>	<u>Granular Li<sub>2</sub>O Sample</u>	<u>Li<sub>2</sub>O Dust mg/g granules</u>
a	Non-Dedusted 10- by 30-mesh	1.09
a	Dedusted 10- by 30-mesh	0.12
a	Dedusted 4- by 10-mesh	0.09
b	Non-Dedusted 10- by 30-mesh	0.19
b	Dedusted 10- by 30-mesh	0.13
b	Dedusted 4- by 10-mesh	0.08
c	Dedusted 4- by 10-mesh	0.21

Notes: a. Monofilament polypropylene cloth, 6% open area, No. 6722200, Chicopee Mfg. Co., Cornelia, Ga.

b. Multifilament polypropylene cloth, no visible open area, 60 x 36 count, 2/2 twill weave, 630 mil yarn size, 8.7 oz./sq. yd., No. 6720600, supplier as above.

c. Monofilament polypropylene netting, 25% open area, 52 mesh, No. 6951500, supplier as above.

fabric of equivalent porosity appears desirable since this material can withstand higher temperatures than the polypropylene fabric.

### 3. SOLID Li<sub>2</sub>O CONFIGURATION DEVELOPMENT

The swelling and sintering properties of Li<sub>2</sub>O<sub>2</sub> on decomposing, as described in section I, were used to form solid and potentially self-supporting Li<sub>2</sub>O configurations. Two variations of the technique were evaluated, one used Li<sub>2</sub>O<sub>2</sub> powder and one used Li<sub>2</sub>O<sub>2</sub> granules. In the first case, a Li<sub>2</sub>O cylinder containing 15 axial holes (further described in section 4 "Configuration Tests" under Run No. 361-26) was prepared by decomposing Li<sub>2</sub>O<sub>2</sub> powder. The mold was an aluminum cylinder with perforated plates at each end. Glass rods inserted through the perforations and extending through the cylinder formed the axial holes. Figure 40 shows this shape after decomposition and removal of the plates and rods. The oxide had low strength, tended to crack into loose pieces, and was left in its casing to expedite handling. A second and larger shape (further described under Run No. 361-21) was made in similar fashion except that granular Li<sub>2</sub>O<sub>2</sub>, produced by pelletizing the powder to 0.8 g/cc pellet density and crushing and sieving, was used. Decomposition at 288 C for 24 hours yielded a hard, sound shape as shown in figure 41. The oxide was tightly bound in the aluminum cylinder and the possibility of breakage precluded removing it from the case.

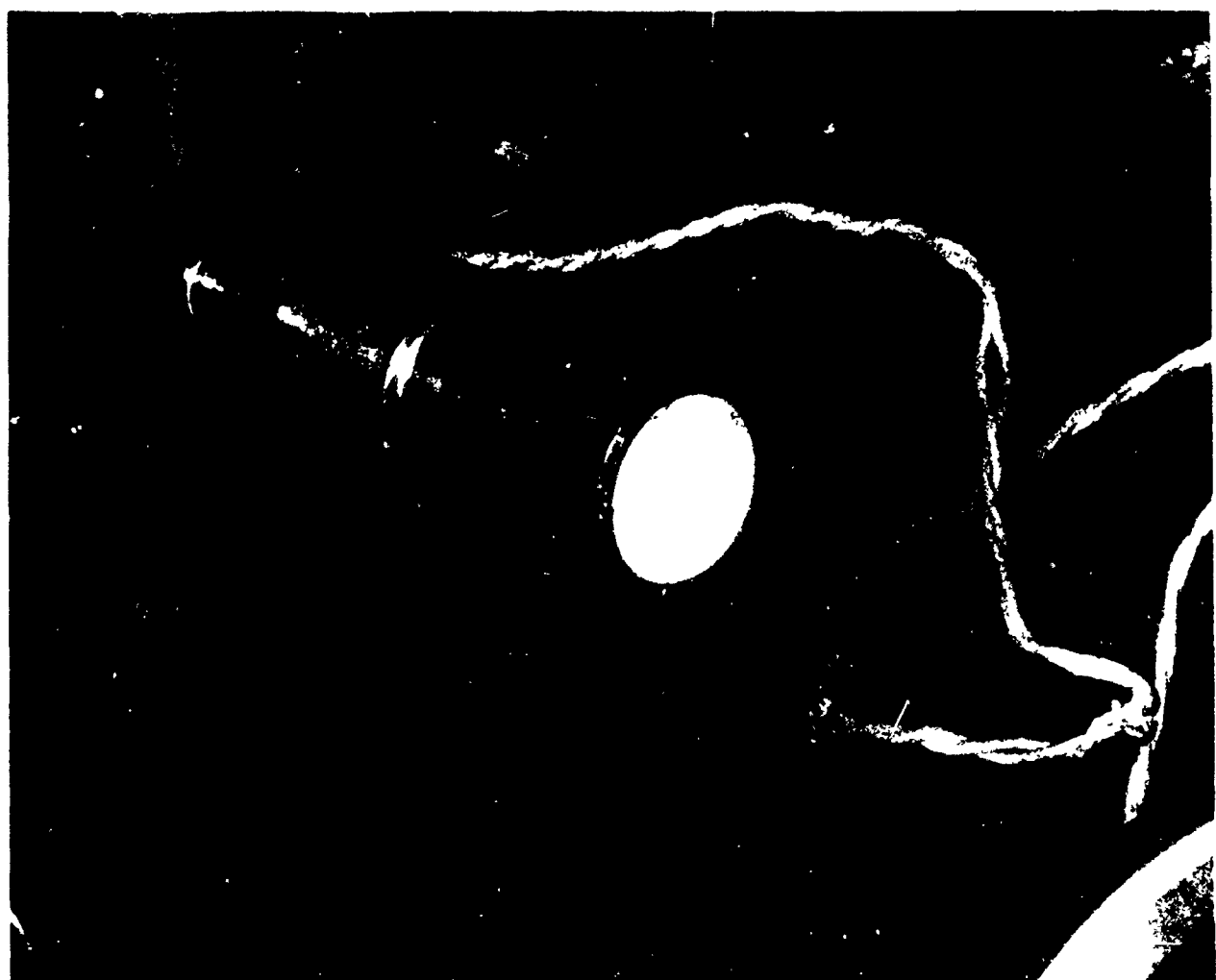


Fig. 40. Pierced Cylinder Configuration, Decomposed  $\text{Li}_2\text{O}_2$  Powder

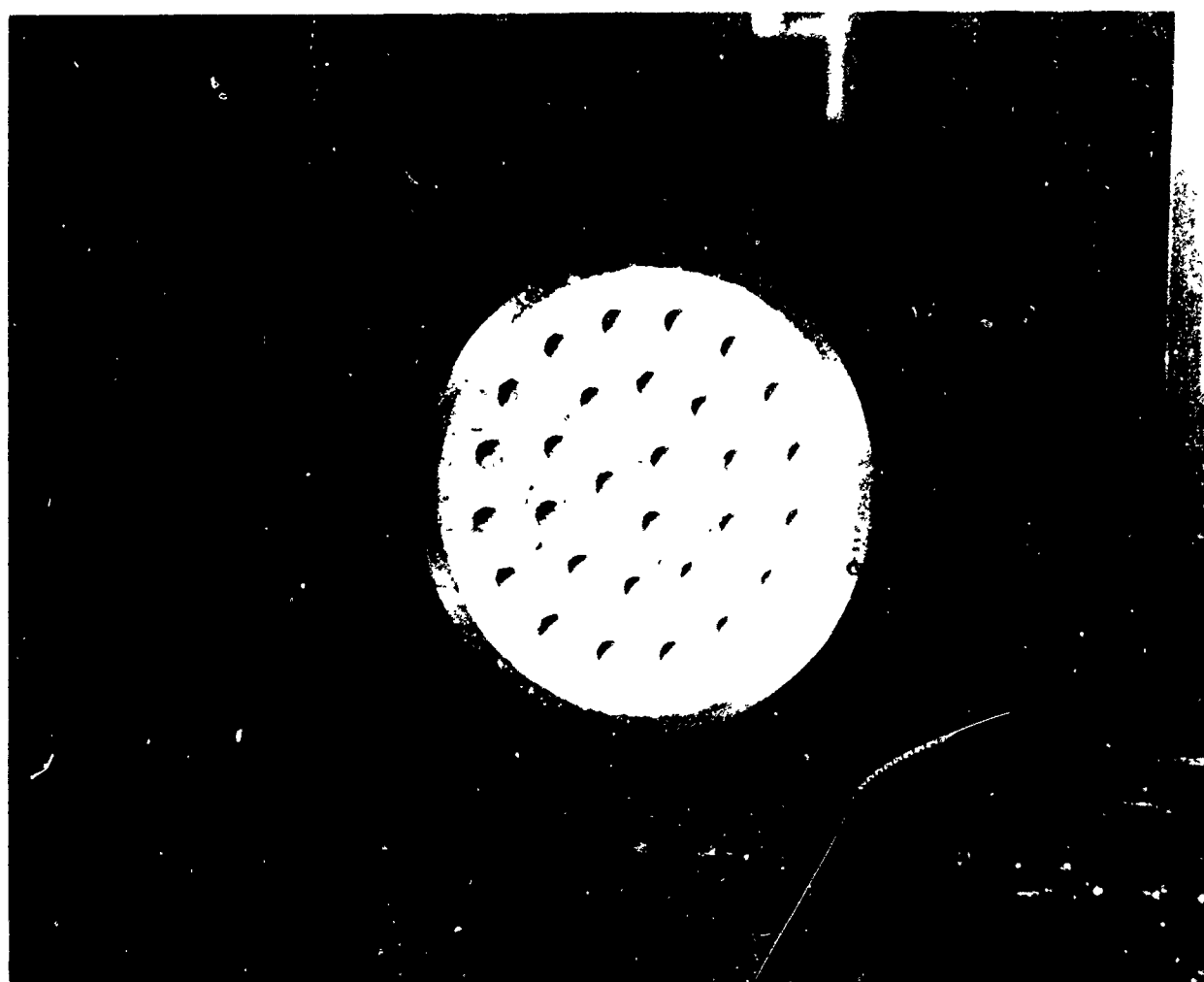


Fig. 41. Pierced Cylinder Configuration, Decomposed  $\text{Li}_2\text{O}_2$  Granules

#### 4. CONFIGURATION TESTS

##### Dynamic Test: Runs 361-26 and 361-30

The granular and pierced cylinder forms of the oxide were compared under dynamic conditions with the configurations housed in identical aluminum cylinders. Gas was drawn through each sample at 126 liters/min by connecting the cylinders to the suction side of the humidity control circuit (position A, figure 36). Table XX gives test data. The profiles of figure 42 can best be compared during the first hour where CO<sub>2</sub> feed rates were roughly the same (40 g/hr for run 361-26 and 49 g/hr for run 361-30). The superior absorption rate of the granular form, by virtue of greater surface area exposed to the gas, is evident. A constant CO<sub>2</sub> feed rate was maintained on the granular sample. CO<sub>2</sub> feed to the cylindrical sample was reduced (point A, figure 42) to demonstrate that almost complete utilization of the solid form was feasible.

##### Passive and Semipassive Test: Run 361-21

A large, pierced-cylinder configuration prepared via Li<sub>2</sub>O<sub>2</sub> granule was tested under passive and semipassive conditions. With the configuration initially positioned for passive operation (location A, figure 36), CO<sub>2</sub> absorption was poor. Relocating the unit directly in front of the chamber gas circulating fan as shown in figure 43 yielded a moderate absorption rate. Later in the run, chamber relative humidity was deliberately increased to 90%. No significant change in absorption rate resulted. This indicated maximum H<sub>2</sub>O diffusion rate into the sample had already been attained at 50% R.H. and was limited

TABLE XX  
TEST DATA OF RUNS 361-26 AND 361-30

Run No. Configuration Type		361-26 Pierced Cylinder(a)	361-30 4- by 10-Mesh Granular
Li <sub>2</sub> O charge	- g	88.1	99.0
Configuration size: diam.	- cm	6.3	6.3
	length - cm	13.0	13.0
Configuration density - g Li <sub>2</sub> O/cc		0.22	0.26
Theo. CO <sub>2</sub> capacity	- g	130	145
Sample weight gain	- g	108.3	126.7
Total CO <sub>2</sub> feed	- g	105.0	143.0
Average CO <sub>2</sub> feed	- g/hr	33.3	47.7
2% breakthrough:			
Time	- hr	3.0	2.0
g CO <sub>2</sub> feed/g Li <sub>2</sub> O charge		0.91	0.97
Final CO <sub>2</sub> concentration - %		2.55	3.92
Total run time	- hr	4.5	3.0
Product Analysis:			
	% Li <sub>2</sub> O	2.9	0
	% Li <sub>2</sub> CO <sub>3</sub>	93.3	89.9
	% LiOH	3.8	5.3
	% LiOH·H <sub>2</sub> O	0	4.8

Notes: (a) 15 axial holes, each 0.6 cm diameter

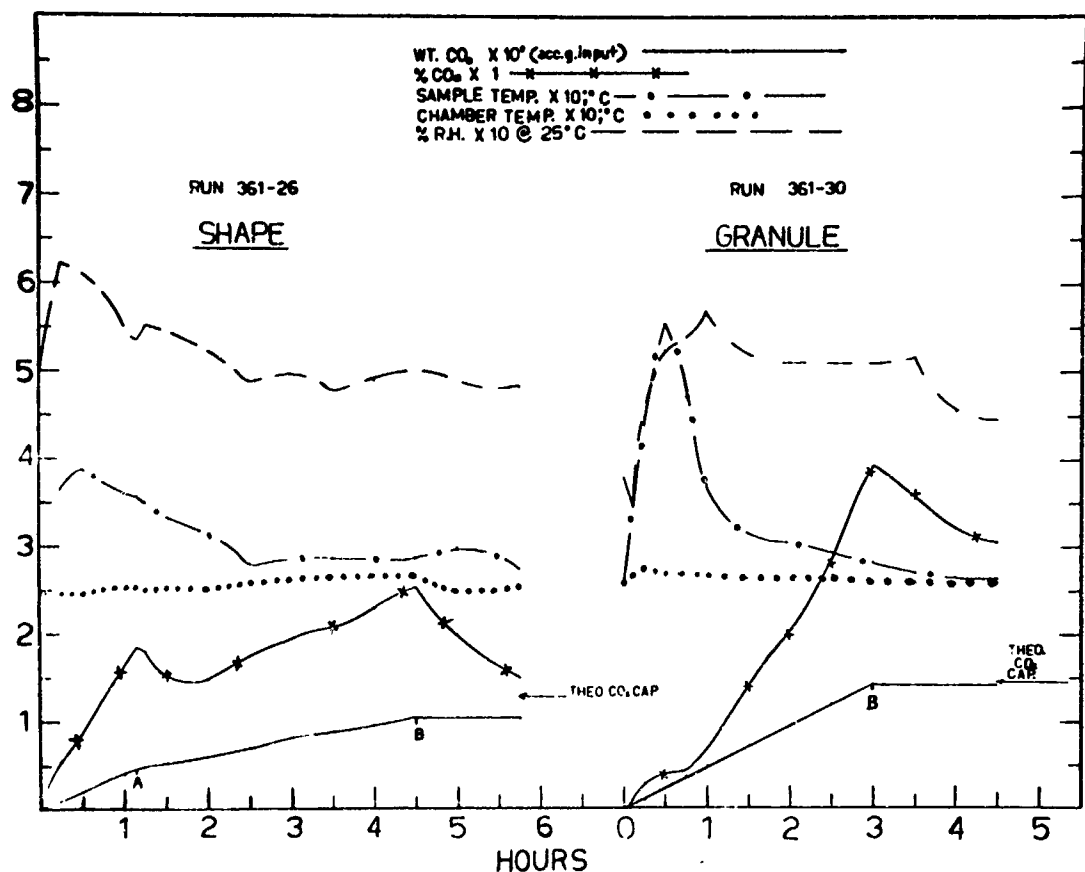


fig. 42. Test Profiles (Runs 361-26 and 361-30)

Notes: A - CO<sub>2</sub> feed decreased

B - CO<sub>2</sub> feed terminated

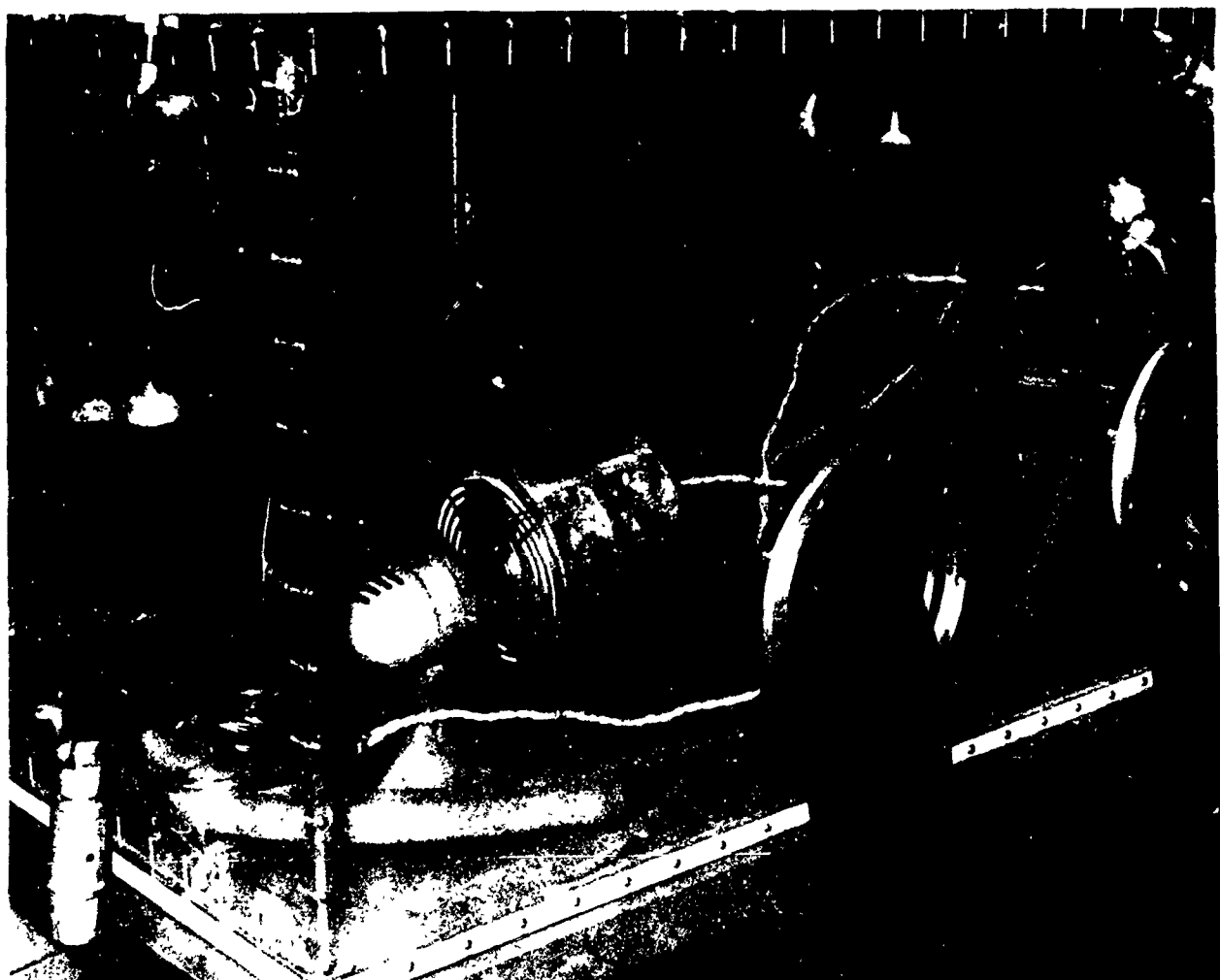


Fig. 43. Apparatus Arrangement, Pierced Cylinder Configuration

by configuration design and  $\text{Li}_2\text{O}$  density rather than ambient humidity. The experimentation outline and the resulting effects are illustrated in the profiles of figure 44. Table XXI gives test data. Reaction product analyses indicate the configuration was porous enough, relative to moisture, for complete conversion of the  $\text{Li}_2\text{O}$  to hydroxide.

Passive Tests: Runs 361-29 and 361-34

Two belt-type configurations consisting of granular  $\text{Li}_2\text{O}$  contained in a series of fabric pouches were tested to study the effect of granule size and bed thickness. The pouches were made of identical fabric but in one case contained 4- by 10-mesh granule, and in the second, contained 10- by 30-mesh granule with pouch width reduced to decrease average  $\text{Li}_2\text{O}$  bed thickness. The support fabric was monofilament polypropylene (fabric type a, Table XX) with an average air permeability of 1.02  $\text{m}^3/\text{min}$  as measured under ASTM Standard Specification D737-46 (i.e., - cfm air through 1 sq. ft. of fabric at 0.5 inches  $\text{H}_2\text{O}$  pressure). The belts were suspended in a passive arrangement (location A, figure 36) as illustrated in figure 45 so that chamber gas flow induced by the circulating fan was mainly parallel to the belt length. The test profiles of figure 46 and the fan voltage adjustments noted thereon suggest that gas velocity changes make little effect on  $\text{CO}_2$  absorption rate. Test data given in table XXII indicate the 10- by 30-mesh granule small pouch design was the better of the two-belt configurations.

Passive Tests: Runs 361-43 and 361-46

The above configuration was further studied by

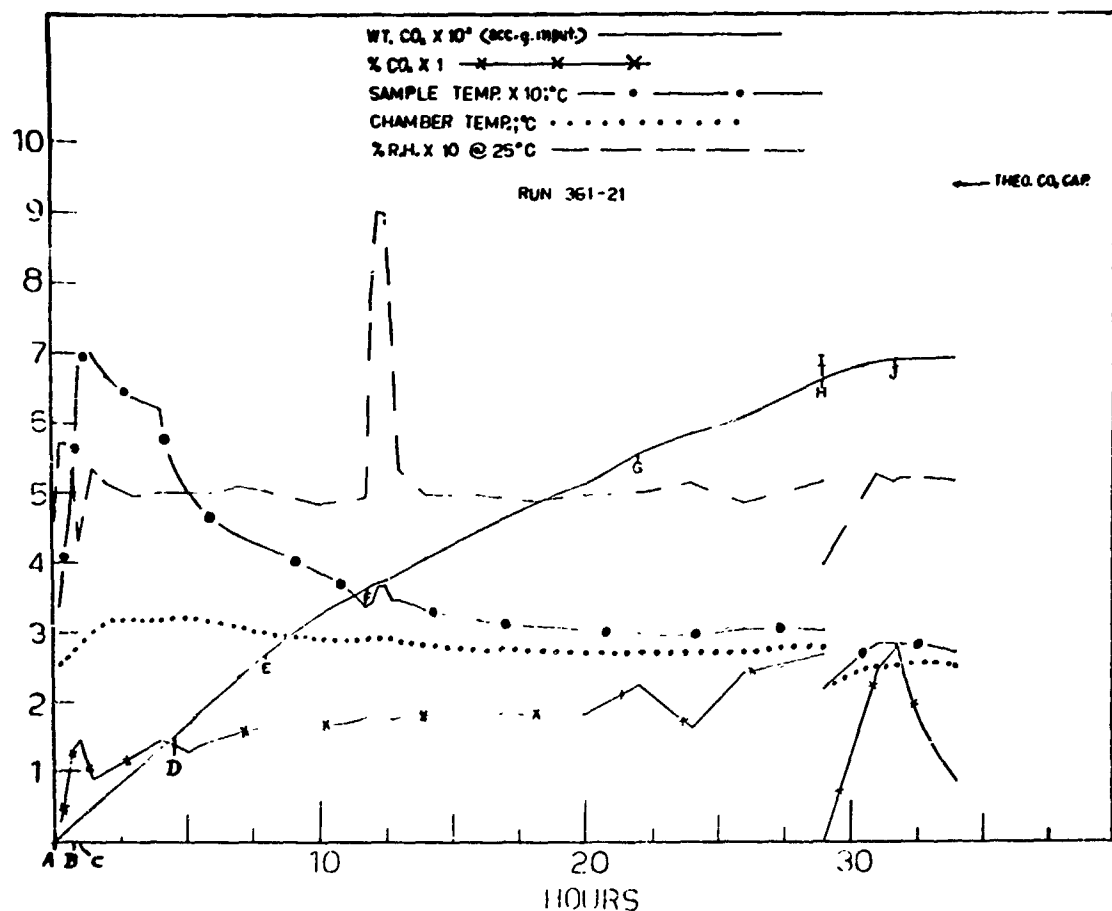


Fig. 44. Test Profiles (Run 361-21)

Notes:

- A. & B. Fan on at 55 Volts Sample positioned at (A) passively.
- C. Sample positioned directly in front of Fan
- D. Increase Fan to 110 Volts
- E. Decrease CO<sub>2</sub> input rate
- F. Determined the affect of increasing relative humidity
- G. New CO<sub>2</sub> cylinder
- H. CO<sub>2</sub> Input off - all power off for 16 hrs
- I. CO<sub>2</sub> Input on - all power on
- J. CO<sub>2</sub> Input off

TABLE XXI  
 TEST DATA, RUN 361-21  
 PIERCED CYLINDER, SEMIPASSIVE EXPOSURE

Configuration Type	<u>Pierced Cylinder(a)</u>	
Li <sub>2</sub> O charge	- g	639
Li <sub>2</sub> O config. size: diam.	- cm	16.3
length	- cm	14.7
volume(b)	- liter	3.07
Configuration density	- g Li <sub>2</sub> O/cc	0.21
Li <sub>2</sub> O density	- g/cc	0.25
Theo CO <sub>2</sub> capacity	- g	942
Sample weight gain	- g	809.8
Total CO <sub>2</sub> feed	- g	698
Average CO <sub>2</sub> feed	- g/hr	22.1
2% breakthrough:		
Time	- hr	14.0
g CO <sub>2</sub> feed/g Li <sub>2</sub> O charge		0.644
cumulative avg. CO <sub>2</sub> feed	- g/hr	29.4
Final CO <sub>2</sub> concentration	- %	2.8
Total run time	- hr	31.5
Product analysis:		
% Li <sub>2</sub> O		0
% Li <sub>2</sub> CO <sub>3</sub>		74.2
% LiOH		19.7
% LiOH·H <sub>2</sub> O		6.1

Notes: (a) 29 axial holes, each 1.0 cm diameter

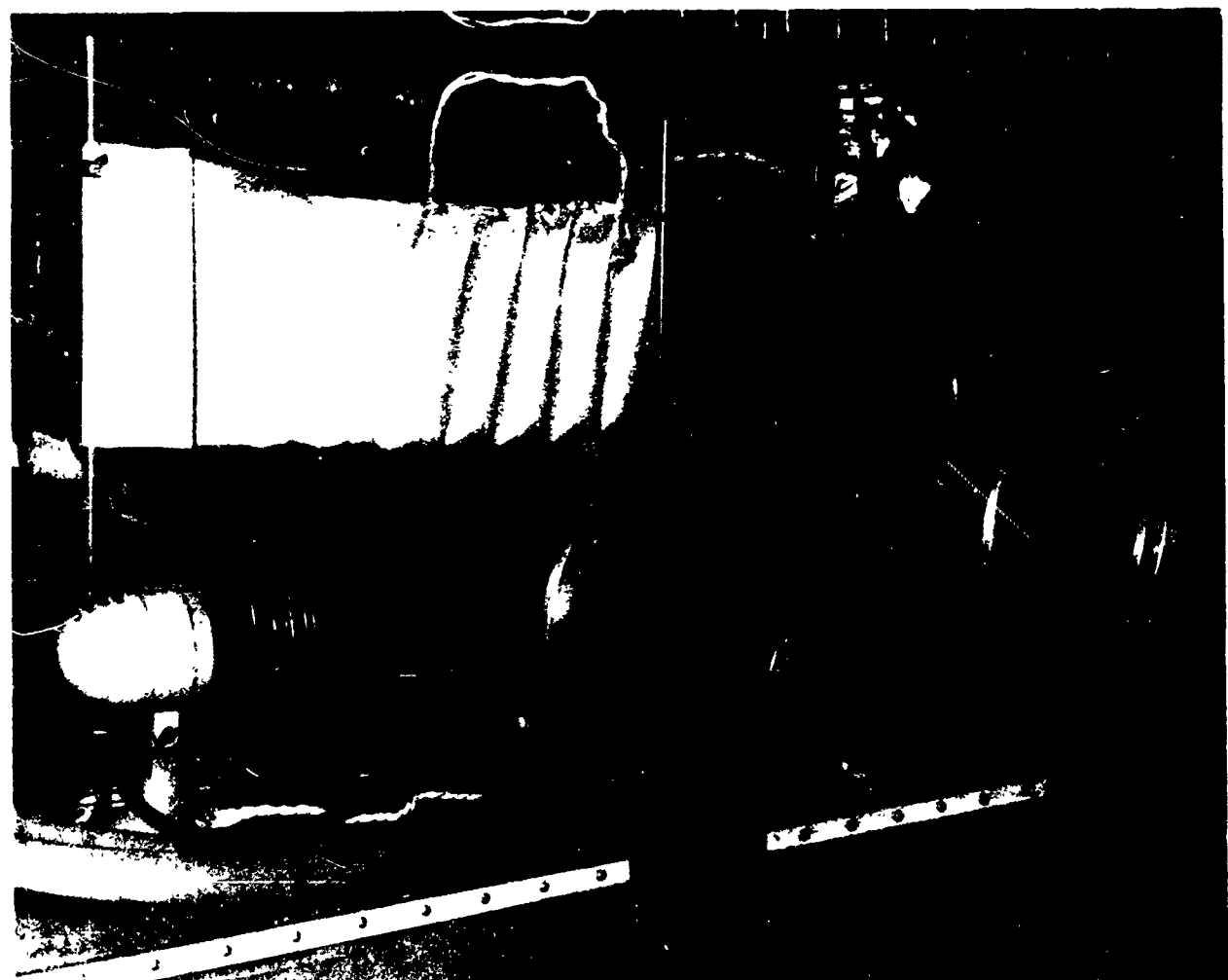


Fig. 45. Apparatus Arrangement, Passive Belt Configuration

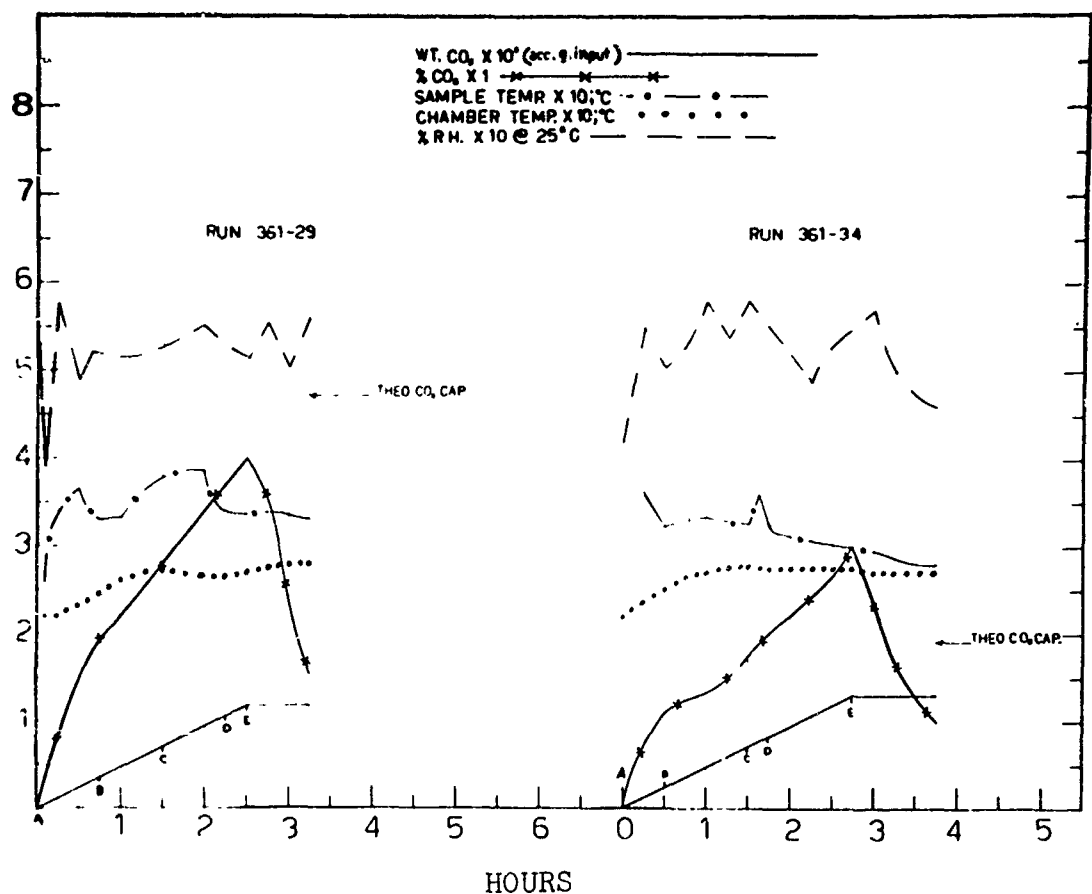


Fig. 46. Test Profiles (Runs 361-29 and 361-34)

Notes: A Fan at 55 V  
 B Fan at 110 V  
 C Fan at 55 V  
 D Fan at 110 V  
 E CO<sub>2</sub> Input off

Configuration type Run No.	Granule Belt	
	<u>361-29</u>	<u>361-34</u>
Granule mesh size	4 by 10	10 by 30
Li <sub>2</sub> O charge	- g	321      129
Configurations:		
Total belt length	- cm	76      76
number of pouches		11      22
width empty pouch	- cm	6.2      3.0
pouch bed height	- cm	20      20
Li <sub>2</sub> O bulk density	- g/cc	0.26      0.29
Gas velocity	- m/min	(a)      (a)
Theo. CO <sub>2</sub> capacity	- g	473      191.5
Sample weight gain	- g	46.5      167.4
Total CO <sub>2</sub> feed	- g	117.8      128.2
Average CO <sub>2</sub> feed	- g/hr	47.1      46.9
2% breakthrough:		
Time	- hr	0.83      1.75
g CO <sub>2</sub> feed/g Li <sub>2</sub> O charge		0.124      0.638
Final CO <sub>2</sub> concentration	- %	4      3
Total run time	- hr	2.5      2.75
Product analysis:		
% Li <sub>2</sub> O	33.6	0
% Li <sub>2</sub> CO <sub>3</sub>	43.1	76.4
% LiOH	23.4	20.7
% LiOH·H <sub>2</sub> O	0	2.9

Notes: (a) Gas velocities with fan at 55 volts, 7.6 m/min parallel and 3.0 m/min perpendicular to belt.  
At 110 volts, 30.4 m/min parallel and 14.6 m/min perpendicular.

similarly testing two narrow pouch type belts containing low (0.14 g/cc) and high (0.24 g/cc) bulk density 10- by 30-mesh granules. The belts were made of multifilament polypropylene fabric because of superior dust retention (table XIX, fabric b versus fabric a) although ASTM air permeability at 0.59 m<sup>3</sup>/min was only half that of the previous fabric. Pouch side seams were sewn with Nylon thread and the tops were sealed by folding over and stapling. To compensate for the reactivity difference caused by bulk density difference, a greater charge of high density granule was used. Also, pouches of the high-density belt (run 361-46) were only partially filled to increase granule and cloth exposure area. The resulting test profiles, figures 47 and 48 were almost identical. The test data of table XXIII indicate performance of the low density configuration was best.

Passive Eight Hour Mission: Run 397-1

A belt design was selected compromising the advantages and penalties established by previous tests. The resulting configuration was passively exposed to a constant rate of CO<sub>2</sub> input of 49.1 g/hr through the entire run. The run profile is shown in figure 49. Table XXIV gives configuration design details and test data.

Dynamic Test: Runs 361-48 and 390-6

The performance of granular beds at two bulk densities, 0.26 and 0.35 g/cc, was tested using the induced draft canister illustrated in figure 32 and described in section III. Figure 50 shows the apparatus arrangement with the canister located in position A (figure 35). The canister blower discharge was

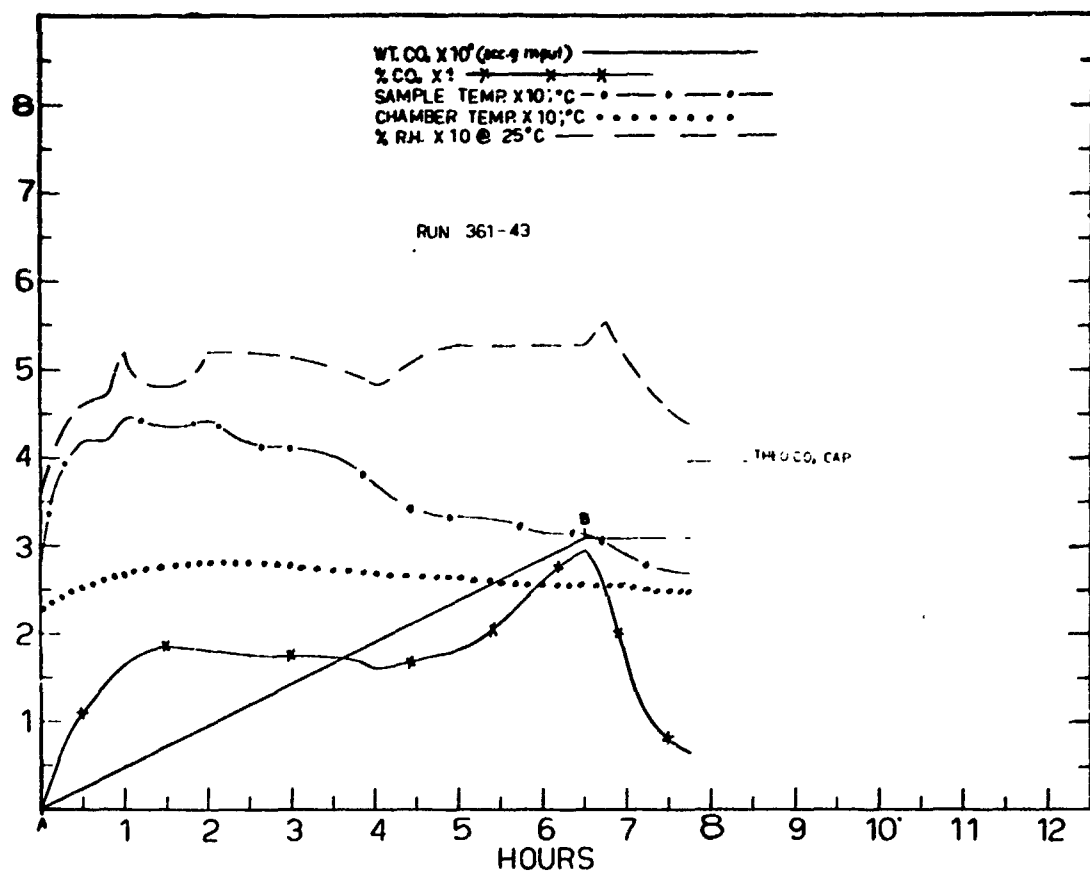


Fig. 47. Test Profiles (Run 361-43)

Notes: A. Start CO<sub>2</sub> Input - Fan at 50 Volts

B. End CO<sub>2</sub> Input

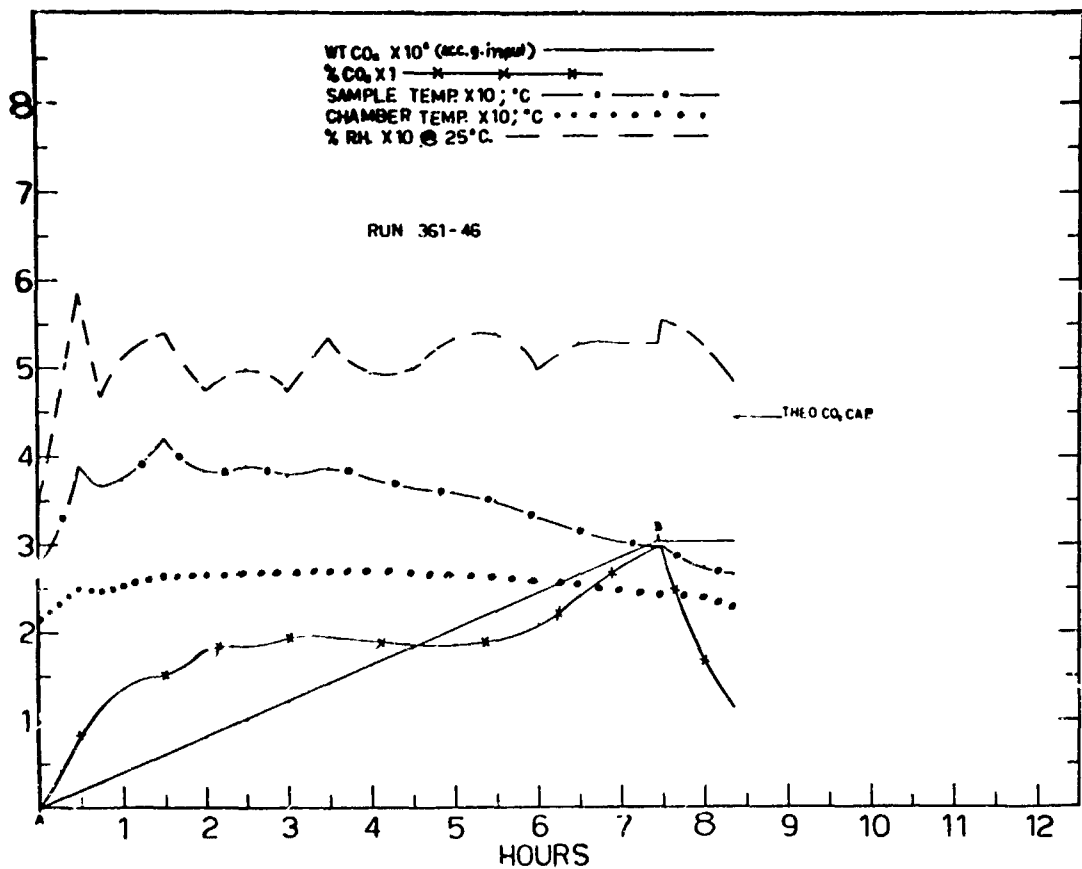


Fig. 48. Test Profiles (Run 361-46)

Notes: A. Start CO<sub>2</sub> Input - Fan at 50 Volts  
 B. End CO<sub>2</sub> Input

TABLE XXIII  
TEST DATA, RUNS 361-43 AND 361-46  
GRANULE BELT, PASSIVE EXPOSURE

Configuration type Run No.	Granule Belt	
	<u>361-43</u>	<u>361-46</u>
Granule mesh size	10 by 30	10 by 30
Li <sub>2</sub> O charge	- g	270.4
Configuration:		
Total belt length	- cm	114
number of pouches		30
width empty pouch	- cm	3.8
pouch bed height	- cm	20
		13
Li <sub>2</sub> O bulk density	- g/cc	0.14
Theo. CO <sub>2</sub> capacity	- g	398
Sample weight gain	- g	342.4
Total CO <sub>2</sub> feed	- g	309.5
Average CO <sub>2</sub> feed	- g/hr	47.6
2% breakthrough:		
Time	- hr	5.25
g CO <sub>2</sub> feed/g Li <sub>2</sub> O charge		0.913
Final CO <sub>2</sub> concentration	- %	2.9
Total run time	- hr	6.5
Product analysis:		
% Li <sub>2</sub> O	0	0
% Li <sub>2</sub> CO <sub>3</sub>	84.0	77.5
% LiOH	7.0	22.0
% LiOH·H <sub>2</sub> O	8.9	0.5

Note: Gas velocities with fan at 55 volts, 6.1 m/min parallel and 3.0 m/min perpendicular to belt.

TABLE XXIV  
TEST DATA RUN 397-1  
GRANULE BELT, PASSIVE 8-HOUR MISSION

Configuration type	<u>Granule Belt</u>	
Granule mesh size		10 by 30
Li <sub>2</sub> O charge	- g	540.8
Configuration:		
Total belt length(a)	- cm	140
number of pouches		38
width empty pouch	- cm	3.8
pouch bed height	- cm	20
pouch bed thickness	- cm	1.5
Li <sub>2</sub> O bulk density	- g/cc	0.19
Theo. CO <sub>2</sub> capacity	- g	796
Sample weight gain	- g	634.8
Total CO <sub>2</sub> feed	- g	555
Average CO <sub>2</sub> feed rate	- g/hr	49.1
%% breakthrough:		
Time	- hr	9.0
g CO <sub>2</sub> feed/g Li <sub>2</sub> O charge		0.808
Final CO <sub>2</sub> concentration	- %	2.85
Total run time		11.5
Product Analysis:		
% Li <sub>2</sub> O		0
% Li <sub>2</sub> CO <sub>3</sub>		78.3
% LiOH		10.9
% LiOH·H <sub>2</sub> O		10.8

Notes: (a) Belt fabric multifilament polypropylene,  
0.59 m<sup>3</sup>/min ASTM air permeability.  
Gas velocities 6.1 m/min parallel and 3.0  
m/min perpendicular to belt.

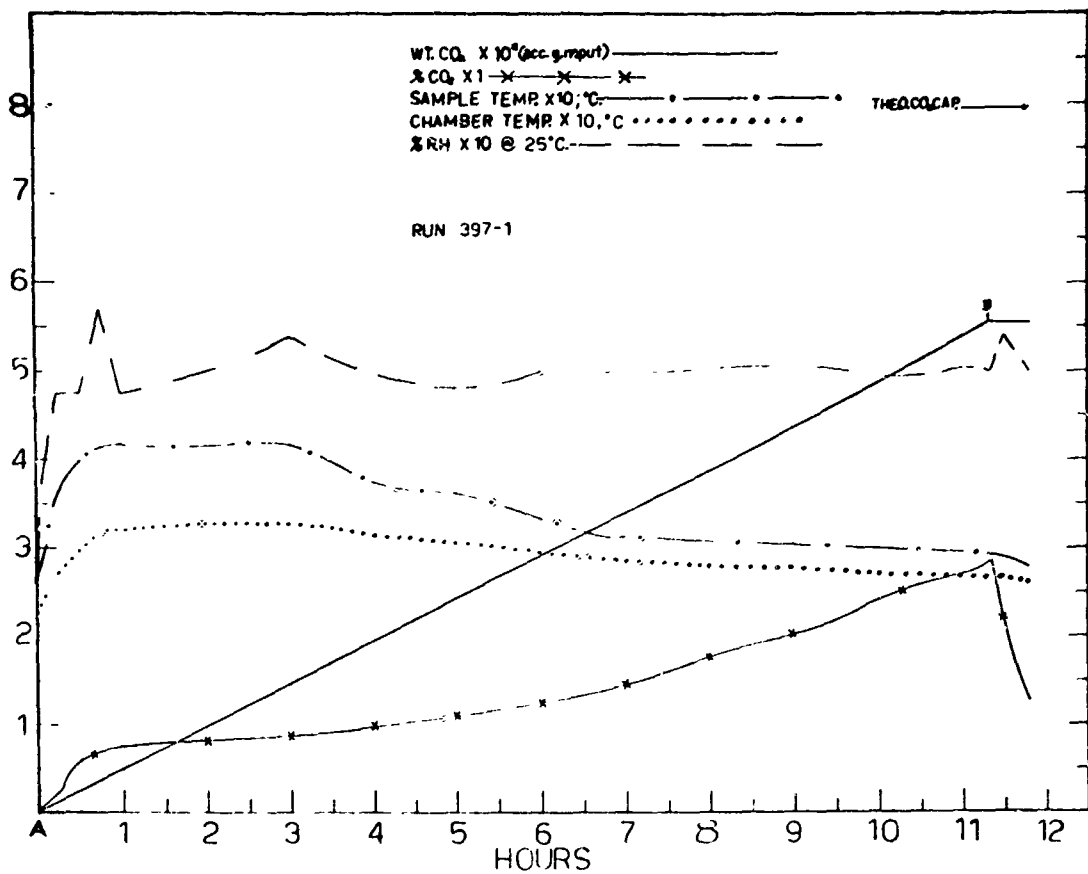


Fig. 49. Test Profiles, Passive 8-Hour Mission (Run 397-1)

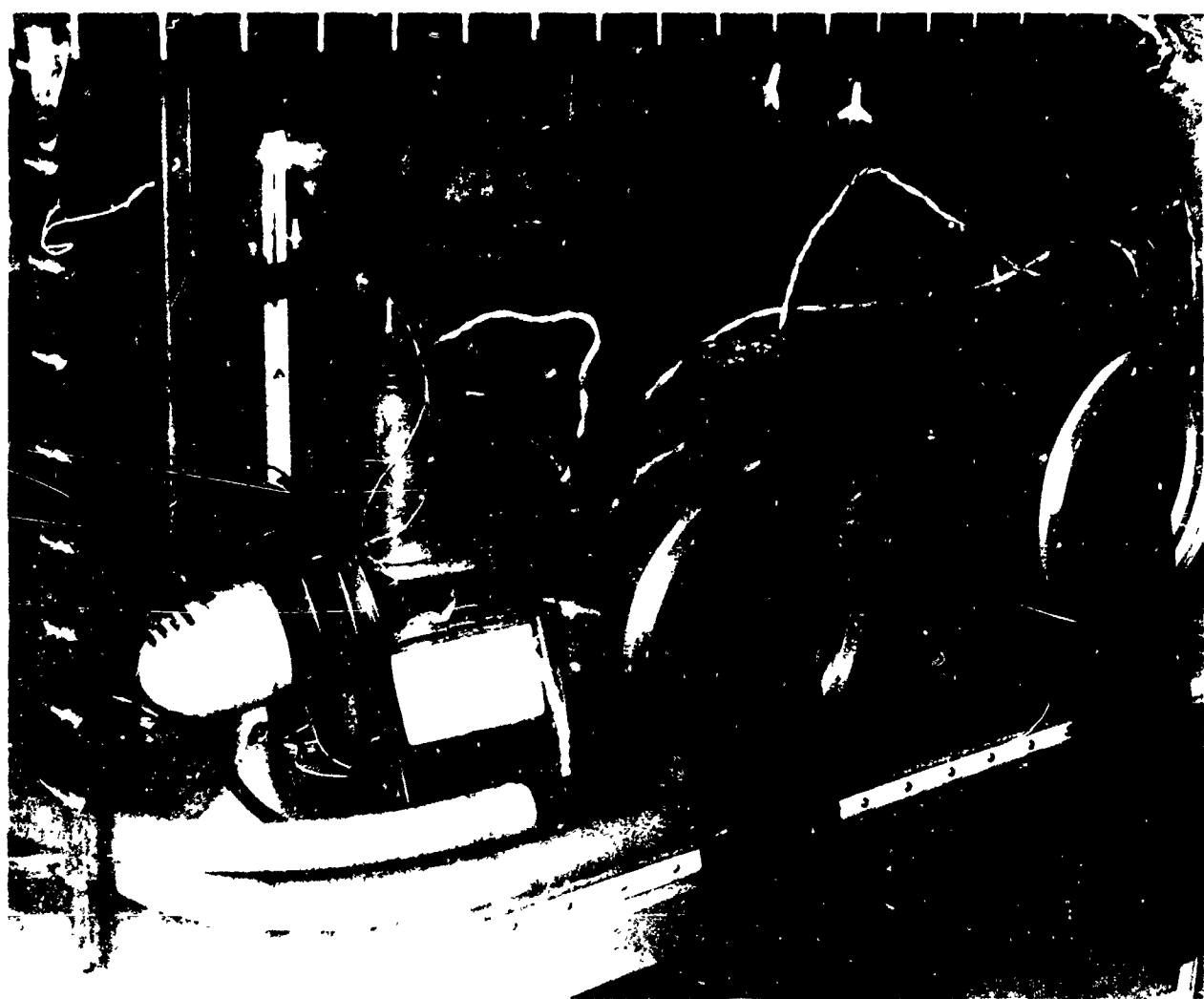


Fig. 50. Apparatus Arrangement, Dynamic Granular Bed

directed toward the suction side of the humidity control circuit so that most of the reaction heat was promptly removed. The chamber circulating fan was left on during tests. Maximum gas velocity measured in the chamber, excluding the canister blower discharge region, was 3 m/min. As shown in the low density bed profiles (Run 361-48) of figure 51, high initial canister exhaust temperature reflected ample moisture availability and rapid  $\text{CO}_2$  absorption. Bulk density of the second bed (0.35 g/cc, Run 390-6) was clearly too high for reactivity. Bed characteristics and test data are given in table XXV. Dismantling and inspection on test completion (Run 361-48) revealed no evidence of granule sintering anywhere in the bed. The test results coupled with the findings of section III suggest that granular bulk densities up to about 0.3 g/cc are feasible at appropriate gas flow rates through the bed. The estimated conditions for maintaining 1%  $\text{CO}_2$  concentration with 46 g/hr  $\text{CO}_2$  feed over an 8-hour mission are 350 g of 4- by 10-mesh  $\text{Li}_2\text{O}$  at 0.25 to 0.28 g/cc bulk density. Gas volume recirculated through the bed should be at least 200 liters/min. With  $\text{CO}_2$  partial pressure at 7.6 mm Hg, moisture partial pressure in the chamber should be 11 mm Hg minimum based on the finding that 1.44  $\text{H}_2\text{O}/\text{CO}_2$  molar ratio is required for efficient absorption.

Semipassive Test: Run 397-3

A granular oxide supported bed configuration consisting of concentric cylindrical beds was fabricated from 12 mesh polypropylene netting. Axial gas flow channels were provided between the beds and between the outermost bed and its aluminum

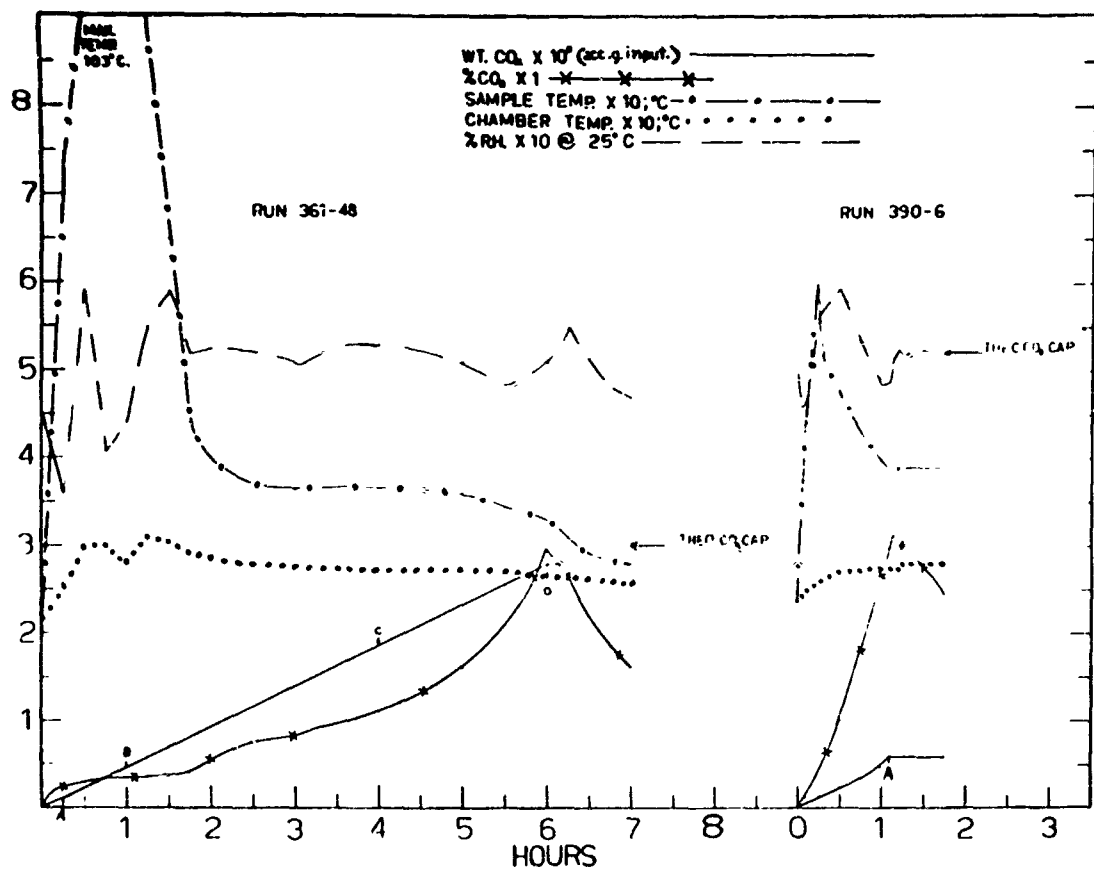


Fig. 51. Test Profiles (Runs 361-48 and 390-6)

Configuration type Run No.	Granular Bed	
	361-48	390-6
Granule mesh size	4 by 10	4 by 14
Li <sub>2</sub> O charge	- g	205 354.4
Configuration:		
bed diameter	- cm	13.4
bed depth	- cm	5.7
initial gas flow	- liters/min	190 (c)
pressure loss (a)	- cm H <sub>2</sub> O	0.63 (b)
Li <sub>2</sub> O bulk density	- g/cc	0.256 0.348
Theo. CO <sub>2</sub> capacity	- g	302 522
Sample weight gain	- g	289.2 44.6
Total CO <sub>2</sub> feed	- g	280.5 50.9
Average CO <sub>2</sub> feed	- g/hr	46.7 46.2
2% breakthrough		
Time	- hr	5.4
g CO <sub>2</sub> feed/g Li <sub>2</sub> O charge		1.227 0.115
Final CO <sub>2</sub> concentration	- %	2.95 2.98
Total run time	- hr	6.0 1.1
Product analysis:		
% Li <sub>2</sub> O	0	83.0
% Li <sub>2</sub> CO <sub>3</sub>	89.6	12.4
% LiOH	2.1	4.6
% LiOH·H <sub>2</sub> O	8.3	0

Notes: (a) Initial pressure loss through Li<sub>2</sub>O bed only, filters removed.  
 (b) Initial pressure loss with filters and hardware in was 1.65 cm H<sub>2</sub>O, increasing to 2.54 cm H<sub>2</sub>O after 4 hours.  
 (c) Declined to 170 liters/min as pressure loss increased.  
 Absorber hardware (case, blower, filters, etc.) weight 623 g

case. Figures 52 and 53 show the assembly. Of necessity, the beds were filled with relatively low assay oxide (84.6%  $\text{Li}_2\text{O}$ , 10.4%  $\text{LiOH}$ , 5.0%  $\text{Li}_2\text{CO}_3$ ), but this apparently was not detrimental to overall performance. Filling holes in the netting were plugged with glass wool. A few oxide granules came through the netting during handling but, as previously demonstrated, a much finer mesh is feasible. Table XXVI gives dimensions of the unit and the gas velocities imparted by a propellor fan connected by duct to one end of the case. The test setup is shown in figure 54. Gas temperature was measured at the exhaust end between the No. 2 and 3 beds. The unit contained no filters, and pressure loss through it was low, about 0.3 cm  $\text{H}_2\text{O}$  at 0.9 to 1.5  $\text{m}^3/\text{min}$  gas flow (30 to 50 cfm) and 21.2 watts power to the fan. Table XXVII gives test data and figure 55 shows profiles. The unit, exposed to constant rate  $\text{CO}_2$  input of 48.9 g/hr maintained 1% or less  $\text{CO}_2$  concentration over eight hours.

## 5. ANALYSIS OF RESULTS

For granular  $\text{Li}_2\text{O}$ , test experience indicates a good bulk density compromise between reactivity and volume efficiency is 0.20 g/cc for passive exposure and 0.26 g/cc for semipassive or dynamic exposure. Depending on gas velocity, the density under dynamic exposure can be somewhat higher but the maximum appears to be about 0.28 g/cc. These values are initial reference points, since the optimum bulk density as related to an overall system will vary with mission length, power availability, and the relative importance of weight versus volume constraints.

A rough appraisal of passive versus dynamic configuration

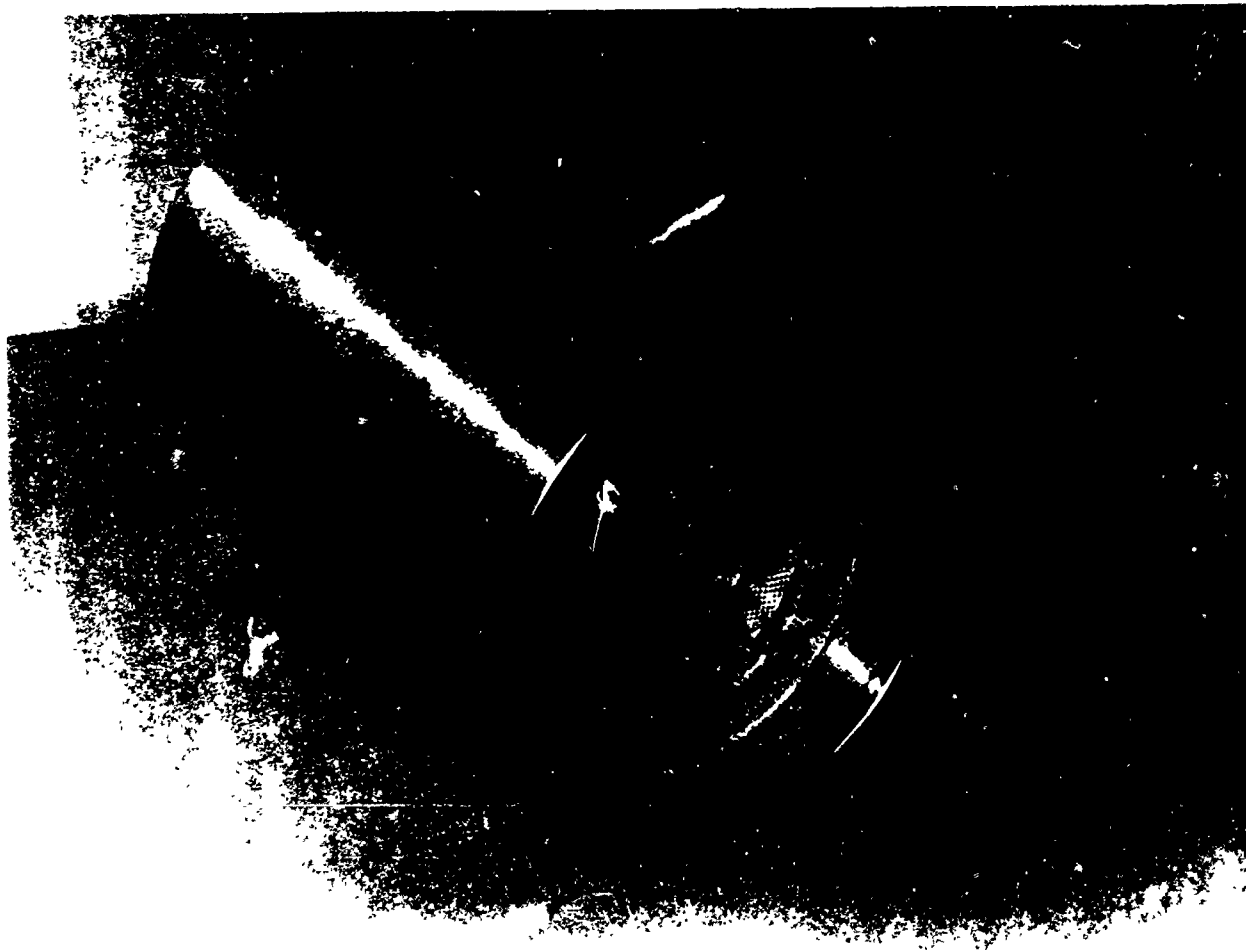


Fig. 52. Semipassive Granular Configuration



Fig. 53. Granular  $\text{Li}_2\text{O}$  Bed For Semipassive Configuration

TABLE XXVI  
CONFIGURATION DIMENSIONS AND GAS VELOCITIES, RUN 397-3

Li <sub>2</sub> O Cylinder No.	Bed Dimensions			Bed Volume cc
	Outside Diam. cm	Inside Diam. cm	Length cm	
1	4.2	2.0	20	200
2	7.4	5.4	20	400
3	11.6	9.0	20	840
4	16.6	13.5	20	1460
Case	---	17.5	30	---

Fan Power	Chamber Gas Velocity Parallel To Main Flow		
	- watts	8.3	21.2
Location (a):			
Behind Fan	- m/min	3.0	5.5
Corner No. 1	- m/min	6.1	8.8
Corner No. 2	- m/min	3.6	7.0
Position A	- m/min	10.0	13.4
Corner No. 3	- m/min	3.4	8.2
Center of Chamber	- m/min	1.5	6.1

Fan Power	Gas Velocity At Li <sub>2</sub> O Bed Exit		
	- watts	8.3	21.2
Location (b)			
Bed centerline	- m/min	13.7	61.0
2.5 cm from center	- m/min	6.1	15.2
5.1 cm from center	- m/min	3.0	15.2
7.6 cm from center	- m/min	21.3	47.0

Notes: (a) Chamber locations as defined in figure 21.  
 (b) Velocity traverse across bed exit face, location measured from axial centerline of bed.

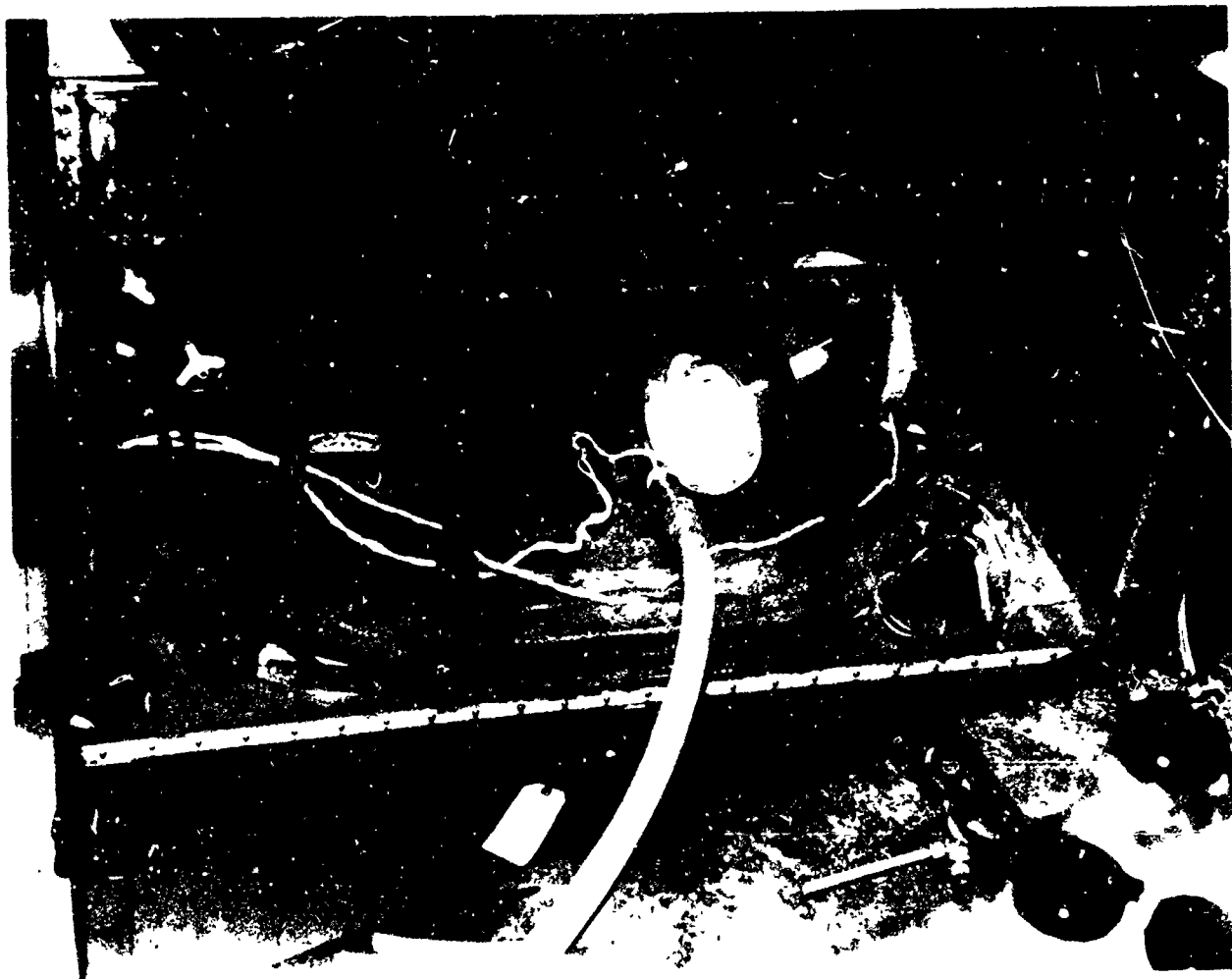


Fig. 54. Apparatus Arrangement, Semipassive Test

TABLE XXVII  
TEST DATA, SEMIPASSIVE 8-HOUR MISSION,  
RUN 397-3

Configuration type	<u>Concentric Cylinders</u>	
Granule mesh size		4 by 10
Li <sub>2</sub> O charge	- g	768.5
Li <sub>2</sub> O bulk density	- g/cc	0.26
Configuration density	- g Li <sub>2</sub> O/cc	0.152 (a)
Theo. CO <sub>2</sub> capacity	- g	1030 (b)
Sample weight gain	- g	949.4
Total CO <sub>2</sub> feed	- g	930
Average CO <sub>2</sub> feed	- g	48.9
2% breakthrough:		
Time g CO <sub>2</sub> feed/g Li <sub>2</sub> O charge	- hr	18.0 1.144 (c)
Final CO <sub>2</sub> concentration	- %	2.83
Total run time	- hr	19.0
Product analysis:		
% Li <sub>2</sub> O		0
% Li <sub>2</sub> CO <sub>3</sub>		91.3
% LiOH		4.5
% LiOH·H <sub>2</sub> O		4.2

Notes: (a) Based on volume of external case  
 (b) Based on sample analysis 84.6% Li<sub>2</sub>O and 10.4% LiOH  
 (c) Based on sample weight

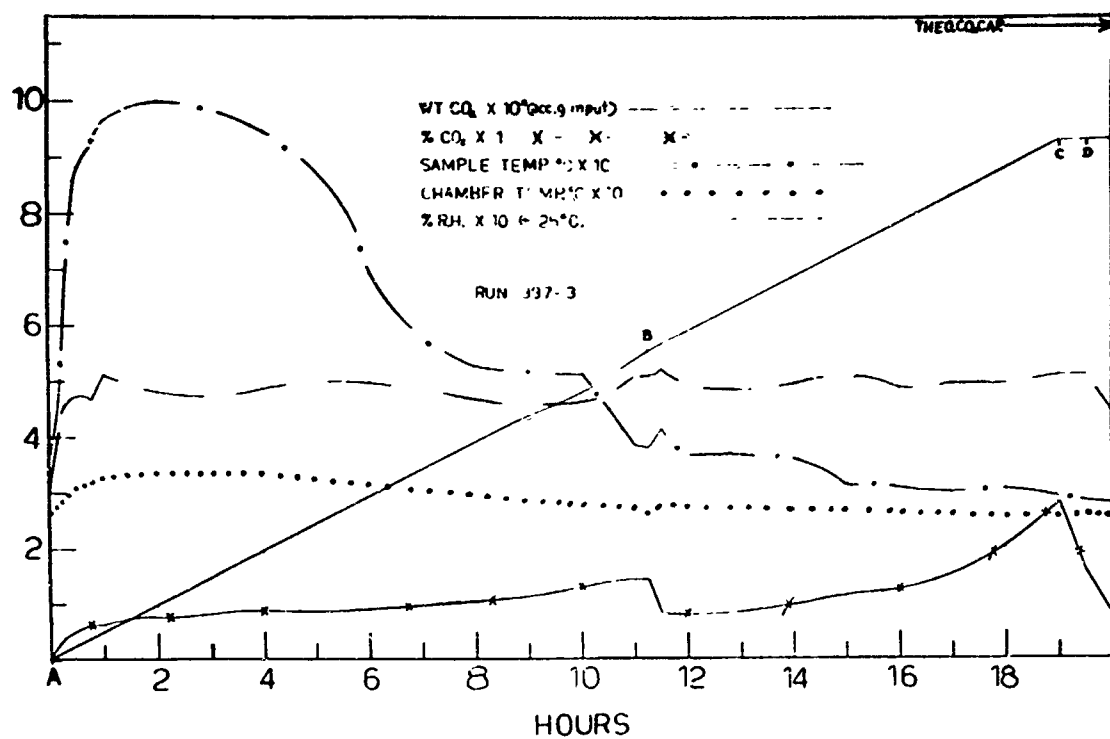


Fig. 55. Test Profiles, Semipassive 8-Hour Mission  
(Run 397-3)

Notes:

- A. Fan power, 8.3 watts
- B. Fan power, 21.2 watts
- C. CO<sub>2</sub> input off
- D. Power off

can be derived by extrapolating test results to a 9-hour run terminating at 2%  $\text{CO}_2$  breakthrough as shown in table XXVIII. Under these conditions the estimates indicate the passive belt system is advantageous from a weight standpoint but inferior on a volume basis.

Dynamic system weight performance would improve in missions requiring larger  $\text{Li}_2\text{O}$  charges. For example the dynamic  $\text{CO}_2$  absorption unit reported under Contract No. AF 33(615)-1588, if filled with 4- by 10-mesh  $\text{Li}_2\text{O}$  at 0.25 g/cc, would contain about 2100 g of absorbent and have a total weight of 3150 g. With about 80% utilization as indicated by Run 361-48, this  $\text{Li}_2\text{O}$  charge would remove 2500 g  $\text{CO}_2$  yielding a weight performance of 0.79 g  $\text{CO}_2$ /g system weight. The weight performance of passive belt systems would probably improve slightly in longer missions. Although the fabric to  $\text{Li}_2\text{O}$  weight ratio would remain essentially constant for larger belts, it seems likely that oxide utilization would improve as additional area was exposed to the atmosphere.

Absorbent-grade  $\text{LiOH}$  meeting specification MIL-L-20213D has a minimum capacity of 0.75 g  $\text{CO}_2$ /g  $\text{LiOH}$  but commonly absorbs 0.8 g/g before 2% breakthrough. In comparison, the oxide forms reported herein performed as follows to 2% breakthrough--

- a. 0.8 g  $\text{CO}_2$ /g  $\text{Li}_2\text{O}$  for a granular belt configuration under passive exposure (Run 397-1).
- b. 1.14 g  $\text{CO}_2$ /g  $\text{Li}_2\text{O}$  for a granular bed, concentric cylinder configuration under semipassive exposure (Run 397-3), representing 42% weight improvement.

TABLE XXVIII  
COMPARISON OF PASSIVE BELT AND DYNAMIC BED

Configuration type		Passive belt-pouch	Dynamic flow-through packed bed
Run No.		397-1	361-48
Granule mesh size		10 by 30	4 by 10
Li <sub>2</sub> O bulk density	- g/cc	0.190	0.256
CO <sub>2</sub> feed rate	- g/hr	49.1	46.7
At 2% breakthrough:			
cumulative CO <sub>2</sub> feed	- g	442	252
time	- nr	9.0	5.4
Li <sub>2</sub> O charge	- g	541	205
Comparison basis:		test data only	extrapolated test data
At 2% breakthrough, 9 hr:			
cumulative CO <sub>2</sub> feed	- g	442	419
Li <sub>2</sub> O charge	- g	541	341
hardware weight	- g	226 (a)	623 (a)
system weight	- g	767	964
Li <sub>2</sub> O bulk volume	- cc	2850	1335
System performance			
g CO <sub>2</sub> feed/g system weight		0.58	0.43
g CO <sub>2</sub> feed/cc Li <sub>2</sub> O bulk volume		0.16	0.31

Notes: (a) Includes fabric weight for passive system; case, blower, filters and screens for dynamic system.

c. 1.23 g CO<sub>2</sub>/g Li<sub>2</sub>O for a granular-packed bed configuration under dynamic exposure (Run 361-48), representing 52% weight improvement.

SECTION V  
TESTS AT ONE-THIRD ATMOSPHERE

1. GENERAL CONSIDERATIONS

The performance of  $\text{Li}_2\text{O}$  configurations under one-third normal pressure and in an oxygen atmosphere is of interest since these conditions are frequently selected for space capsule environments. The three basic modes of operation--passive, semi-passive, and dynamic, were investigated using configurations and oxide forms judged best from tests at normal pressure. Partial pressures of the constituent gases in the test atmosphere selected were 160 mm Hg  $\text{O}_2$ , 11 mm Hg  $\text{H}_2\text{O}$ , and 7.6 mm Hg  $\text{CO}_2$ .

2. APPARATUS

A low-pressure test chamber was assembled from two bell jars and fitted with instrumentation and a 100 liters/min gas recirculation circuit as shown in figure 56. Chamber  $\text{CO}_2$  concentration was determined by measuring per cent transmission through a gas cell with sodium chloride windows at 4.2 microns wave length. Transmission was calibrated with 0, 0.5, 1.0, and 4.0%  $\text{CO}_2$  in oxygen (corrected to 760 mm Hg pressure) using a spectrophotometer (Perkin-Elmer Infracard Model 137B, Perkin-Elmer Corp., Norwalk, Conn.). Traps were located just upstream of the vacuum pump to absorb  $\text{CO}_2$  and  $\text{H}_2\text{O}$  lost during any pressure adjustments. The chamber and piping were evacuated and purged with dry oxygen for 15 minutes before starting each test.

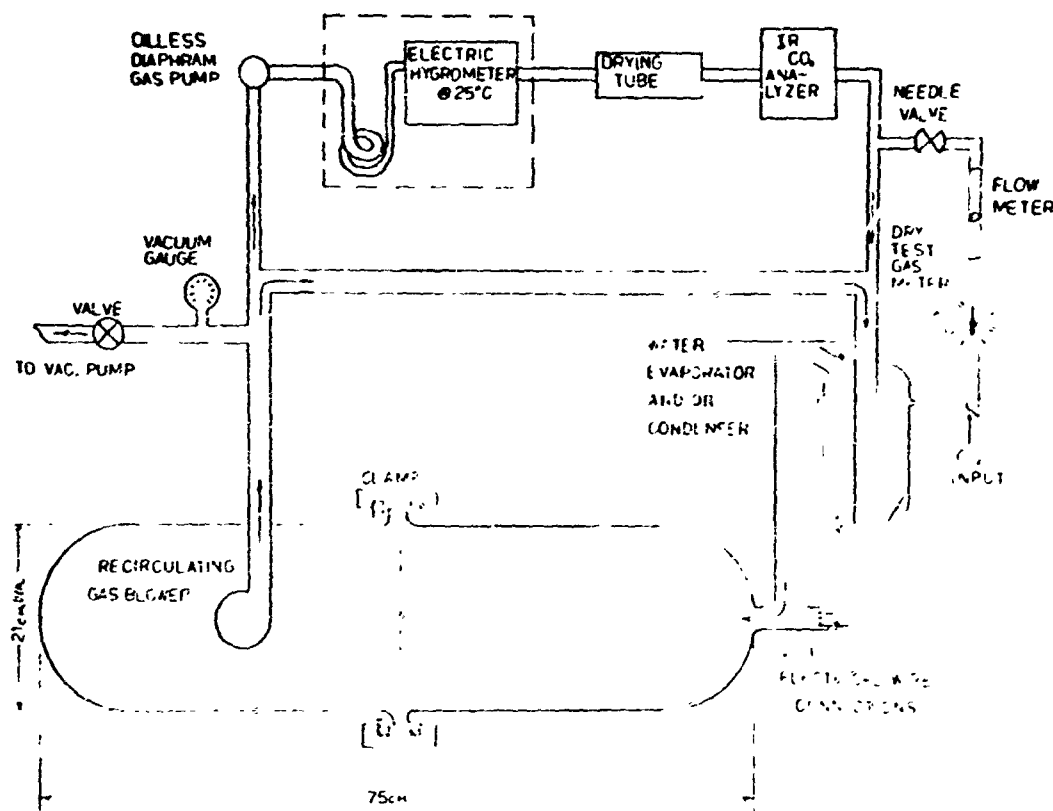


Fig. 56. Apparatus Arrangement, One-third Atmosphere Tests

### 3. CONFIGURATION TESTS

#### a. Dynamic Exposure, Packed Granular Bed Run 397-16

The dynamic test canister (described in section III and figure 32), charged with 376 g of 4- by 10-mesh granules at 0.23 g/cc bulk density, was tested with chamber gas circulating at 190 liters/min. The run was terminated when the canister inlet screen failed because of excessive localized temperature (225 °C or higher). Up to this point, feed rates indicated 76.0 g CO<sub>2</sub> and 39.4 g H<sub>2</sub>O had been absorbed, corresponding to 1.26 H<sub>2</sub>O/CO<sub>2</sub> molar ratio. Test data were as follows:

Time hrs:min	Effluent gas temp °C	% R.H. at 25 °C	Cumulative CO <sub>2</sub> Input g	Chamber Pressure mm Hg	Chamber CO <sub>2</sub> %
0:30	56	10	23.5	159	0.12
0:45	60	26	36.2	174	0.30
1:00	67	4	48.0	174	0.03
1:15	89	50	60.6	189	0.45
1:30	130	43	76.0	191	0.55

Inspection of the bed indicated the CO<sub>2</sub> concentration increase logged at 1.25 hr resulted from sintering and gas channeling. Samples drawn from sintered regions of the bed had the following analysis:

Sample Appearance	% Li <sub>2</sub> CO <sub>3</sub>	% Li <sub>2</sub> O	% LiOH
Fused solid	46.7	41.6	11.7
sintered granules	31.7	29.8	38.9
unsintered granules	17.9	63.7	18.4

The apparatus arrangement, in which the canister inlet directly faced the test chamber gas inlet, apparently caused the difficulty. Feed gas containing CO<sub>2</sub> and moisture (100% R.H., in an attempt to increase low humidity in the chamber) had little chance to mix with the chamber gas. The resulting high CO<sub>2</sub> concentration stream directed at the bed face caused localized overheating. Time limitations precluded a test re-run.

b. Passive Exposure, Granular Belt  
Run 390-46

A tight-weave fabric belt configuration was tested. Because of test chamber space limitations the belt was simply laid along the jar wall length and being flexible, conformed to its curvature. Although only half its area was thus directly exposed to the gas stream, performance was apparently unaffected. Test data are given in table XXIX and profiles in figure 57. One notable difference from the passive belt exposure at one atmosphere (as reported in section IV, figure 49) was higher fabric temperature. Reaction zone movement along the belt, starting from the chamber gas inlet end, could be observed by a progressive yellowing of the belt. Generally, chamber CO<sub>2</sub> concentration ran lower than in the one atmosphere test. Lower resistance to CO<sub>2</sub> diffusion within the granule pores because of fewer inert molecules in the carrier gas may have been a significant factor. Absorption was initially poor as atmosphere humidity could not be maintained in the relatively small chamber because of moisture removal by the oxide. CO<sub>2</sub> feed was

TABLE XXIX

TEST DATA, RUNS 390-46 AND 397-19

GRANULE BELT, PASSIVE EXPOSURE  
PIERCED CYLINDER, SEMIPASSIVE EXPOSURE

Configuration type		<u>Granule Belt(a)</u>	<u>Pierced Cylinder(b)</u>
Run No.		390-46	397-19
Granule mesh size		10 by 30	---
Li <sub>2</sub> O charge	- g	414.6	594.6
Configuration:			
total belt length	- cm	78	---
number of pouches		26	---
width empty pouch	- cm	3.3	---
pouch bed height	- cm	20	---
diameter	- cm	---	13.4
length	- cm	---	14.0
fabric or canister weight	- g	226	246
Li <sub>2</sub> O bulk density	- g/cc	0.19	0.30
Theo. CO <sub>2</sub> capacity	- g	611	875
Sample weight gain	- g	531.3	475
Total CO <sub>2</sub> feed	- g	511	439
Average CO <sub>2</sub> feed rate	- g/hr	44	48
2% breakthrough:			
time	- hr	---	8.2
g CO <sub>2</sub> feed/g Li <sub>2</sub> O charge		1.22	0.664
Final CO <sub>2</sub> concentration	- %	1.45	2.42
Product analysis:			
% Li <sub>2</sub> O		0	18.4
% Li <sub>2</sub> CO <sub>3</sub>		88.8	67.4
% LiOH		8.4	14.1
% LiOH·H <sub>2</sub> O		2.7	0

Notes: (a) Fabric, multifilament polypropylene No. 6720600  
 (b) 44 axial holes, each 0.6 cm diameter, 1.2 cm  
 minimum center to center.

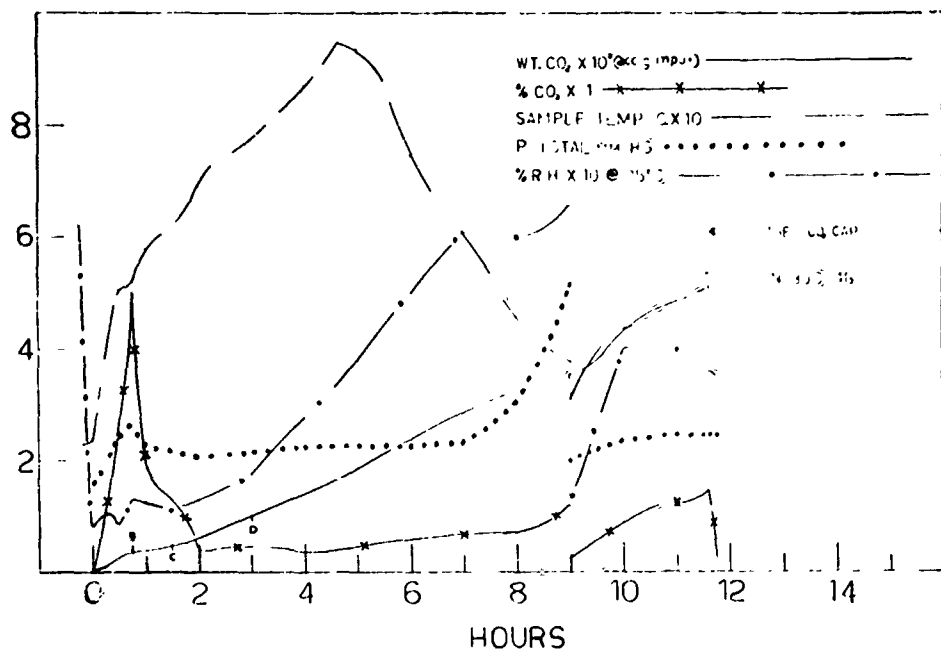


Fig. 57. Test Profiles, Passive 8-Hour Mission At One-third Atmosphere (Run 390-46)

Notes: A. Start CO<sub>2</sub> input  
 B. CO<sub>2</sub> input rate reduced  
 C&D. CO<sub>2</sub> input rate increased - 100% R.H. input  
 E. Leak corrected, no CO<sub>2</sub> lost from system  
 F. CO<sub>2</sub> input off.

increased as humidity recovered and, as shown in the profile, good absorption was realized during the balance of the run.

c. Semipassive Exposure, Pierced Cylinder  
Run 397-19

Two pierced-cylinder configurations were prepared using techniques previously described, and the one appearing structurally superior was tested. To avoid the risk of breaking the piece while stripping it from the mold, the outer cylindrical case was left in place. The axial holes were smooth and without visible cracks or dust. Chamber gas was passed through the unit at 311.5 liters/min, entering at the face marked "1" in the cross-section diagram of figure 58. The exhaust end faced the test chamber gas inlet port. Pressure drop across the shape was 0.25 cm H<sub>2</sub>O. Test data and profiles are given in table XXIX and figure 59. Inspection revealed no evidence of sintering in any portion of the bed. Chemical analyses of samples drawn from various regions of the bed as located in figure 58 are given below. These indicate excellent conversion of the oxide at the surface of the axial holes and in between them.

<u>Composite Sample Location</u>	<u>Li<sub>2</sub>CO<sub>3</sub></u> %	<u>Li<sub>2</sub>O</u> %	<u>LiOH</u> %	<u>LiOH·H<sub>2</sub>O</u> %
(1) bed inlet face	95.8	0	1.6	2.6
(2) between axial holes	89.9	0.7	9.4	0
(3) walls of axial holes	96.6	0	1.4	1.9
(4) near case wall	19.4	53.5	27.1	0
(5) bed exhaust face	92.2	1.4	6.4	0

Because of the axial hole placement and the metal case almost half of the oxide was inaccessible to the gas. About 2%

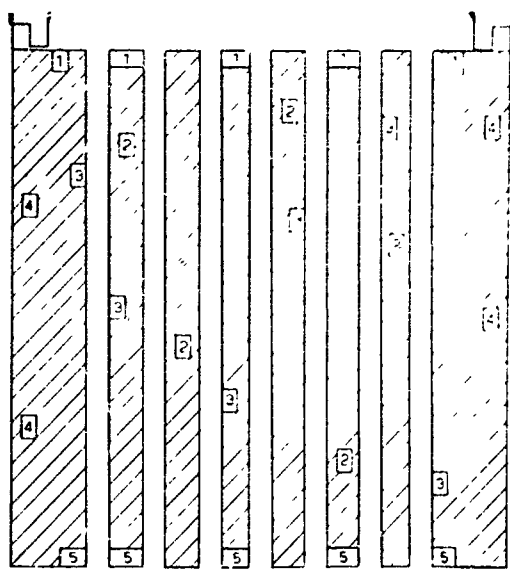


Fig. 58. Cross-section of Pierced Cylinder Configuration

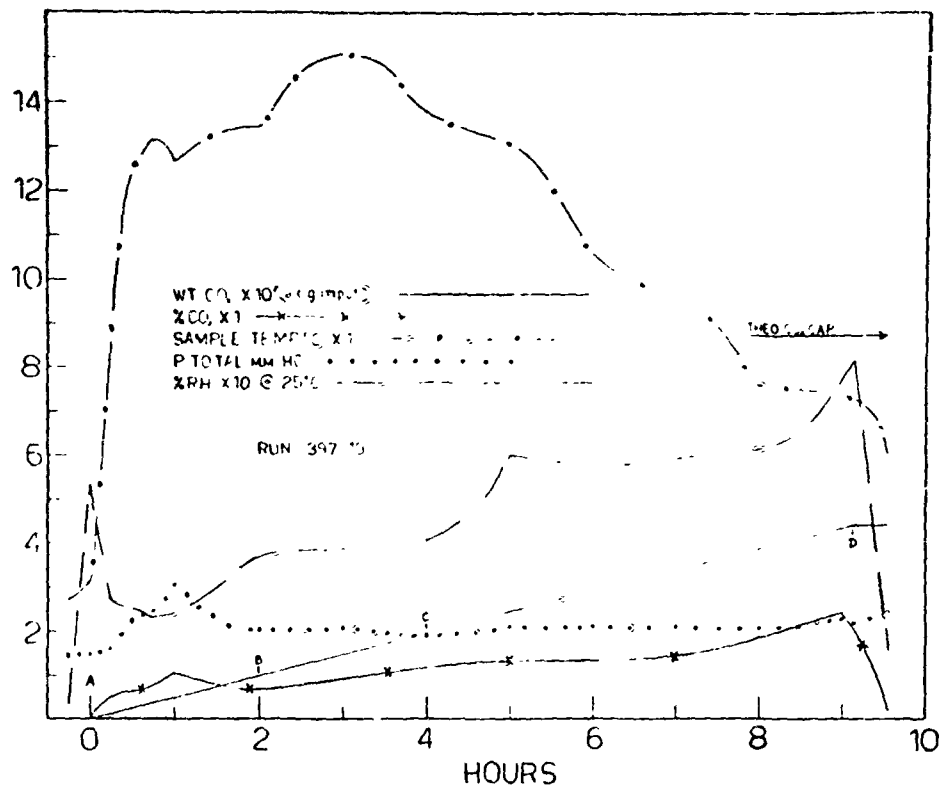


Fig. 59. Test Profiles, Semipassive 8-Hour Mission At One-third Atmosphere (Run 397-19)

Notes: A. Start CO<sub>2</sub> input  
 B. Input recirculating gas at 100% R.H.  
 C. Input recirculating gas below 100% R.H.  
 D. End CO<sub>2</sub> input

more holes, which could easily be located in the outer ring of oxide, would reduce the configuration density (g Li<sub>2</sub>O/cc total cylinder volume) to 0.28 but would also increase utilization to above 90%.

#### 4. ANALYSIS OF RESULTS

The tests indicate lithium oxide based absorption systems are applicable under one-third atmosphere conditions. The passive belt configuration absorbed CO<sub>2</sub> at an average rate of 44 g/hr, and following an initial humidity problem, maintained chamber CO<sub>2</sub> concentration below 1% (7.6 mm Hg) for about 6 hours. Oxide conversion to carbonate was almost 90%. The semipassive, pierced-cylinder configuration averaged 48 g/hr CO<sub>2</sub> absorption, and its conversion can be readily increased by providing additional flow channels. This porous, solid configuration appears to have excellent potential. In future work, structural strength might be further improved by providing a matrix of inert fibrous material in the Li<sub>2</sub>O<sub>2</sub> before decomposing. Testing of the dynamic-packed bed configuration was prematurely terminated, but the initial data indicate high CO<sub>2</sub> absorption rate. The sintering resulting from a high concentration CO<sub>2</sub>-H<sub>2</sub>O stream indicates design of the gas intake and its location relative to the CO<sub>2</sub> source are important. Bed intake area should be large so the reaction and corresponding heat are not localized. In general, operating at one-third atmosphere versus normal pressure resulted in lower chamber CO<sub>2</sub> concentration and higher temperatures.

## SECTION VI

### EFFECT OF ATMOSPHERE COMPOSITION

#### 1. GENERAL CONSIDERATIONS

Excluding CO<sub>2</sub> and moisture, closed environmental systems may be based on three types of atmospheres: O<sub>2</sub>, O<sub>2</sub>-N<sub>2</sub>, and O<sub>2</sub>-He. An oxygen partial pressure close to 160 mm Hg is a requirement of any system (reference 10). The effect of these atmosphere variations on CO<sub>2</sub> absorption is of interest. This was investigated by the gravimetric analysis technique, using small samples of granular Li<sub>2</sub>O passively exposed to the various gas compositions at 50% relative humidity. The effect of humidity variations in the O<sub>2</sub> and O<sub>2</sub>-N<sub>2</sub> systems was also studied. Since moisture is a prime factor during initial absorption, the merit of partially hydrating the oxide before exposure was explored.

#### 2. APPARATUS

Three-gram samples of 10- by 30-mesh Li<sub>2</sub>O, contained in a 1.2 cm diameter by 16 cm high basket of 100-mesh (43.5% open area), stainless steel screen, were suspended in the gravimetric apparatus (described in section I and figure 2). The sample depth was about 9.8 cm and gas flow was 2.8 liter/min equivalent to 520 cm/min velocity based on the chamber cross-section. Premixed gas cylinders: 1% CO<sub>2</sub> - 99% O<sub>2</sub>; 1% CO<sub>2</sub> - 21% O<sub>2</sub>-78% He; and 1% CO<sub>2</sub> - 21% O<sub>2</sub>-78% N<sub>2</sub> were purchased from the Mathieson Company. Humidity was controlled by a series of sulfuric acid (H<sub>2</sub>SO<sub>4</sub>) solutions with their densities checked before and after the runs.

### 3. EXPERIMENTAL DATA

Table XXX gives data and reaction product analyses for three series of tests:

(1)  $\text{Li}_2\text{O}$  exposed to  $\text{O}_2$ ,  $\text{O}_2\text{-N}_2$ , and  $\text{O}_2\text{-He}$  atmospheres at 50% relative humidity. The corresponding gravimetric curves are shown in figure 60.

(2)  $\text{Li}_2\text{O}$  exposed to  $\text{O}_2$  and  $\text{O}_2\text{-N}_2$  atmospheres at 25, 50, and 75% R.H. Figure 61 shows gravimetric curves.

(3) Partially hydrated  $\text{Li}_2\text{O}$  exposed to  $\text{O}_2$ ,  $\text{O}_2\text{-N}_2$ , and  $\text{O}_2\text{-He}$  atmospheres. Gravimetric curves are shown in figure 62.

### 4. ANALYSIS OF RESULTS

With 1%  $\text{CO}_2$  concentration (1% = 7.6 mm Hg) the effect of atmospheric moisture on  $\text{CO}_2$  absorption rate is greatest in the range 0 to 50% R.H. Since  $\text{LiOH}$  formation must precede  $\text{CO}_2$  removal, the  $\text{H}_2\text{O}/\text{CO}_2$  molar ratio must exceed unity for reasonable  $\text{CO}_2$  absorption rate during initial absorption. This ratio at 22 C, 25% R.H. is only 0.65, too low for efficient absorption. Runs 2a and 2b (table XXX) reflect this water deficiency, showing poor utilization and residual  $\text{Li}_2\text{O}$  after 8 hours exposure. With higher humidity and a molar ratio exceeding unity (22 C, 50% R.H., 1.32 moles  $\text{H}_2\text{O}/\text{mole CO}_2$ ), the  $\text{CO}_2$  absorption rate nearly doubles as in Runs 2c and 2d. At 75% R.H. the additional moisture merely increases  $\text{LiOH}\cdot\text{H}_2\text{O}$  content as illustrated by Runs 2e and 2f.

Results on the effect of gas composition,  $\text{O}_2$  versus  $\text{O}_2\text{-N}_2$  atmospheres, show some inconsistencies. However, the bulk of

TABLE XXX  
ABSORPTION TESTS IN VARIOUS ATMOSPHERES

Run No. (a)	Rel. Hum. %	Gas Comp.	Run Time hr.	Absorbed Gases Millimoles		Mole Ratio H <sub>2</sub> O/CO <sub>2</sub>	Li <sub>2</sub> O Used %	Reaction Product Analysis	
				H <sub>2</sub> O	CO <sub>2</sub>			Li <sub>2</sub> O	Li <sub>2</sub> CO <sub>3</sub>
1-	---	---	---	---	---	---	91.0	2.1	6.8
1a	50	O <sub>2</sub>	3.7	46	33	1.39	96.6	47.7	45.7
1b	50	O <sub>2</sub> +N <sub>2</sub>	3.7	60	16	3.75	96.0	64.0	0.0
1c	50	O <sub>2</sub>	41	41	65	0.63	0.0	73.1	18.2
1d	50	O <sub>2</sub> +He	3	79	48	1.65	49.8	55.1	22.1
1e	50	O <sub>2</sub> +N <sub>2</sub>	3	82	30	2.73	31.2	0	46.5
2-	---	---	---	---	---	---	94.7	3.3	2.0
2a	25	O <sub>2</sub>	42.6	33.0	1.29	11.9	48.2	39.9	0.0
2b	25	O <sub>2</sub> +N <sub>2</sub>	43.0	41.6	1.034	42.7	56.1	37.8	0.0
2c	50	O <sub>2</sub>	46.6	65.0	0.72	66.8	0.0	72.4	18.1
2d	50	O <sub>2</sub> +N <sub>2</sub>	45.6	64.6	0.70	66.4	0.0	73.6	9.0
2e	75	O <sub>2</sub>	57.8	69.4	0.83	71.3	0	67.5	7.32
2f	75	O <sub>2</sub> +N <sub>2</sub>	71.3	63.4	1.12	65.1	0	73.58	9.08
3-	---	---	---	---	---	---	58.0	3.6	38.4
3a	25	O <sub>2</sub>	15.5	42.2	0.36	51.2	0.6	52.6	0.0
3b	25	O <sub>2</sub>	13.6	60.7	0.22	73.6	0.0	77.5	11.1
3c	25	O <sub>2</sub> +N <sub>2</sub>	15.5	40.6	0.38	49.2	1.6	61.1	0.0
3d	25	O <sub>2</sub> +He	2.5	60.8	0.04	73.7	0.0	80.2	3.4
3e	75	O <sub>2</sub> +N <sub>2</sub>	43.1	50.6	0.85	61.4	0.0	64.0	24.5
3f	75	O <sub>2</sub> +He	5.6	77.5	0.07	93.9	0	89.6	6.1

Notes: (a) 0.22 g/cc Li<sub>2</sub>O bulk density for Run Nos. 1  
0.21 g/cc Li<sub>2</sub>O bulk density for Run Nos. 2  
0.25 g/cc Li<sub>2</sub>O bulk density for Run Nos. 3

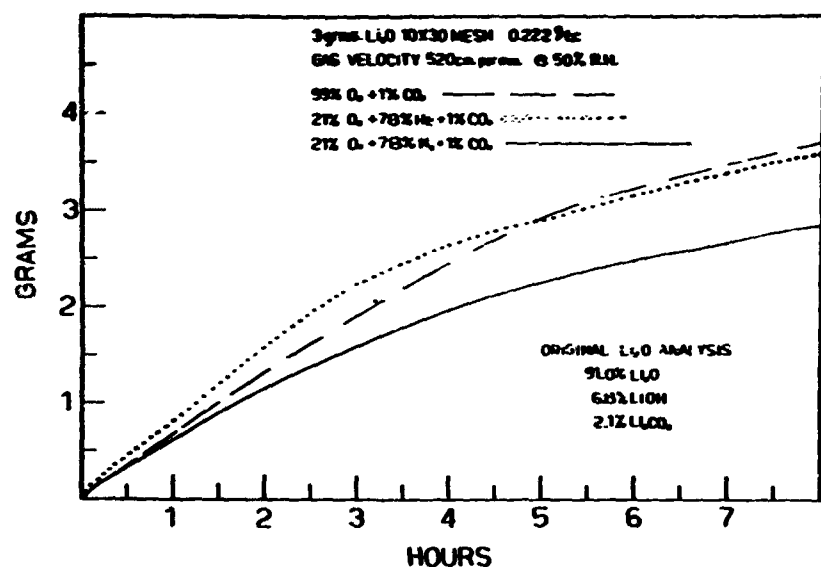


Fig. 60. Gravimetric Curves For O<sub>2</sub>, O<sub>2</sub>-N<sub>2</sub>, and O<sub>2</sub>-He Atmospheres At 50% Relative Humidity.

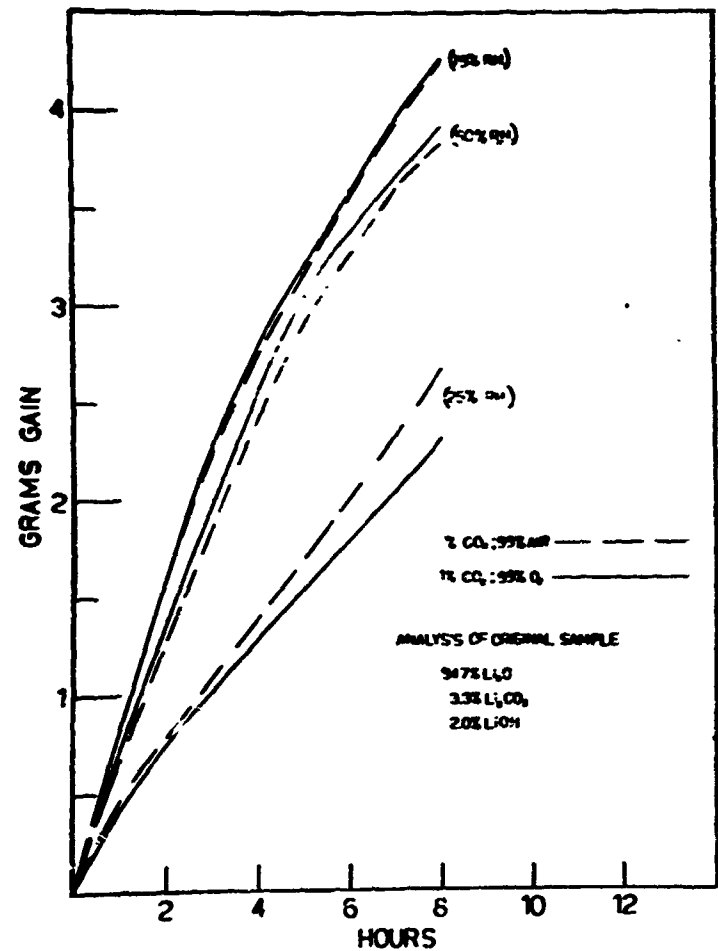


Fig. 61. Gravimetric Curves For O<sub>2</sub> and O<sub>2</sub>-N<sub>2</sub> Atmospheres  
At 25, 50, and 75% Relative Humidity

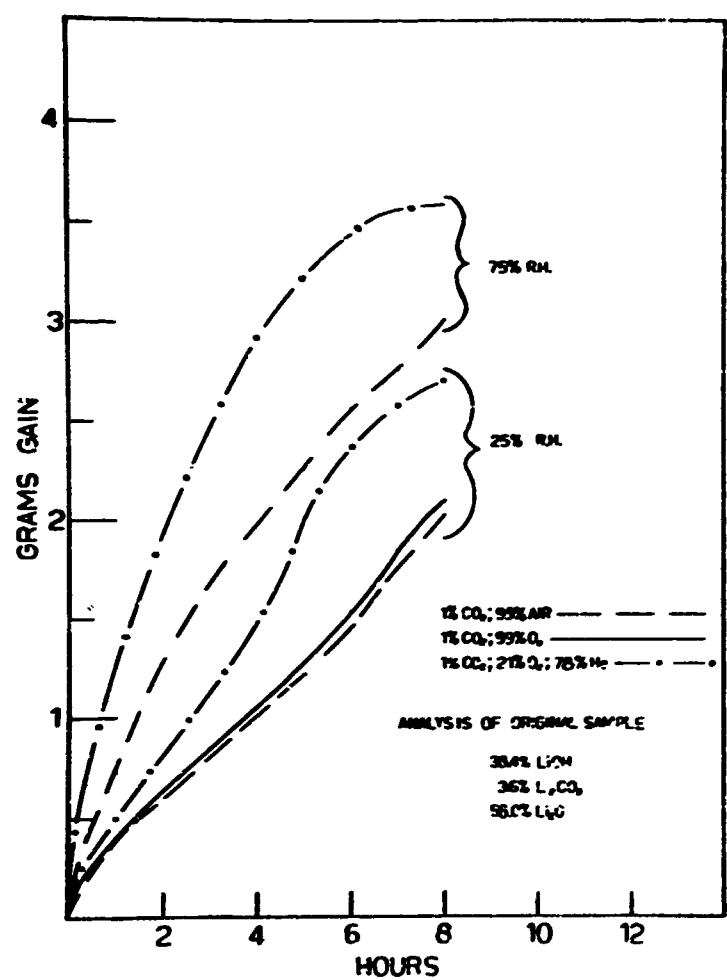


Fig. 62. Gravimetric Curves For Partially Hydrated Li<sub>2</sub>O

the data, the Run 2 series, wherein these atmospheres were studied over a wide humidity range, indicate absorbent performance is above the same in either atmosphere. The gravimetric curves at various humidities are shown in figure 61. Helium had a significant effect on the absorption process. The higher diffusion rates occurring in  $O_2$ -He versus  $O_2$  and  $O_2$ - $N_2$  atmospheres are best illustrated in figure 62. The small size and high velocity of the He molecule improves diffusion of the  $CO_2$  and moisture.

Exploratory results indicate that partial hydration of  $Li_2O$  has merit. This step pre-supplies moisture in the form of  $LiOH$ , thereby improving  $CO_2$  absorption under low humidity conditions. Comparison of Runs 2a and 3a ( $O_2$  atmospheres) and Runs 2b and 3c ( $O_2$ - $N_2$  atmospheres) illustrates improved oxide utilization under 25% relative humidity. With partially hydrated absorbent, the  $H_2O/CO_2$  molar ratio of the gas does not have to exceed unity.

## SECTION VII

### CONCLUSIONS

#### 1. LITHIUM OXIDE PREPARATION AND PERFORMANCE

The bulk density of various forms of  $\text{Li}_2\text{O}$  has been substantially increased while retaining good reactivity. Absorbent  $\text{Li}_2\text{O}$  shapes and granular forms can be prepared with bulk densities ranging between 0.18 and 0.28 g/cc. At the present state of knowledge, reactivity declines sharply at bulk densities exceeding about 0.30 g/cc. The granular oxide can meet standard hardness specifications for granular  $\text{LiOH}$ , currently a widely used absorbent. Key factors in preparing the improved density oxide are high-surface lithium peroxide (about  $18 \text{ m}^2/\text{g Li}_2\text{O}_2$ ), decomposition temperature, and techniques in processing the  $\text{Li}_2\text{O}_2$  to  $\text{Li}_2\text{O}$ .

Granular  $\text{LiOH}$ , currently the best chemical absorbent available, will typically remove 0.8 g  $\text{CO}_2/\text{g LiOH}$  before the 2% breakthrough point. In the reported work the corresponding performance attained with various forms of  $\text{Li}_2\text{O}$  was as follows:

- a. 0.8 g  $\text{CO}_2/\text{g Li}_2\text{O}$  for a granule belt configuration passively exposed (Run 397-1).
- b. 1.14 g  $\text{CO}_2/\text{g Li}_2\text{O}$  for a granule bed concentric cylinder absorber under semipassive exposure (Run 397-3).
- c. 1.23 g  $\text{CO}_2/\text{g Li}_2\text{O}$  for a granular-packed bed under dynamic exposure (Run 361-48).

A variety of processes were studied for producing the oxide in supported and self-supported forms. For supported beds, the

best process involved pelletizing high surface area  $\text{Li}_2\text{O}_2$  powder, thermally decomposing, and crushing and sieving the resulting  $\text{Li}_2\text{O}$  cake. This technique yielded granular  $\text{Li}_2\text{O}$  with improved bulk density while maintaining good reactivity. The swelling and sintering properties of  $\text{Li}_2\text{O}_2$  on decomposition can be used for preparing self-supported shapes. Testing indicates that good absorption can be realized with such shapes but higher strength would be desirable. The conflicting requirements of high density for strength and low density for reactivity suggest that pursuit of mechanical compaction techniques will not be fruitful. Further development should probably be aimed at using some reinforcing technique such as a matrix of inert fibrous material.

Two techniques were developed for reducing the potential dusting of granular  $\text{Li}_2\text{O}$ . Controlled abrasion in a rotary gas flushed dedusting apparatus largely removed adherent dust and dust producing granule edges. This treatment also improved bulk density. The fabric encasement of granular  $\text{Li}_2\text{O}$  displays also appears promising. Contrary to expectation, a high percentage of open area in the fabric proved unnecessary. Good diffusion and absorption was obtained with a relatively tight fabric which can also serve as a dust filter. Development efforts on directly coating the  $\text{Li}_2\text{O}$  granules were unsuccessful.

## 2. EFFECT OF ATMOSPHERE VARIATIONS

Tests at one-third normal atmospheric pressure revealed that absorption rates were improved at reduced pressure. A study of

atmosphere composition indicated no significant difference in absorption rate in  $O_2$  and  $O_2-N_2$  atmospheres. A marked improvement in  $CO_2$  and  $H_2O$  diffusion rates was found in  $O_2-He$  atmospheres.

Atmospheric moisture, in terms of adequate  $H_2O/CO_2$  molar ratio, is required during initial  $CO_2$  absorption. With 7.6 mm Hg  $CO_2$  partial pressure, the 0 to 50% relative humidity range is the most critical. The corresponding minimum water vapor pressures required for efficient absorption are about 11 mm Hg for a dynamic granular bed and 15 mm Hg for a passive granular display. In general, the  $H_2O/CO_2$  molar ratio of the environmental chamber input to granular  $Li_2O$  configurations should be about 1.44 for dynamic systems and 2.0 for passive systems. The ratio for human exhalation is about 2.4. Exploratory work indicates that partial hydration of the  $Li_2O$  has merit. This step pre-supplies moisture in the form of  $LiOH$  thereby improving  $CO_2$  absorption under low humidity conditions.

### 3. CONFIGURATION DESIGN

Gravimetric analysis work has confirmed the importance of the molar volume relations between reaction product and substrate. Density limitations can be estimated from these relations thereby providing guidelines for absorbent design and further experimentation. For granular  $Li_2O$ , experience indicates that a good bulk density compromise between reactivity and volume efficiency is about 0.20 g/cc under passive exposure and 0.26 to 0.28 g/cc under semipassive or dynamic exposure.

Various Li<sub>2</sub>O forms were developed, capable of absorbing 46 g CO<sub>2</sub>/hr under passive, semipassive, or dynamic conditions. For reporting purposes, the following definitions have been adopted for these exposure modes--

Passive - Gas velocity past or through the absorbent configuration is essentially the same as the gas velocity within the chamber itself and is relatively low. There is no pressure loss across the configuration. Any power required for this nominal gas circulation is chargeable to other systems, such as humidity or temperature control.

Semipassive - The configuration requires a positive gas flow, causes a measurable pressure loss, and does impose a power penalty. The major gas flow is through channel voids in the configuration and its direction is essentially parallel to the exposed absorbent surfaces.

Dynamic - The configuration requires a positive gas flow, causes a pressure loss, and imposes a power penalty. The major gas flow is through bulk voids with gas flow through multiple circuitous paths.

Factors to be considered in selecting the best exposure mode for a given mission length include-- ambient atmosphere (composition and humidity), weight and volume penalties assessed for power consumption, and the relative importance of weight versus volume. These factors are not yet firmly defined. However, the reported results suggest that passive exposure could be employed in missions up to about 12 hours duration. Beyond this point semipassive or dynamic exposure would appear preferable because

of higher volume efficiency. General guidelines for designing  $\text{Li}_2\text{O}$  based systems for the various exposure modes can be summarized as follows:

a. Passive Exposure

The absorbent requirement is estimated to be 50 to 60 g of 10- by 30-mesh granular  $\text{Li}_2\text{O}$  per manhour. However, this value is greatly dependent on chamber pressure. For example only 38 g  $\text{Li}_2\text{O}/\text{hr}$  was required to absorb 44 g  $\text{CO}_2/\text{hr}$  in a one-third atmosphere test. A tight-weave, multifilament fiberglass fabric envelope should provide adequate  $\text{CO}_2$  and moisture diffusion while retaining even fine particles (10 microns)  $\text{Li}_2\text{O}$  dust.

b. Semipassive Exposure

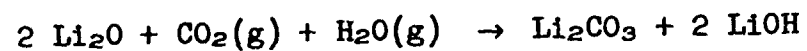
Tests with pierced cylinders indicate that a configuration density (i.e., - g  $\text{Li}_2\text{O}/\text{cc}$  total volume including channel voids) of about 0.28 g/cc is suitable. The oxide shape should preferably be formed by decomposing granular  $\text{Li}_2\text{O}_2$  as described in section IV-3. A pressure loss of 0.3 cm  $\text{H}_2\text{O}$ , or less, at 1.5  $\text{m}^3/\text{min}$  is feasible.

c. Dynamic Exposure

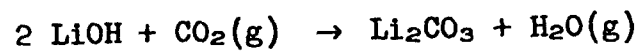
The best choice is considered 4- by 10-mesh granular  $\text{Li}_2\text{O}$  at about 0.28 g/cc bulk density. The absorbent requirement is estimated to be 38 g  $\text{Li}_2\text{O}$  per manhour. A pressure loss of 0.6 cm  $\text{H}_2\text{O}$ , or less, at 0.2  $\text{m}^3/\text{min}$  gas flow is feasible.

In configuration design, the increased heat evolution of  $\text{Li}_2\text{O}$  based systems, as noted below, should be recognized. The

bed should not be directly exposed to the CO<sub>2</sub> and H<sub>2</sub>O concentrations of human exhalation, since excessive temperature and absorbent sintering can result. The problem can be eliminated by diluting the gas to 1% CO<sub>2</sub> and 50% R.H. before processing.



H<sup>25</sup>; - 86.8 Kcal/mole CO<sub>2</sub> absorbed



H<sup>25</sup>; - 20.4 Kcal/mole CO<sub>2</sub> absorbed

## REFERENCES

1. Markowitz, M. M., Dezmelyk, E. W., A Study of the Application of Lithium Chemicals to Air Regeneration Techniques in Manned Sealed Environments, Technical Documentary Report AMRL-TDR-64-1, Aerospace Medical Research Laboratories, Wright-Patterson Air Force Base, Ohio, February 1964.
2. Bach, R. O., Boardman, W. W., Jr., Robinson, J. W., Jr., Application of Lithium Chemicals for Air Regeneration of Manned Spacecraft, Technical Documentary Report TR-65-106, Aerospace Medical Research Laboratories, Wright-Patterson Air Force Base, Ohio, June 1965.
3. Boryta, D. A. and Markowitz, M. M., Lithium Oxide as a Carbon Dioxide Absorbent, Unpublished Research Report, Foote Mineral Company, Exton, Pa., August 1964.
4. Pilling, N. B. and Bedworth, R. E., "The Oxidation of Metals at High Temperatures," J. Inst. Metals 29, 577(1923).
5. Cohen, A. J., "Lithium Hydroperoxide 1 Hydrate, Lithium Peroxide, and Lithium Oxide," Inorganic Synthesis, Vol. V, T. Moeller, editor, McGraw-Hill Book Company, New York, pp. 1-6, 1957.
6. Markowitz, M. M., Boryta, D. A., "A Convenient System of Thermogravimetric Analysis and of Differential Thermal Analysis," Anal. Chem., 32, 1588(1960).
7. Gregory, N. W., Mohr, R. H., "The Equilibrium  $2\text{LiOH(g)} = \text{Li}_2\text{O(g)} + \text{H}_2\text{O(g)}$ ," J.A.C.S. 77, 2142-4(1955).
8. Yuji Ueda, "Thermodynamic Studies of Lithium Hydroxide and Lithium Chloride," Sci. reports, Tohoku Univ. A22: 448-74 (1933).
9. Keating, D. A., Weiswurm, K., Potassium Superoxide Passive Air Regeneration Studies for Manned Sealed Environments, WADD Technical Report 60-707, Life Support Systems Laboratory Aerospace Medical Division, Wright-Patterson Air Force Base, Ohio, December 1960.
10. Keating, D. A., Design Parameters for the Engineering of Closed Respiratory Systems, WADC Technical Report 59-766, Aerospace Medical Laboratory, Wright-Patterson Air Force Base, Ohio, December 1959.
11. McGoff, M. J., Potassium Superoxide Atmosphere Control Unit, Technical Report AMRL-TR-65-44, Aerospace Medical Research Laboratories, Air Force Medical Division, Wright-Patterson Air Force Base, Ohio, September 1965.

12. Markowitz, M. M., The Absorbing Story of Lithium Hydroxide, Foote Prints 34, 9(1965).
13. Standard Methods of Chemical Analysis, N, Howell Furman, Ph.D., editor, D. Van Nostrand Company, Inc., Princeton, New Jersey, p. 298.

## Security Classification

## DOCUMENT CONTROL DATA - R &amp; D

(Security classification of title, body of abstract and indexing annotation must be entered when the overall report is classified)

1. ORIGINATING ACTIVITY (Corporate author) Foote Mineral Company Research and Engineering Center Exton, Pennsylvania 19341	2a. REPORT SECURITY CLASSIFICATION UNCLASSIFIED
3. REPORT TITLE CONFIGURATION INVESTIGATION FOR LITHIUM OXIDE CARBON DIOXIDE CONTROL SYSTEMS	2b. GROUP N/A

4. DESCRIPTIVE NOTES (Type of report and inclusive dates) Final Report, December 1965-December 1966		
5. AUTHOR(S) (First name, middle initial, last name) Daniel A. Boryta Eugene W. Dezmelyk		
6. REPORT DATE October 1967	7a. TOTAL NO. OF PAGES 144	7b. NO. OF REFS 13
8a. CONTRACT OR GRANT NO. AF 33(615)-3382	9a. ORIGINATOR'S REPORT NUMBER(S) Foote Mineral Company Research Report No. FOOTE-1266	
b. PROJECT NO. 6373	9b. OTHER REPORT NO(S) (Any other numbers that may be assigned this report) AMRL-TR-67-62	
c. Task No. 637302		
d.		

10. DISTRIBUTION STATEMENT Distribution of this document is unlimited. It may be released to the Clearinghouse, Department of Commerce, for sale to the general public.		
11. SUPPLEMENTARY NOTES	12. SPONSORING MILITARY ACTIVITY Aerospace Medical Research Laboratories Aerospace Medical Div., Air Force Systems Command, Wright-Patterson AFB, Ohio 45433	

13. ABSTRACT The bulk density of lithium oxide shapes and granules has been increased substantially while retaining good reactivity. Absorbent forms of the oxide can be prepared in the bulk density range of 0.18 to 0.28 g/cc. For granular oxide, results indicate a reason- able compromise between reactivity and absorbent volume efficiency is about 0.20 g/cc in passive systems and 0.26 to 0.28 g/cc in semipassive or dynamic systems. The improvement results from use of high (about 18 m <sup>2</sup> /g) surface area lithium peroxide raw material and techniques in processing the peroxide to oxide. Tests indicate the oxide forms developed can equal (passive exposure) or exceed (semipassive or dynamic expo- sure) the 0.8 g CO <sub>2</sub> /g LiOH capacity of granular lithium hydroxide before 2% breakthrough. Dusting of the granular oxide form was reduced by controlled abrasion and fabric encase- ment techniques. Tests at one-third and normal atmospheres indicated higher carbon dioxide absorption rates at the lower pressure. A marked improvement was found in oxygen-helium as compared to oxygen and oxygen-nitrogen atmospheres. Atmospheric moisture conditions required for efficient absorption were defined. Exploratory work indicates partial hydration of the oxide is one method for initiating absorption under low humidity conditions. Gravimetric analysis work, which confirmed that density limita- tions are presently imposed by reaction product-substrate molar volume relations, should provide useful guidelines for absorbent design and further experimentation.		
---	--	--

Security Classification

14 KEY WORDS	LINK A		LINK B		LINK C	
	ROLE	WT	ROLE	WT	ROLE	WT
Environmental control Configuration investigation Lithium oxide Carbon dioxide control Life support Alkali metal oxides Carbon dioxide absorption Space vehicles Passive absorption Semipassive absorption Dynamic absorption						